Using neutrons to protect our works of art

Amélie Castel

THÈSE

Pour obtenir le grade de

DOCTEUR DE L'UNIVERSITÉ GRENOBLE ALPES

Spécialité : MEP : Mécanique des fluides Energétique, Procédés

Arrêté ministériel : 25 mai 2016

Présentée par

Amélie CASTEL

Thèse dirigée par **Yahia RHARBI**, Directeur de recherches
et codirigée par **Philipp GUTFREUND**
et **Bernard CABANE**

préparée au sein du **Laboratoire Laboratoire Rhéologie et Procédés**
dans **l'École Doctorale I-MEP2 - Ingénierie - Matériaux, Mécanique, Environnement, Energétique, Procédés, Production**

Utilisation des neutrons pour la protection des oeuvres d'Art

Using neutrons to protect our works of art

Thèse soutenue publiquement le **10 juillet 2020**,
devant le jury composé de :

Monsieur Yahya RHARBI
Chargé de recherche, CNRS DELEGATION ALPES, Directeur de thèse
Madame Lay-Theng LEE
Directeur de recherche CNRS, unité mixte CEA-CNRS, Laboratoire Leon-Brillouin, CEA, Rapporteur
Monsieur Carlos MARQUES
Directeur de Recherche, CNRS, Rapporteur Président
Madame Giovanna FRAGNETO
Directeur de recherche, Chaire Grands Instruments Européens Université Grenoble Alpes, Institut Laue Langevin, Examinateur
Madame Debora BERTI
Professeur, CSGI, Examinateur

If the picture needs varnishing later,
I allow a restorer to do that, if there's any restoring necessary.
Edward Hopper

A ma famille.

REMERCIEMENTS

Cette thèse a été réalisée au sein du groupe de recherche Large Scale Structures (LSS) de l'Institut Laue Langevin (ILL) de Grenoble et du Laboratoire Rhéologie et Procédés (LRP) de Grenoble. Ce projet doctoral a été porté par la collaboration étroite et le soutien sans faille de plusieurs acteurs du monde des sciences, de l'art et de mon entourage et je tiens particulièrement à leur exprimer ma gratitude à travers ces quelques écrits.

En premier lieu, j'adresse mes sincères remerciements à mon directeur de thèse, Yahya Rharbi et mes deux encadrants, Philipp Gutfreund et Bernard Cabane. Je vous remercie pour votre soutien, votre implication et la transmission du savoir nécessaire à l'élaboration de ce projet. Tout cela m'a été précieux et j'ai ainsi pu apprendre beaucoup sur les polymères, les gels et la réflectivité de neutron. Merci aussi pour ces nombreuses discussions scientifiques constructives et stimulantes au cours de nos réunions régulières ainsi que de votre patience indéfectible. Grâce à ces échanges, le projet a évolué efficacement en s'axant premièrement dans la construction et le développement des idées ; et dans un second temps, en explorant la compréhension, l'analyse et la discussion des résultats. Travailler avec vous a été un grand plaisir et je vous remercie de m'avoir transmis une part de vos passions scientifiques respectives.
Bernard, je vous suis notamment très reconnaissante d'avoir toujours cru en moi et d'être toujours présent dans chaque étape de ma vie professionnelle scientifique, merci beaucoup. Et je me permets de rappeler que sans vous ce projet n'aurait pas vu le jour.

Je remercie sincèrement les rapporteurs et tous les membres de mon jury de l'honneur qu'ils font à ce projet ainsi qu'à moi-même de participer à la lecture de ces travaux et pour leurs présence à ma soutenance. Je remercie vivement Lay-Theng Lee et Carlos Marques d'avoir accepté de rapporter ce travail. Je remercie aussi Giovanna Fragneto et Debora Berti pour leur participation au jury de thèse. Merci à vous de m'avoir apporté vos expertises et d'avoir évalué mon travail.

Merci à Bruno Jean et Marco Maccarini d'avoir suivi le projet en tant que comité de thèse pour l'université, vos conseils ont permis de mieux aborder le travail de thèse et de bien redéfinir le rôle de chacun.

Merci à l'équipe du Large Scale Structures (LSS) et sa directrice Giovanna Fragneto pour leur accueil. J'ai beaucoup appris à votre contact quotidien. Une pensée particulière pour Yuri Gerelli qui en plus de ses conseils et de son soutien, m'a transmis ses connaissances sur l'utilisation et le fonctionnement du QCMD, merci. Je remercie toutes les personnes à l'ILL avec qui j'ai eu la chance de partager tant au travail qu'en dehors.

Mes doux remerciements à mes amis et collègues de l'ILL :
Une grande pensée pour Marta qui dès son arrivée dans le bureau a été un petit soleil quotidien et s'est très vite placée comme une alliée dans les bons et les moins bons moments. De cette rencontre est née une belle amitié. Merci pour ton oreille attentive et ton soutien constant. Francesca, il serait difficile de ne pas mentionner ses talents de cuisinière qui étaient un ravissement gustatif au cours de ces 3 années passées à l'ILL. Merci de m'avoir partagé un peu d'Italie ! J'ai aussi une douce pensée pour Elodie, Oonagh et Bruno avec qui j'ai eu la joie de faire de la poterie à l'ILL sur ma première année, sans oublier les autres doctorants avec qui j'ai pu partager quelques soirées, discussions et bout de vie : Loreto, Silvia, Andreas, Murias, Peter, Marion, Charlotte, Palmerina, Quentin, Stanislav, Stella, Kristijan, Tetiana, Irina, Javier et Giuseppe. Sans oublier mes deux copines des cours d'anglais Virginie et Maria, nos repas et discussions vont me manquer!

Merci aussi aux personnels de l'ESRF qui m'ont prodigués des conseils avisés et m'ont permis d'utiliser les instruments : microscope optique et l'AFM.

Je remercie l'ensemble des membres du LRP et sa directrice Nadia El Kissi pour m'avoir si bien intégrée dans l'équipe. J'ai beaucoup apprécié le soutien, l'écoute et la bienveillance de l'ensemble du personnel. Je ne pourrais jamais suffisamment exprimer ma gratitude à l'ensemble de l'équipe. Hélène Galliard, pour son implication active les deux premières années, pour m'avoir appris à utiliser les rhéomètres du laboratoire et pour ses précieuses astuces. Mohamed Karrouch, Didier Blèses et Eric Faivre, pour avoir été présents pour moi à chaque fois que j'en ai eu besoin. Frédéric Hugenell, pour nos discussions, son aide précieuse et son expertise dans l'utilisation de la DSC. Vincent Verdoot, pour sa contribution sur cette dernière année. Merci aussi à Denis Roux pour nos quelques échanges au détour du couloir sur l'avancement de mon projet, c'était toujours intellectuellement fructueux.

Mes remerciement affectueux à mes amis et collègues du LRP :
Je remercie chaleureusement ma team Girl Power, Alice, Mathilde et Candice, nos soirées filles sont un petit bonheur et d'une grande détente. Alice, merci pour toute la force que tu m'as transmise et l'amitié que tu me portes. Mathilde, merci d'être cette femme entière et vraie qui m'a fait passer des moments forts. Candice, merci d'être un exemple à suivre et de m'avoir rassurée forte de ton expérience.
Je pense aussi à tous ceux qui ont rendu cette période de ma vie agréable au travail et en dehors autour d'un verre ou d'un plateau de charcuterie/fromage : Hugues, Moctar et William, qui ont été là depuis le début jusqu'à la fin de ma thèse, et aussi Diego, Mehdi, Louis, Mohamad, Hanna, David, Revaz, Ouattara, Ayoub, Antoine, Adriana, Alexis et Clément.
Un grand merci à Martinien, reparti avant la fin de ma thèse au Gabon. Les moments passés ensemble en France et nos discussions ont fortement contribué à mon épanouissement durant cette période active de ma vie. J'espère avoir l'occasion de venir te rendre visite prochainement.

Également, j'ai une grosse pensée pour Marguerite Szyc et Olivier Nouaille, deux grands soutiens depuis mes débuts dans le monde de la restauration d'œuvre d'art.

J'en profite aussi pour remercier et témoigner de ma grande affection et reconnaissance à mes proches qui ont été d'une grande aide psychologique : Clémence, ma très chère amie, merci pour ta bienveillance ; Anne-Sophie, mon amie "invisible" et ma grande confidente, toujours là ! ; Léa, l'heureuse retrouvaille Grenobloise ; Fanny, merci chat pour ton soutien sur ces dernières semaines d'écritures, les plus difficiles ! Je ne risque pas d'oublier mes soirées aux Dr. D et mes belles découvertes gustatives ; Jérémie, mon copain de lecture, Batman forever! ; Laetitia, T-Chan, toujours avec moi en pensée ; Stéphanie, tu suis mon parcours depuis presque 10 ans et tu m'a vu passer de la jeune élève à la femme d'aujourd'hui ; Laurie, ma cousine adorée et Houssen ; Stefan, Ghislain, Romain, Audrey et mes copines du lycée que j'ai vu récemment avec grand plaisir (Anaïs, Bianca, Tiphaine et Marie). Merci tout simplement d'être dans ma vie ainsi que pour l'amitié et l'amour que vous me portez. Nos échanges et nos rires contribuent à mon épanouissement. Vos encouragements et votre soutien m'ont grandement aidée dans l'accomplissement de ce projet.

Je remercie aussi mon frère Jonathan, ma soeur Amandine et ma belle-soeur Mélanie, toujours présents dans ma vie pour suivre activement chaque étape et me soutenir dans mes choix. J'ai aussi une douce pensée pour mes neveux et nièces, Grégoire, Alice, Thibaud et les deux derniers nés au cours de ces trois ans de projet doctoral Océane et Baptiste.

Pour finir, je ne peux pas écrire ces remerciements sans penser à mes parents qui m'encouragent et me soutiennent dans tous mes projets. Au-delà du fait que mon existence ne tient qu'à vous deux, je ne serais pas la personne que je suis sans votre aide et les valeurs que vous avez su me transmettre, merci pour tout !

Merci !!!

TABLE OF CONTENTS

LIST OF TABLES

LIST OF FIGURES

RÉSUMÉ

Le gonflement et la dissolution des vernis des peintures de chevalet : Contribution à la compréhension macroscopique et nanoscopique des mécanismes physiques en jeux pendant le traitement d'enlèvement des vernis altérés.

Les œuvres d'art ne durent pas éternellement. Elles sont composés de matériaux évolutifs qui vieillissent dans le temps. Ainsi, les vernis des peintures de chevalet perdent leur aspect visuel initial par dépôt de poussières et des suies en suspension dans l'air, par oxydation et par modification structurelle (effet des radicaux libres). A cause de ces processus, les vernis perdent leur transparence et jaunissent, ce qui empêche une bonne appréciation de l'œuvre d'art.

Afin de renverser l'évolution de ces processus, les peintures sont périodiquement restaurées avec remplacement des anciens vernis. Ce traitement majeure, qui requiert le gonflement et la dissolution de la couche de vernis polymère par des solvants qui peuvent être pénétrants et polaires. Ces solvants peuvent altérer considérablement la composition et la cohésion des matériaux originaux de l'oeuvre qui sont situés sous les couches de vernis. Il est donc urgent de mieux comprendre les processus employés dans les opérations de restauration, particulièrement lors du remplacement des vernis.

Conscient de cette urgence, restaurateurs et scientifiques ont proposé d'utiliser les gels aqueux/solvant pour transférer seulement les quantités de solvants nécessaires à la dissolution du vernis. Les images macroscopiques obtenues avant et après application de ces gels démontrent bien l'efficacité de ce procédé. Toutefois, il apparait des lacunes dans la compréhension des phénomènes qui entre en jeu.

C'est dans ce contexte que s'inscrivent ces travaux de thèse. Ils visent à mieux comprendre la physique des films polymères au contact de mélanges solvant/non solvant et solvant/gel, en suivant les mêmes processus que ceux employés dans la restauration des œuvres d'art. Dans la thèse, on a utilisé la réflexion de faisceaux de neutrons (réflectivité de neutron et diffusion de neutrons aux petits angles), combinée à des visualisations locales (microscopie optique et AFM). La résine polymère choisie est le Laropal®A81, le solvant est l'alcool benzylique et l'hydrogel est le Pemulen TR-2.

La réflectivité de neutrons permet d'observer in situ le comportement physique de films polymères ultraminces déposés sur des blocs de silicium, pendant la cinétique de gonflement par le bon solvant puis par le mauvais solvant suivi de la dissolution et la disparition du film de vernis. L'eau utilisé est le D_2O, qui a un densité de longueur de diffusion (SLD) très élevée par rapport à celles du polymère et du solvant. Ceci permet de différencier par leurs contrastes les distributions spatiales du solvent et du non-solvant. On a ainsi déterminé le SLD du Laropal®A81, puis modélisé l'épaisseur du Laropal®A81 et la rugosité des différents éléments. Ensuite, en utilisant ces valeurs d'épaisseur et de SLD, on a calculé les fractions volumique des différentes composants dans le film de vernis. On a discuté les variations de ces fractions de BA ϕ_{BA} et du D_2O ϕ_{D_2O} qui ont pénétré dans les films en fonction des paramètres investigués c'est-à-dire, l'influence de la concentration de solvant et l'effet de la température pour le cas avec le gel/solvant.

En parallèle, un diagramme de phase ternaire utilisant les paramètre d'interaction de Flory-Huggins a été tracé pour le cas du système solvant/non-solvant en utilisant les résultats de NR, les mesures de viscosité intrinsèque et les mesures de turbidité à température ambiante. Les paramètres d'interaction $\chi_{LA/BA}$, $\chi_{W/BA}$ et $\chi_{LA/W}$ ont été obtenus par calcul du diagramme de phase en utilisant un modèle de Flory-Huggins. La compréhension des phénomènes a été déduite de l'analyse des spectres de NR, complétée par les observations faites en microscopie optique et AFM. L'AFM a surtout permis d'obtenir le profil en profondeur (axe z) des objets apparues dans le films en présence du mélange BA/W.

Une expérience de diffusion aux petits angles de neutrons (SANS) sur des films épais (0.5-1.5 µ m) a donné des spectres d'intensités en fonction du temps évolué. Ces spectres ont été modélisés suivant la loi de Porod. L'aire des interfaces a été tracée en fonction des valeurs de $\chi_{BA/LA}$. Ces résultats ont été complétés par des mesures de QCM-D montrent la cinétique du gonflement et de la dissolution sur des heures et jours après la mise en contacte avec le système solvant/non-solvant.

En conclusion, nos études expérimentales ont permis de mieux comprendre le gonflement et la dissolution des films de Laropal®A81 épais et minces déposés sur des blocs de silicium et exposés à un mélange binaire solvant/non-solvant et des gels aqueuses contenants du solvant.

SUMMARY

The swelling and dissolving of varnish of easel paintings: Contribution to the macroscopic and nanoscopic understanding of the physical mechanisms involved during the removal process of altered varnishes.

Artworks do not last forever. They are composed of changing materials which age with the passage of time. Indeed, the varnishes of easel paintings lose their initial visual appearance due to deposits of dust and soot suspended in the air, by oxidation and by structural modification, e.g. the effect of free radicals. Because of these processes, the varnishes lose their transparency and turn yellow, thus preventing a good understanding of the work of art.

In order to reverse the evolution of these processes, paints are periodically restored and the old varnishes replaced. This major treatment requires the swelling and dissolution of the layer of polymeric varnish using solvents that can be penetrating and polar. These solvents can significantly alter the composition and cohesion of the original materials of the painting that are located under the varnish layers. It is therefore imperative to understand the processes used in restoration operations better, in particular when replacing varnishes.

Conscious of this urgency, conservators and scientists have proposed the use of aqueous gels/solvents to transfer only the quantities of solvents necessary for the dissolution of the varnish. The macroscopic images obtained before and after application of these gels demonstrate the efficiency of this method. However, the physical and chemical processes involved are still poorly understood.

The aim of this thesis is to understand the physics of polymer films in contact with solvent/non-solvent and solvent/gel mixtures better, following the same processes used in the restoration of works of art. To study the physical processes of this method, we have used neutron beam reflection, in our case neutron reflectivity and small angle neutron scattering (SANS) combined with local visualizations, in particular optical microscopy and Atomic Force Microscopy (AFM). The polymer resin chosen is Laropal®A81, the solvent is benzyl alcohol and the hydrogel is Pemulen TR-2.

The neutron reflectivity allows us to observe in situ the physical behaviour of ultrathin polymer films deposited on silicon blocks. This behaviour is observed during the kinetics of swelling by the good solvent then by the bad solvent followed by the dissolution and disappearance of the varnish film. The water used is D2O, which has a very high scattering length density (SLD) compared to those of the polymer and the solvent. It is therefore possible to differentiate by their contrasts the spatial distributions of the solvent and the non-solvent. The SLD of the Laropal®A81 was first determined. Then the thickness of the Laropal®A81 was modelled, as well as the roughness of the various elements. By using these thicknesses and SLD values, the volume fractions of the various components in the varnish film were calculated. The variations of these fractions of BA ϕ_{BA} and D_2O ϕ_{D_2O} which have penetrated into the films have been discussed as a function of the investigated parameters, i.e. the solvent concentration and the effect of the temperature in the case of the gel/solvent.

In parallel, a ternary phase diagram using Flory-Huggins interaction parameters was plotted for the case of the solvent/non-solvent system using NR results, intrinsic viscosity measure-

ments, and turbidity measurements. The interaction parameters, χ_{LABA}, $\chi_{W/BA}$ and $\chi_{LA/W}$, were obtained by calculating the phase diagram using a Flory-Huggins model. The understanding of the phenomena was deduced from the analysis of the NR spectra, supplemented by the observations made in optical microscopy and AFM. The AFM allowed us to obtain the depth profile (z axis) of the objects appearing in the film in the presence of the BA/W mixture.

A Small Scattering Neutron Experiment (SANS) on thick films (0.5-1.5 µm) gave spectra of intensities as a function of evolved time. These spectra were modelled according to Porod's law. The interface area was plotted according to the values of $\chi_{BA/LA}$. These results were supplemented by QCM-D measurements showing the kinetics of swelling and dissolution over hours and days after contact with the solvent/no-filler system.

In conclusion, our experimental studies allowed a better and detailed understanding of the swelling and dissolution of thick and thin Laropal®A81 films deposited on silicon blocks and exposed to a solvent/non-solvent binary mixture and to aqueous gels containing good solvent.

LIST OF ABBREVIATIONS

FRMII	. . . . .	Forschungs-Neutronenquelle Heinz Maier-Leibnitz
ILL	. . . . .	Institut Laue-Langevin
LRP	. . . . .	Laboratoire de Rhéologie et Procédés
NR	. . . . .	Neutron reflectivity
NS	. . . . .	Neutron scattering
N-S	. . . . .	Navier-Stocks
SANS	. . . . .	Small Angle Neutron Scattering
SLD	. . . . .	Scattering length density

INTRODUCTION

Since prehistory, humans have left traces of their existence. Consequently, works of art and artifacts have a major place in our lives. They are a historical marker, a means of expression or propaganda, of political and economic issues. Art is a universal marker of the present and the past and it is an important part of our identity. Preserving it, is therefore essential for future generations. In this context, conservators and restorers are the guarantors of this preservation and transmission. Hence, first they optimize the storage and the exhibition environment. Second, if necessary, they proceed to restoration to preserve their aesthetic and historical roles. According to Cesare Brandi's book 'Teoria del restauro' [1] which is the reference book for conservation and restoration heritage, restoring a work of art is defined as: "il retauro deve mirar al ristabilimento della unità potenziale dell'opera d'arte, purchè ciò sia possibile senza commettere un falso artistico o un falso storico, e senza cancellare ogni traccia del passagio dell'opera d'arte nel tempo." (C. Brandi. 1963 p.36). It means that during restoration treatments, the restorer must act only in order to perpetuate and stabilize the piece of art without compromising its integrity or that of the artist. It is not a question of modifying the piece of art to form a new one. We have to take into account that the aging of the materials is an integral part of the history of the work of art. If a restoration action is necessary and inevitable, it must use reversible products and materials, and the restorers must limit their actions to the strictest necessary.

However, the restoration treatments are sometimes risky for the works of art and the slightest misstep can be irreparable. The history of restoration includes references to destruction due to over-extensive restoration or due to the action of new species transferred during treatments [2], [3], [4] and [5]. Eugène Delacroix, a famous French artist wrote in particular: " Ce n'est pas un tableau restauré qu'on vous donne, mais un autre tableau, celui du misérable barbouilleur qui s'est substitué à l'auteur du tableau véritable..." [6] which is good example of the controversy between supporters of minimalist conservation-restoration or supporters of advanced restoration. Other opponents of radical restorations have also distinguished themselves, such as Professor Gombrich and Professor Kurz of the Warburg Institute, and Professor Stephen Rees Jones of the Courtauld Institute [2] in their time.

However whatever the outcome of the debate on the degree of restoration needed, the removal of varnish coating is essential because varnishes deteriorate, develop micro-cracks, turn yellow and become more acidic with time [7]. Restorers usually remove this protective layer with solvents which are often penetrative and polar,inducing an irreversible modification of the physico-chemical composition of the painting. In its 'life', the same work of art can therefore undergo several restoration campaigns in only 100 years of life. Unfortunately, each restoration can contribute to the weakening of the constituent materials and the disappearance of the materials of the work of art. The real problem comes mainly from the difficulty of the restorers in controlling the action of solvents during the removal the varnish. Indeed, the presence of the patina and glazes (layer transparent colored on top of the paint layer [8]) complicates the removal of the varnish. A strong argument advanced by the opponents of strong cleaning is the destruction of the patina and glazes by this cleaning treatment. These layers are very thin and sensitive and constitute the last layer of the artist to magnify his work. Destruction was already mentioned by Vasari who gives the artificial patina recipes used in his time [9]. Another

argument mentioned by Stephen Rees Jones is varnish leaching of the binder of the paint layer [2]. Many paintings have organic varnishes and the current synthetic varnishes replacement also have disadvantages that make it necessary to remove them after a while, therefore finding sustainable solutions to limit the destruction during this treatment is a current issue. So, the removal of the old varnish layer is a delicate and a risky treatment which has been controversial since the end of the war. The study of chemical materials on artworks is common. Scientists

use several surface spectroscopy techniques such as for example Raman, Photoluminescence, or X-Ray fluorescence (XRF). In the case of bulk materials, chemical and physical information cannot be obtain just by surface spectroscopy. To perform the treatment and investigate the physical phenomena, some studies on the fundamental physics governing the varnish removal process by the use chemical and physical characterization techniques have been carried out in the past, but this remains incomplete and is mainly based only on the R.L. Feller, Graham and Stolow datas [10], i.e. on works of the middle of the twentieth century. The most recent study is that of Michalski [11] in which he collects the scattered data of the latter experiments and some others to propose a partial model of the physical aspects of varnish removal from oil paint. Also he gives a chart of solvent penetration as a function of the time. Since the twentieth century, restoration varnishes have evolved [7]. Many restorers favor the use of these new varnishes as the varnish Laropal®A81 of this study and many paintings have a synthetic varnish. That does not change the problem of the restorers of the removal of varnishes. Removing them from the surface of a painting without risk to the paint layer remains a challenge. And there is a need to have a better comprehension of the fundamental physics governing the process. And the understanding of diffusion of solvent into polymers is also important in others area (for example to identify chain architectures and mechanisms), and the mechanisms that govern the diffusion behaviour are not fully understood. [12]

A major part of science research for cultural heritage in the world focuses on the macroscopic/nanoscopic understanding, on the investigation of the degradation and on the evolution of materials; this project is a part of that research. The aim of this study is to understand mainly by the use of neutrons, the nanoscopic behavior of ultrathin, thin and thick films of a synthetic polymer resin (Laropal®A81), which is commonly used by art restorers as a varnish resin and retouching resin on paintings, when they are in contact with solvent/water mixture and gel/solvent mixture; and to observe the impact of several external effects (temperature, shear) on polymer/nonsolvent/solvent and polymer/gel/solvent systems. The basic idea is to answer several questions about physico- chemical mechanisms of swelling and dissolution of layers of polymeric varnish that lead to its disappearance on the paint layer when the restorer treats the varnish with a solvent: How does the film of varnish disappear? Is it layer by layer, dewetting or erosion? Is there nucleation or spinodal decomposition during the process?

This study is composed of 5 chapters:

In the **Chapter 1**, the context of the thesis will be introduced. First, the history, the place and the role of the varnish in a painting will be discussed briefly. Then, the instability, the reasons that lead restorers to remove these varnishes and the traditional way of the restorers to remove this layer when it becomes undesirable will be explained. Finally, the effects that this treatment of the removal of the varnish coating may have on the paint layer and the current way to offset these effects will be discussed. Second, the theory of polymers physics focusses on the swelling and the dissolution processes by a solvent/non-solvent mixture will be exposed in order to understand the removal of varnish layer treatment. Flory-Huggins theory, interaction parameters and phase diagram theory will be developed. Then, the last step of the disappearance of the polymer film: rupture, dewetting and drop formation of the thin polymer film will be addressed.

Chapter 2 is a view of scientific knowledge necessary to understand the physics behind the experiments carried out and gives the scientific context of this project. Three important parts constitute this chapter: Neutron Scattering, Polymer and Compremental information (QCM-D and Rheology). First, we will explore the basic Physics of polymers and some hypothesis about solvent/nonsolvent/polymer behaviors. Then, Neutron scattering techniques including neutron reflectometry and SANS will be addressed. The basics of QCM will be quickly addressed and we will finish on the basics of rheology.

The materials, the preparation of samples, the instruments and the methods of analysis will be explained in the **Chapter 3**.

The microscopic and nanoscopic behavior of the polymer model films in contact with a small amount of solvent in water investigated by few techniques (mainly by NR) is exposed in an article published the 13th January 2020 in Soft Matter [13]. This paper is shown unchanged in **Chapter 4**.

As in the previous chapter, **Chapter 5** explores the behavior of the polymer model films by NR but this time in contact with a solvent in a gel of water.

The last chapter, **Chapter 6** presented in the form of a paper, investigates the temporal evolution of the polymer model films immersed in a mixture compounds of a small amount of solvent in water in order to understand the origin of instabilities during and after the swelling film.

CHAPTER 1
STATE OF ART

The aim of this chapter is to give the context and the motivation of this PhD project. I begin with a brief, simple view of the historical context of varnish [14], and the organisation and the materials present in an easel painting. This part may appear simplistic to the eyes of a professional or to restorers but will be sufficient and necessary for the comprehension of a wider audience. The role of the varnish and its effects on the paint layer is developed. And we will also address a quick look at the state of the art on methods for removing the varnish layer.

1.1 Restoring a varnish layer, an issue !

1.1.1 A protective and aesthetic layer

A varnish layer is defined as a fluid substance which gives, after hardening, a transparent and amorphous smooth film, and this for a protective and optical purpose [15]. Based on current knowledge, the word "varnish" appeared in the seventeenth century but its use on painted works was widespread well before. Throughout the centuries, preparation techniques have evolved and it were composed of drying oils, gums, resins and/or egg whites. The first varnishes used were natural varnishes. There are two categories: either called 'greasy varnishes' prepared from natural resin and drying oil or so-called 'lean varnishes' prepared from natural resin and alcohol or gasoline. Then, after the discovery and the formulation of synthetic resins, the trend moved to synthetic varnishes (acrylic, ketonic, polyurethane, etc.) prepared from resin dissolved in organic solvents. These varnishes have the advantage of being stronger and have the reputation of being more easily removable because these polymers do not cross-link.

Natural varnishes

The use of the first protective coatings goes back to ancient Egypt and maybe well before, with the Egyptians sarcophagus. The oldest, on Egyptians sarcophagus dating from 1200-1300 BC, was discovered by A.P. Laurie. The first mentions of the protective layers are those of Vitruve [16] in the 1st century BC and Pline l'Ancien [17] in the 1st century AD with the 'atramentum' d'Appelle (the 4th century BC) but the exact composition of these layers remains unknown. Subsequently, There are many varnish recipes mentioned in various sources [18], [19], [20].

Before the 18th century and more particularly until the appearance of alcohol and gasoline varnishes ('lean varnishes'), according to Theophilus [21], varnishes were formulated with boiling natural resins (sandaraque, rosin, copal, shellac, amber, mastic) from vegetable and animal substances origins ('greasy varnishes'). Over time, the varnish composition has been redesigned (towards the end of the eighteenth century by J. F. Watin [22]. But real changes did not come until the 19th century. At this period, there was reflection about the essential and useless elements which compose varnishes and about the notion of an'ideal varnish': transparency, colorless, elastic, protective, reversible easily and with non-polar solvents or with low polarity. In parallel, the 19th century marks the arrival in Europe (from Asia and subsequently implanted in Southern Europe) of a complex natural resin from the trees of the Dipterocarpaceae family: the Damar resin. This resin was already observed on the old works of art at this age but little used by European restorers. It is the most common natural resin used nowadays by restorers because of its exceptional optical qualities. Many restaurateurs still agree that even the best synthetic varnishes still cannot match it on this point. But unfortunately it tends to yellow quickly,

to bleach [23], change in solubility, loose its flexibility and crack with time, especially if it is exposed to light.

Synthetic varnishes

The 20th century marks the emergence and the development of numerous polymers in industry and opened new possibilities in art restoration domains particularly to use synthetic resin for varnish layers. The interest was to develop more stable, transparent and reversible coatings. It was only after the 14-18 war that synthetic varnishes began to be used gradually in restoration workshops and in the range of products for artists. The first synthetic varnishes tested are those with high molecular weight resins. In 1928, the poly(vinyl acetate) (PVAc) is considered to be the most stable material for old paintings [24] but compared to conventional varnishes with alcohol, optical properties were unsatisfactory. The surface became matt and the colors darker. Followed by acrylic resins: Lucite 44 and 45 which become insoluble in contact with the light, then the Paraloid®B72 [25] resin soluble in ketones, esters, aromatic and chlorinated hydrocarbons which presented the best optical qualities of the four resins, used still as an adhesive [26]. Around 1960, restorers became interested in low molecular weight resins in order to find a resin with not only the properties of resistance, transparency and reversibility but also with optical properties close to those of natural resins. Ketone resins like the Laropal®K80 [7] [27] [24] [28] was studied. It was observed, that they have good optical qualities but bad aging properties in contact of light rays. Then, they tried hydrocarbons resins like Regalrez 1094 [28] [29] which have a better stability but aldehyde resins are the most successful, such as Laropal®A81. These are the most stable and optically closest to natural resins.

Nowadays, many restorers continue using natural resins because of their optical properties considered superior to those of synthetic varnishes. But Laropal®A81 seems a promising resin more and more used by painting conservators.

1.1.2 Disposition and optical aspect of the varnish on a painting

A painting is a complex mixture of organic materials (natural varnish, binder, cellulosic support) and in-organics materials (synthetic varnish, pigments, fillers, drying agent) which interact with each other. It is therefore a series of layers with a specific role independent of each other. In other words, each layer has its own composition, characteristics and function in the work of art.

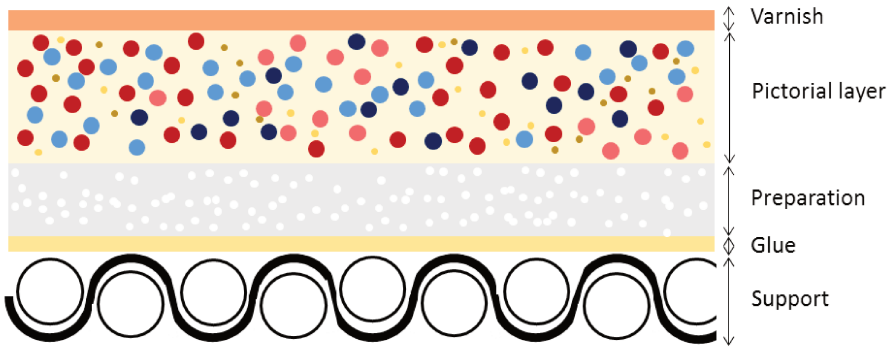

Figure 1.1 – Schematic of the stratigraphy of a painting (not to scale)

Supports are mainly a canvas stretched on a frame or a wood panel. They are the foundations of a painting. The sizing, a mixture of animal skin in the water, prepares the support to make it waterproof and cohesive for the preparation layer that follows the classical stratigraphy. The preparation, a mixture of animal glue and a load (so-called "lean" preparation) or oil and

white lead (so-called "fat" preparation), prepares the support for the pictorial layer. In particular, it limits the migration of the oil or binder towards it, thus avoiding oxidation or weakening of the support. It also makes it possible to regularize and erase the irregularities of the support: asperities of the wood and frame of the canvas. It can be colored by a pigment for brown, red or yellow preparations, carbon black for gray preparations. Colored preparations appeared gradually during the 16th century for oil paintings and were described by Giorgio Vasari [30]. The principle is to give more depth to the pictorial layer. Clear preparations were used particularly during the period of neoclassicism and the impressionists. The pictorial layers also called the colored layers, are constituted of pigments finely ground or vegetable (indigo and saffron) and animal (purple or sepia) dyes in a binder (often oil). Most of natural pigments from plant or animal origin are sensitive (discoloration or mutation) to ultraviolet light, temperature changes, pH changes and humidity. Finally, most paintings present a varnish layer because of its protective and aesthetic role (brightness, brilliance and color saturation) [31]. It is the first layer beyond the pictorial layers therefore the one directly in contact with the external environment. It constitutes a barrier against all the harmful external elements (dirt, volatile elements, light rays, etc.) which favor the deterioration of other fragile materials composing the paint and more particularly the pictorial layers and it allows saturation of the colors of the pigments in the binder in order to sublimate them.

In essence, a painting is not a static object but one in slow and constant evolution. And this aging evolution is accelerated by the type of storage or the place of exhibition. Indeed, the materials that compose the work of art are very sensitive to numerous parameters such as pressure, temperature and humidity. Surprisingly, it is also these same parameters which allow art restorers to restore them [3].

1.1.3 Degradation and instability of varnish, removal of the varnishes and effects on other layers

Why the varnish can be removed on paintings?

It is commonly decided to remove the varnish when it impedes the understanding and the appreciation of the work of art. Varnish is not perceived as an original material, unlike the pigment layer, the preparation, the glue and the support because it has not been applied by the artist but by a restorer for the purpose of protecting the colored layer of abrasive exterior elements. So unlike other original materials, it is agreed that it can be removed from the surface.

What is the degradation of the varnish?

Several degradation of varnishes are due to environmental effects or some other more specific reasons and lead a restorer to act on the varnish which obscures the images beneath. For example, the oxidation reactions of the varnish lead to yellowing, cracking and increase of acidity (Fig.1.2). A thin varnish layer can cause the loss of colored matter and cracking of the material and become a risk factor for the paint layer. Also, anything that affects the deep layers (support, gluing and preparation) has a direct impact on the upper layers (colored layer and varnish)making them thinner and more sensitive.

Figure 1.2 – Detail of *L'Enfant, la Vierge et Sainte Anne*, oil on canvas, painting before (left) and after (right) the removal of the varnish layer. At the left of the picture the varnish is yellow and inhomogeneous

How restorers procede to remove a varnish?

Traditionally, restorers remove the varnish by applying, via a circular motion directly on the surface, a cotton swab soaked in organic solvents. The task is sometimes difficult (oxidized layers) and the varnish cannot be removed with low polar or apolar solvent [18]. Restorers are then forced to use very polar solvents, strong and penetrating solvents [7] [24] [27] [32]. To reduce the amount of strong solvents, restorers mix two solvents with different polarities. For example, they combine a polar solvent and an apolar solvent following the solvents parameters [33], the Teas Diagram [34] [35] [36] [37] such as a predicting tool or restorers lists of solvents. These lists from Cremonesi [38] or Masschelein Kleiner [39] propose numerous solvent mixtures for specific cleaning treatments to remove the unwanted elements on pictorial layers. These lists are known and applied by most of restorers in the world.

...and what about the effect on the paint layer?

In 1971, Stolow wrote about organic varnishes: 'Unfortunately, no varnish has yet been found or devised which adequately fulfills the aesthetic and physical requirements and is also absolutely durable' [10]. In the twentieth century, the advent of the use of synthetic resins as a restoration varnish has changed the game a little with new competitive resins in terms of stability and resistance to external agents. They are used as alternative varnishes to traditional organic resins[1]. Even if the resins are chosen for their good resistances, stability and transparency, they do not escape the effect of time, yellowing or fouling [8]. Without forgetting that in this very wide choice of existing resins, the restorer can easily get lost and paintings can pay the price with synthetic varnishes difficult or impossible to remove with low-polar solvents. The use of toxic and penetrating solvents repeatedly and over time lead to a risky situation for the user and the paint layer.

Nowadays, the negative effects of the removal of vanish (solubilization, binder depletion, bleaching, embrittlement, swelling and cleavage of the colored layer, etc.) are known by most scientists and restorers. Therefore, they are looking for alternative methods to remove the varnish and deposit a fresh new layer without damaging the paint and deep layers. This approach

[1] for the most part Damar or Mastic

of 'how to do better to remove the vanish layer ?' is fairly recent because until the 20th century restorers used solvent cleaning methods without asking any questions about the possible impact of these very penetrating and abrasive treatments. Nevertheless it is a regular treatment of works of art: about half a century in the life of an array of paintings in a museum. The first writings that mention the possible dangers of solvent action on paint film date back to the mid-nineteenth century. In 1851, H. Deon [40] mentioned the negative effects on the use of more and more polar solvents for the cleaning and the removal of the varnish on paintings and in particular the difficulty of dissociating the varnish from the paint, which in some cases form a single heterogeneous layer. In 1930, a committee of the Conference on the Examination and Conservation of Works or Art met in Rome with the object of defining a 'good varnish'.

Afterwards, the solubility, the swelling and the leaching effects of organic solvents on varnish and paint films were studied by Graham for Linoxyn films [41] and Stolow for drying-oil films [42] [43] [44]. Since 1985, the book of Feller, Stolow and Jones serves as a reference on the behavior of resins and solvents used in varnishes of paintings. In addition, Sutherland showed that varnishes may affect the oil paint film. There is extraction of fatty acids from the paint film into the varnish layer depending on the solvent used and the component of the resin [45] [46]. Synthetic varnishes, contrary to what one might think, have not changed the situation. Certainly, they are more stable in time, and for some, more resistant and less rigid therefore less restrictive for the layers below ; but most of them have shown other failures. Namely, that there are problems of adhesion, insolubility and resistance to solvents, increased sensitivity to dust especially on varnishes with low glass transition temperature (T_g) or they could have a too high viscosity. In addition, many restorers find that gasoline varnishes (Dammar and Mastic) can better saturate the colors, give more depth and provide the ideal look of shading or shine and control the light. Others opted for a mixture of one or more layers of natural varnish on which are deposited layers of synthetic varnish. The idea was to combine the advantages of each. So there is not just a simple model of paintings but an infinite combination of material and layer thickness that makes each object unique. The ideal varnish has not been found and old master paintings still have altered.

Restorers are therefore very interested in alternative solutions (gel, microemulsion or laser) to remove varnish and to apply a new coating in the best conditions. And restorers and curators are interested in the investigation of how to remove old varnish coatings in the best condition and the investigation of the 'ideal varnish' to apply a new fresh varnish.

1.1.4 How to counter these effects?

In the 2000s, Wolbers opened the way to use some gels for the cleaning of paintings [47]. The scientific literature of the gels is rich due to the many possible applications in many domains. Therefore, research on gels began long before Wolbers highlighted them for application in the field of art restoration, as well as the work of many scientists who are interested in it. To name a few, Graham was mentioned already [41], [48], and Meunier is the discoverer of the famous gel of 1,3:2,4-di-O-benzylidene-D-sorbitol still used [49]. Subsequently, thanks to Wolbers's book [47], many researches have been undertaken to investigate the properties of gels and develop the way for applying them on art (paintings, fresco, ceramics and papers) and more particularly of microgels and nanogels [50], [51] [52] [53] [54]. Several advantages are advanced by the scientists for the use of these systems in art. First, these gels are composed mainly of water maintained in a network while not limiting the transfer of the solvent contained therein. Secondly, the gel would also provide the material to be applied to transfer very small amounts of solvent. Resolving at the same time the problem of the use of toxic solvents for the restorers and theoretically the risk of the solubilization of the paint layers which would be low because of the low solvent concentration. For the reasons previously stated, gels seem a promising tool

for Cultural Heritage so a lot of restorers, conservators and scientists have investigated and applied them [55] [56] [57] [58] [59] [60]. As shown by the many references already mentioned, Baglioni et al. in Florence, is one of the groups most involved in investigating art restoration issues on works of art, in particular easel paintings, wall paintings and frescoes. They propose numerous innovating methods (soft and hard nanomaterials) for the cleaning and the removing of the non-original materials from the paint layer. The reviews of 2006 [61] and of 2014 [54] and the mini-review of 2017 [62] summarize well the state of the art of cleaning products (micelles, microemulsions and gels) proposed and applied for the conservation-restoration of Cultural Heritage.

These products seems to be effective solutions to transfer solvents in the polymeric vanish layer in order to swell, dissolve and remove it. However, one could nevertheless observe that the work undertaken at the moment on these gels demonstrate their effectiveness visually but that there seems to be a lack of understanding of the physical phenomenon involved in the transfer of a solvent by a gel in the varnish as well as the effects on it (swelling, dissolution or other effects). This will be one of the objectives of this project, but before understanding what is happening in a gel/solvent/polymer system, it will be necessary to have a full understanding of what is happening in a water/solvent/polymer system without molecules of gel.

CHAPTER 2
PHYSICS OF NEUTRON SCATTERING AND BACKGROUND

In this chapter, we provide an overview of neutron scattering and the Atomic Force Microscope used to understand the swelling and dissolution processes of the polymer films which composed the second part of this chapter. Then, complementary theory of rheology is quickly addressed.

2.1 Neutron scattering

In 1932, James Chadwick discovered neutrons. In the decades after, thanks to the creation of dedicated high flux sources (ILL, ISIS, LENS, HFIR, ANSTO, LANSCE, FRMII, etc.), it was possible to produce free neutron particles in large quantities allowing the exploration of different areas of research in condensed-matter physics and other areas. Neutron scattering is a powerful tool especially for the study of material science, chemistry, biosciences, and nuclear and elementary particle physics and in engineering sciences as well as magnetism.

Especially for condensed matter investigations neutrons are often applied as a non-invasive probe; they do not change the investigated sample since they do not deposit energy into it. Using them allows e.g. to observe the microscopical structure and dynamics of polymer materials with a high resolution (few Å).

Using neutrons presents undeniable advantages for the investigation of condensed-matter[63]. They interact through short-range nuclear interactions, their wavelengths are comparable to atomic sizes and inter-distance spacing and hydrogen atoms can be replaced by deuterium atoms, which is an advantage to allow better differentiation of the different elements by contrast.

This part is based on the following references [64], [65], [66], [63], [67], [68], [69], [70], [71] and [72].

2.1.1 Neutrons

These remarkable elementary particles are contained in the atomic nucleus. With protons, they constitute the nuclei of atoms but its mass is a little larger (m_n= 1.008664924 u). Neutrons electric charge is supposedly zero. Unlike X-rays which see most of the time only the surface and are highly energetic, neutrons can penetrate deeply into matter and interact with it without being stopped by coulombian barriers (nondestructive particles), hence they are suitable for the study of biological and soft matter samples. Another important particularity of the neutron for neutron scattering is its magnetic moment (μ_n= 1.91304275 μ_N) which is given by the neutron's spin angular momentum -$\gamma\mu_N\widehat{\sigma}$ with γ the gyromagnetic ratio (= 1.913), μ_N the nuclear magneton and $\widehat{\sigma}$ the quantum mechanical Pauli spin operator. Neutrons wear a 1/2 spin which allows polarisation of the neutron beams and to analyse this polarization before and after magnetic field interactions. Furthermore, according to quantum mechanics neutrons do not have only particle properties but can be considered as a wave with a wavelength (traditionally in Å) given by de Broglie's formula:

$$\lambda = \frac{2\pi\hbar}{mv}, \tag{2.1}$$

with the Planck constant h = $2\pi\hbar$ = 1.034 x 10^{-34} Js, m the neutron mass and v the neutron speed. The wavelength is similar to that of X-rays. And its kinetic energy (in eV or meV) is given by:

$$E = \frac{\hbar^2 k^2}{2m_n}. \tag{2.2}$$

A free neutron does not live forever and its lifetime is 886 ± 3 s. General properties of the neutron are summarized in table 2.1.

Table 2.1 – Basic properties of the neutron

mass	1.674927471 x 10^{-27}kg
spin	$\frac{1}{2}$
charge	0
magnetic moment	-1.91304273 μ_N

Nuclear reactions allow us to obtain neutrons by two possibles ways : by accelerated charged particles like electrons and protons, and by fission or fusion. At ILL and MLZ, neutrons are produced by fission of the fuel element Uranium 235 thermalized by deuterium oxide (moderator), hence we will only focus on this reaction 2.3 for the following part. Fission was discovered in 1938 by three German scientists Otto Hahn, Lise Meitner and Fritz Strassmann. During this reaction, the ^{235}U nucleus (heavy nuclei) absorbs a thermal neutron. Then, it becomes excited until it splits into several fragments (fig. 2.1). This releases neutrons but also the energy. The fission reaction is:

$$n + {}^{235}_{92}U \rightarrow \text{fission product 1} + \text{fission product 2} + 3n. \tag{2.3}$$

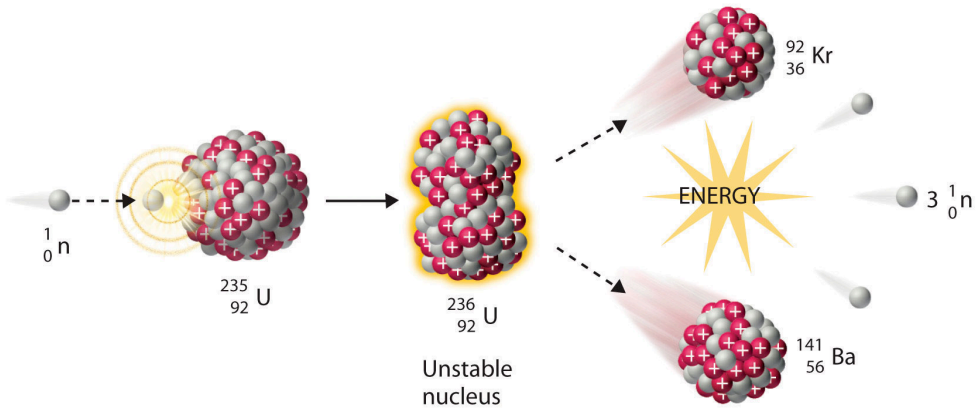

Figure 2.1 – Schematic of Nuclear Fission from reference [73]

After being thermalized neutrons are further cooled down by liquid deuterium (cold moderator at 20 K) to obtain the energy required, such that their velocity distribution equals a Maxwell-Boltzmann function, which allows to perform NR and SANS experiments used in this study. And the average energy of the Maxwell-Boltzmann distribution is given by:

$$E = \frac{3}{2} k_B T, \tag{2.4}$$

where, k_B is the Boltzmann constant and T is the temperature of the moderator (deuterium). At 20 K, the energy is 2.6 meV which corresponds to an average velocity about 700 m.s^{-1} (eq. 2.5) and an average wavelength λ equal to 5.6 Å(eq. 2.1). [70]

$$v = \sqrt{\frac{2E}{m_n}}. \tag{2.5}$$

2.1.2 Neutron Scattering Theory

Neutron-scattering experiments consist in measuring the intensity of neutrons scattered by the sample as a function of the momentum transfer Q and the energy transfer *e* [69]. Unlike X-rays which interact through electromagnetic interactions with the electron cloud of atoms or electron beams which interact through electrostatic interactions; neutrons interact directly through the strong interaction with the nuclei. There exist two interactions between neutrons and matter, with the nuclei of atoms and with their magnetic moment.

2.1.3 Neutron scattering techniques

There are four main kinds of neutron scattering techniques: a) Transmission Measurement, b) Elastic Neutron Scattering, c) Quasi-Elastic and Inelastic Neutron Scattering and d) Neutron Spin-Echo (Fig. 2.2). One difference which allows us to distinguish them is the energy exchange as is shown in the example of the neutron scattering spectrum in Fig. 2.3. We will only develop b) in the following text.

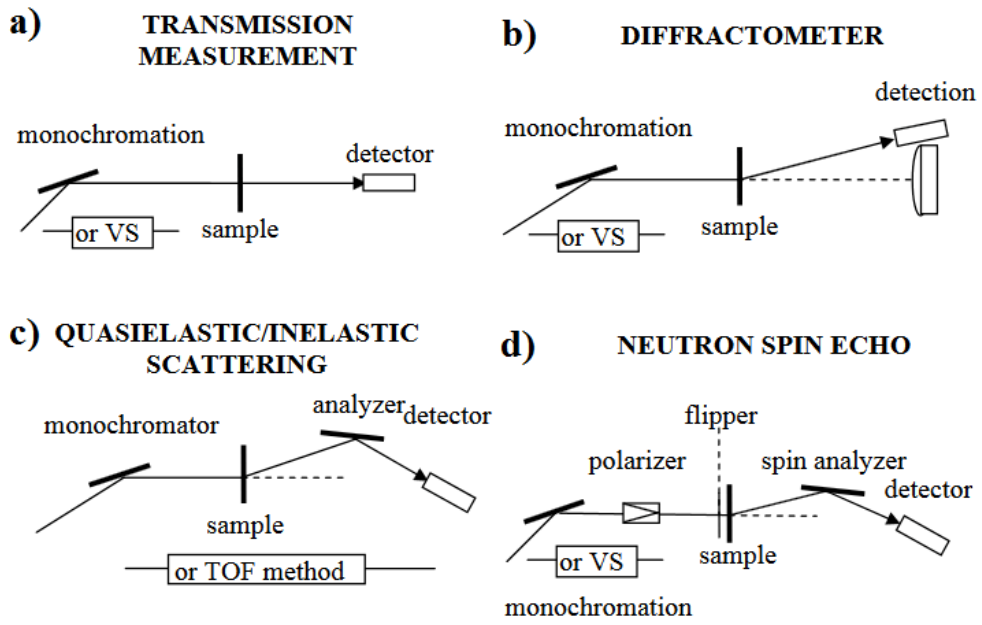

Figure 2.2 – Schematic representation of the four types of neutron scattering methods from reference [63]

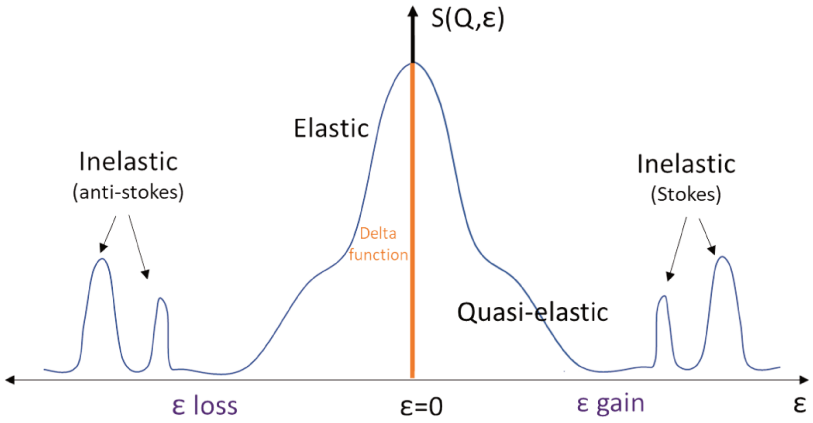

Figure 2.3 – Schematic example of a neutron scattering spectrum as a function of exchanged energy at a given Q

Elastic Scattering is the scattering with no energy exchange ε=0. This means the energy of the incident beam is equal to the energy of the scattered neutrons. It forms the elastic peak in Fig. 2.3. Contrariwise, Inelastic, Quasi-elastic and spin echo scattering involves an energy exchange $\varepsilon \neq 0$.

2.1.4 Scattering on a single fixed nucleus, elastic scattering case

Understanding the theory of neutron scattering requires the use of quantum-mechanical tools such as the solution of the Schrodinger equation:

$$(H_i + V)|\Psi\rangle = E|\Psi\rangle. \tag{2.6}$$

where, H_i is the Hamiltonian consisting of incident neutron kinetic energy operator of the neutron, V is the neutron-nucleus interaction potential. E is the eigenvalue energie. $|\Psi\rangle$ is the wave function. [70] This equation (eq. 2.6) is solved involving perturbation theory, the so-called Born Approximation. It consists of approximating the scattering wave function as a superposition of the neutron beam without a sample, the incident plane wave, plus the scattered wave function from the nucleus without taking into account the cross-terms, neither multiple scattering (in first order). All of neutron scattering except neutron reflectivity can be described by a first order Born approximation.

In the simplest case, the scattering can be defined by a single constant, which describes the strength of scattering, namely the scattering length and the total scattering cross-section (units of cm) for a single nucleus σ_{tot} becomes the equation 2.7. The apparent size of the scattered element is given by the neutron scattering length b.

$$\sigma_{tot} = b^2. \tag{2.7}$$

A cross-section σ (ref [67]) is the probability of the material (sample) to scatter neutrons per second into a unit area (barns). It depends on the material size which is described by the volume specific cross section $\sigma = \Sigma$. The cross-section can be divided into three contributions: [68].

$$\sigma_{total} = \int \frac{d\sigma}{d\Omega} d\Omega = 4\pi b^2 \equiv \sigma_{coh} + \sigma_{inc} + \sigma_{abs}, \tag{2.8}$$

where, σ_{coh}, σ_{inc} and σ_{abs} are the coherent, incoherent and absorption cross sections respectively [70].

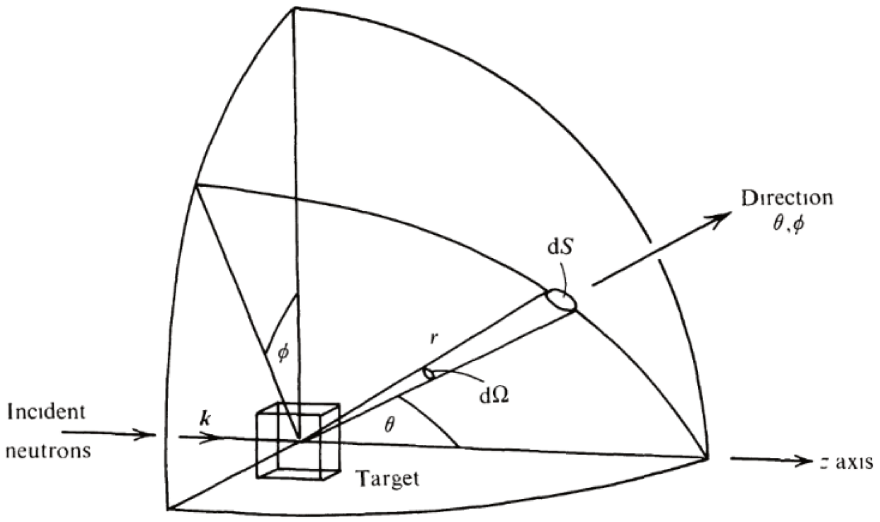

Figure 2.4 – Scattering geometry experiment where r is the point of the scattered neutrons, θ, Φ are the angles, dΩ is the small solid angle and dS is the area of the beam from the reference [68]

Neutron scattering is carried out by a strong interaction between the free neutron and the atomic nucleus of the material. The scattering of free neutrons behaves like a spherical wave.

Taking into account the geometry of the scattering experiment 2.4 (origin point at nucleus position and z-axis along the propagation direction k), the incident neutron wave is:

$$\Psi_{inc} = e^{(ikz)}, \tag{2.9}$$

where, Ψ_{inc} is the incident neutrons, k is the momentum of the incident neutrons and z is the axis.

Now, if one consider a spherically symmetric wave at the point r, the wave function becomes:

$$\Psi_{sc} = -\frac{b}{r}e^{(ikr)}, \tag{2.10}$$

where, Ψ_{sc} is the spherical incident neutron wave and b is the aforementioned scattering length.

When the energy transfer of the neutrons e is too small to be resolved the scattering is considered elastic and the final scattered intensity is integrated over all energies. The magnitude of the wave vector of the incident neutrons k is equal of the wave vector of the scattered neutrons k'. The momentum transfer q is equal to:

$$q = \frac{2\pi}{\lambda} sin(2\theta) \tag{2.11}$$

where, λ is the neutron wavelength and the scattering angle is 2θ.

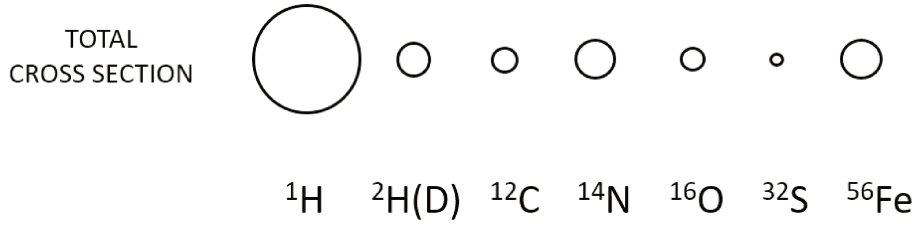

Figure 2.5 – Neutron scattering cross sections for few elements. Circles are drawn to scale from reference [74]

The scattering amplitude is the probability amplitude of the outgoing spherical wave relative to the incoming plane wave [75], defined as:

$$f(\theta) = \left(\frac{m}{2\pi\hbar^2}\right) \int d\vec{r'} e^{-i\vec{q}\vec{r'}} V(\vec{r'}), \tag{2.12}$$

where, f(θ) is the Fourier transform of the interaction potential V($\vec{r'}$)

Its absolute square (eq. 2.13) allows to calculate the scattered intensity.

$$\frac{d\sigma}{d\Omega} = |f(\vec{q})|^2 = \left(\frac{m}{2\pi\hbar^2}\right)^2 \int V(\vec{r'}) e^{i\vec{q}\vec{r'}} d\vec{r'} * \int V(\vec{r}) e^{-i\vec{q}\vec{r}} d\vec{r}, \tag{2.13}$$

where, V($\vec{r}$) is the scattering potential. Replacing V($\vec{r}$) by V($r' \vec{-} r$), the absolute square scattering amplitude becomes:

$$\frac{d\sigma}{d\Omega} = \left(\frac{m}{2\pi\hbar^2}\right)^2 \int V(\vec{r'} - \vec{r}) V(\vec{r'}) * e^{i\vec{q}(\vec{r'} - \vec{r})} d(\vec{r'} - \vec{r}). \tag{2.14}$$

The part $\int V(\vec{r'} - \vec{r})\ V(\vec{r'})\ d\vec{r'}$ is called the pair correlation function.

The Fourier transformation of the scattering potential $V(\vec{r})$ is the scattering amplitude.

So, the intensity measured during a scattering experiment is the Fourier transformation of the pair correlation function of the scattering potential in the reciprocal space [70].

Another important quantity is the scattering length density (SLD) [76], not to be confused with the scattering length, because it allows to calculate the neutron contrast factors. It is the ratio of scattering length per molecule and molecular volume. In the case of an A_mB_n molecule with m atoms A and n atoms B, the SLD is given by:

$$SLD_{AmBn} = \left(\frac{b_{nuclei}}{v}\right)_{AmBn} = \frac{(mb_A + nb_B)}{v} = \frac{N_{av}\rho}{M} \sum_{nuclei} b_{nuclei}, \tag{2.15}$$

where, (mb_A+nb_B) is the scattering length b_{nuclei} per molecule and v is the volume given by v=$\frac{M}{N_{av}\rho}$ with N_{av} is the Avogradro's number (N_{av} = 6.10^{23} mol^{-1}), ρ is the density and M is the molar mass.

2.1.5 Neutron Reflectometry

There are many powerful techniques for the investigation of surface layers such as ellipsometry or optical microscopy ; but only few of them allow us to penetrate the solid/liquid interface, to give informations about interface structure and in particular for ultrathin and thin films. Neutron reflectometry (NR) is one of those and there is no need to prove that it is an indispensable tool and non-destructive probe in the study of polymer films to resolve the internal structure. This term includes two techniques of reflection, specular and off-specular reflectometry (OSS) and grazing incidence small angle scattering (GISANS). Their difference lies in the angles : the outgoing angle θ_f in the case of OSS and the azimuthal angle θ_y in the case of GISANS).

The refractive index n of materials for neutron reflectometry is very often smaller than 1 : n < 1, leading to total external reflection. Neutron reflectivity was observed for the first time in 1944 by E. Fermi and W. H. Zinn [77] and the previous affirmation was well confirmed during their experiment on several materials (graphite, aluminium, glass, iron, nickel, zinc, copper and beryllium).

Basically, when a collimated, monochromatic neutron beam, represented by a wave function e^{ikr} [68] [67] is scattered by a single fixed nucleus into a liquid or solid sample by the strong nuclear forces, the scattering is assumed to be symmetric, because the range of the nuclear forces

is much smaller than the wavelength of thermal or cold neutrons. A part of neutrons is reflected following a particular geometry called grazing incidence geometry. The reflected beam is collected into the detector so that the signal is subsequently analyzed and can give information on the system studied. The reflectivity is the ratio between the number of reflected neutrons and initial neutrons. Reflectivity of flat interfaces (ideal case) is calculated using Fresnel [78] [79]. In reality, flat interfaces do not exist, but a finite roughness or inter diffusion is present. The factor of Nevot-Croce [80] is added to describe real interfaces. Furthermore, neutron reflectivity can be used to study chemically identical species thanks to the sensitivity of neutrons to the nuclei of the material. For example, hydrogen atoms can be exchanged by deuterium. Deuterium atoms contrast better without having any effect on the thermodynamic properties of chemical species. The Flory-Huggins interaction parameter χ (section 2.2.4) is almost the same between protonated and deuterated species [81].

Specular Reflectivity

Nowadays, specular NR has become a standard technique for the investigation of thin films and interfaces [82] similar to optical techniques like ellipsometry. Its spatial resolution is, however, much higher due to the significantly smaller neutron beam wavelength on the order of Å as compared to visible light, giving access not only to total layer thicknesses or material gradients but also to nanoscopic roughness between layers. Moreover, the reflection contrast of layers is not determined by the refractive index as for visible light. In order to characterize the nanoscale structure of interfaces of water/polymer/Si Block systems, a collimated neutron beam (incident beam) is directed at the interface of interest through the Si block, which is practically transparent for neutrons, with an incident angle θ and the reflectivity profile of the reflected beam at an exit angle $\theta_f = \theta$ equal to the incident angle is measured as a function of the momentum transfer perpendicular to the polymer film surface (Fig. 2.6). As can be seen in the figure the difference in momentum transfer normal to the surface before (k_i) and after (k_f) neutron reflection can be defined:

$$q_z = \frac{2\pi}{\lambda} * (\sin\theta_i + \sin\theta_f), \tag{2.16}$$

where λ is the wavelength.

The resolution of the specular experiment is obtained by the combination of the angles resolution and the wavelength resolution. Nowadays, the mechanical precision is so high and allows us not to take it into account here. The formula becomes:

$$\frac{\Delta q_z}{q_z} = \sqrt{\left(\frac{\Delta\theta_i + \Delta\theta_f}{2\theta}\right)^2 + \left(\frac{\Delta\lambda}{\lambda}\right)^2}. \tag{2.17}$$

a. Application on an interface between two semi-infinite media

The scattering length density SLD_{AmNn} of each material is calculated using the reference [76] using the equation 2.15.

The critical momentum transfer q_c (eq. 2.18) and the critical angle of the total external reflection θ_c (eq. 2.19 are obtained from the SLD :

$$q_c = 4\sqrt{\pi SLD}. \tag{2.18}$$

$$\theta_c \approx \lambda\sqrt{\frac{SLD}{\pi}}. \tag{2.19}$$

For neutrons, the refractive index n can be obtained using the equation 2.20. As previously mentioned, n is inferior to 1 for most material in reflectivity experiment.

$$n = \sqrt{1 - \frac{\lambda^2}{\pi} SLD}, \tag{2.20}$$

where, λ = 2π/k. From equations 2.18 and 2.19, it is deductible that n depends of neutron wavelength λ and the SLD. In addition, the Snell's law between the interface of this two media is applicable.

Now, let us consider the Fresnel reflection and the transmission coefficients [71]. The momentum transfer is given by Q_z = $p_{z,f}$ - $p_{z,i}$ = $\frac{4\pi}{\lambda} sin\theta$ where $p_{z,i}$ and $p_{z,f}$ are the projection of the incoming $\overrightarrow{k_i}$ and the outgoing $\overrightarrow{k_f}$ wavevectors on the z-axis. In the context of a single interface between two media, the calculation of the projections $p_{z,0}$ and $p_{z,1}$ of the wavevector $\overrightarrow{k}$ on the z-axis above (0) and below (1) of the interface can be obtained as:

$$p_{z,1} = \sqrt{p_{z,0}^2 - p_{z,c}^2} = \sqrt{p_{z,0}^2 - 4\pi(SLD_1 - SLD_0)}, \tag{2.21}$$

where, $p_{z,c}$ is the critical wavevector of the total external reflection. SLD_0 and SLD_1 are the SLDs of the material above (0) and below (1) the interface, respectively. Moreover, $p_{z,0}$ = $|\overrightarrow{k}| \sin\theta_i$ with $|\overrightarrow{k}| = \frac{2\pi}{\lambda}$.

If $\psi_0(0) = \psi_1(0)$ and their derivatives are $\psi_0'(0) = \psi_1'(0)$, the Fresnel reflection coefficient $r_{0,1}^F$ (eq. 2.24) and the Fresnel transmission coefficient $t_{0,1}^F$ (eq. 2.23) are given by:

$$r_{0,1}^F = \frac{p_0 - p_1}{p_0 + p_1}, \tag{2.22}$$

$$t_{0,1}^F = \frac{2p_0}{p_0 + p_1}, \tag{2.23}$$

where, p_1 = $\sqrt{p_0^2 - p_c^2}$.

Then, the Fresnel reflectivity for a single sharp interface between two semi-infinite media is:

$$r_{j,j+1}^F = \frac{p_j - p_{j+1}}{p_j + p_{j+1}}. \tag{2.24}$$

where, p_j = $\sqrt{p_0^2 - 4\pi SLD_j}$ an p_0 = $\frac{2\pi}{\lambda}$ $\sin\theta_i$.

b. Experimental description Neutron reflectometry can be performed following two methods: the Time of flight (ToF) or the angle dispersive mode. A range of q_z values can be obtained either by varying the neutron wavelength λ as done on FIGARO (ToF method) [83] or by varying the incident angle θ_i at constant wavelength as done on N-Rex$^+$ (angle dispersive method).

In ToF mode, the incident angle is constant and the detector is 3-D with two spatial dimensions plus one temporal dimension due to the low velocity v of each neutron. This methods operates in two points, the white beam is chopped into pulses ($\sim$ 20 µs) with an angle fixed and the beam speed is investigated over a flight path between the chopper to the detector. [64] The wavelength of the neutron is defined from the time of flight from the chopper and the monochromator.

The velocity depends on the wavelengths of the neutrons. In both methods, the wavelengths of cold neutrons is between 2 Å and 27 Å for a velocity around 2000 m.s^{-1} and 150 m.s^{-1}. The wavelength resolution is only of few percent $10^{-2} < \frac{\Delta\lambda}{\lambda} < 10^{-1}$ [84]. In monochromatic mode the neutrons are monochromatized by a monochromator and the sample is rotated to be

placed precisely at the center of the beam. The reflected intensity from the sample is captured and measured on the detector. Then the data are transmitted from the detector to the software or they are therefore first reduced with COSMOS in the case of ILL experiment [83]. This reduction involves the removal of the background and the normalization by the incident beam intensity. The measured NR data is subsequently compared to simulated NR curves calculated by an optical matrix formalism from a slab model [85] and the goodness of fit is calculated. This least-squares fitting procedure is repeated until a convergence is found by using MOTOFIT [86]. The model used here to fit the NR curves consists of an infinitely thick single crystal silicon slab covered by a thin layer of silicon dioxide, which thickness varied between 1 nm and 2 nm among the samples, and several layers of LA on top capped by an infinite layer of liquid. Each of the layers was fitted by allowing its thickness and roughness to change until convergence was found. The SLDs of the LA and water were also fitted, but the SLDs of silicon dioxide and silicon were fixed at the corresponding literature values reported in table 6.1. The roughness of the silicon substrate and silicon dioxide were found to vary between 0.2 nm and 0.5 nm.

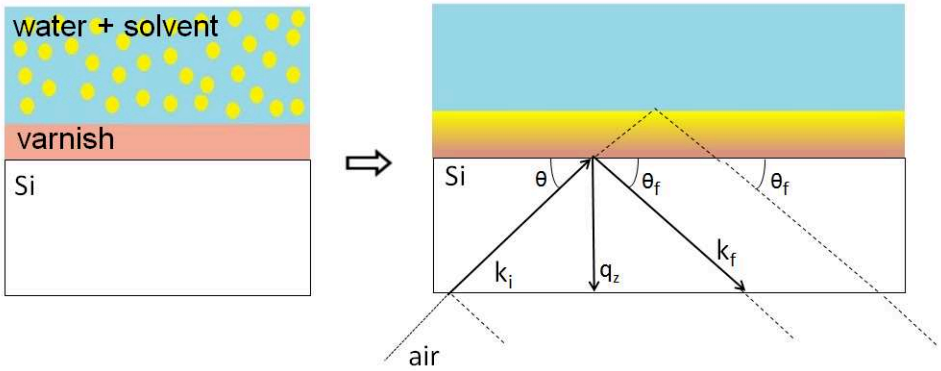

Figure 2.6 – Sketch of the specular reflection geometry at the water/polymer/Si substrate system. Note that the reflection angles are exaggerated for illustration, in a real experiments the neutron beam enters and leaves the silicon substrate from the sides rather than the bottom

Off-Specular reflectivity

This Off-specular reflectivity section is mainly based on the reference [71]. **a.** Application on a single rough surface

Off-specular scattering can be obtained following several methods, the one used here is the distorted wave Born approximation (DWBA) where the small perturbation from the ideal potential is used as a representation of the rough surface of the material. The ideal potential is calculated with Fresnel theory. The ideal potential $\overline{V}(z)$ (eq. 2.26) and the small perturbation (eq. 2.27) from the lateral deviations of $\delta\overline{V}(z)$ give the scattering potential $V(\overrightarrow{r})$ at $z = 0$ (eq. 2.25) [87] [71]. The SLD contrast of two layers is represented by the potential of the small perturbation, the second term of the equation 2.25.

$$V(\overrightarrow{r}) = \overline{V}(z) + \delta\overline{V}(x,z), \tag{2.25}$$

where, the ideal potential is:

$$\overline{V}(z) = \frac{2\pi\hbar^2}{m} \begin{cases} SLD & ; \quad z > 0 \\ 0 & ; \quad z < 0 \end{cases} \tag{2.26}$$

and, the small perturbation is given by:

$$\overline{V}(z) = \frac{2\pi\hbar^2}{m} \begin{cases} SLD & \text{for } z(x,y) < z < 0 \text{ if } \delta z(x,y) < 0 \ ; \\ -SLD & \text{for } z(x,y) > z > 0 \text{ if } \delta z(x,y) > 0 \ ; \\ 0 \text{ otherwise.} \end{cases} \tag{2.27}$$

b. Experimental description

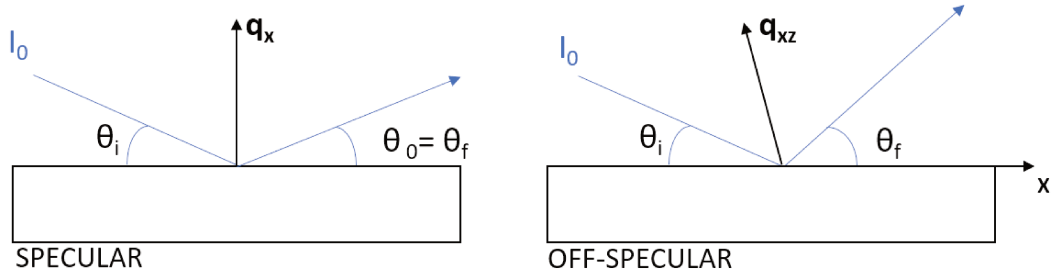

Figure 2.7 – Sketch of the specular reflection geometry vs Off-specular scattering

Off-specular scattering (OSS) [71] is the intensity measured in the incidence plane away from the mirror reflection (incident and reflected angles are not equal, $\theta_i \neq \theta_f$) and gives information about the in-plane structure of the film with the resolution of few µmeters. The OSS intensity is often maximized at the critical momentum transfer q_c (eq. 2.18) due to optical enhancement of the incoming and/or outgoing beam. This behavior is known as Yoneda scattering [88]. Two conditions must be needed for Off specular reflectivity to appear (fig. 2.6): $\alpha_i \neq \alpha_f$ and the momentum transfer $q \neq 0$.

The OSS spectrum can be recorded by two ways, the single wavelength measurement (1) or in Time-of-flight (2). The choice does not depend on the sample but on the measuring instrument.

1) The single wavelength measurement is the easiest way to perform OSS measurements, it allows to do different scans. These scans are performed either (1) with a fixed angle θ_i but q_z and q_x are not constant, or either (2) θ_i and θ_f evolved but only q_x must be changed, not q_z which are kept constant. The case 2 is preferred because the reciprocal spacing of the lateral features out of the specular peak is sharper [71].

2) The ToF measurement is performed with a constant angle $\theta_i = \theta_0$ and a change of the wave vector transfer p_i using several neutron velocities. These incoming neutrons are then reflected and recovered by a 3-D detector as function of their time of flight from the source to the detector.

In this study, as the neutron reflectivity spectra were recorded using 2-D detectors the off specular neutron reflectivity (OSS) is also accessible [89]. The total momentum transfer also comprises an in-plane component:

$$q_x = \frac{2\pi}{\lambda}(\cos\theta_f - \cos\theta_i). \tag{2.28}$$

This allows one to determine SLD variations parallel to the interface but due to the geometry the momentum transfers are typically two orders of magnitude smaller than in specular reflectometry and therefore the spatial resolution is much lower probing micrometer sized structures.

More information are given in the recent and complete review of Lauter et al. [89] where they presents the state of art and the theory of OSS.

2.1.6 Small angle neutron scattering

This part is based on the references [68] and [63]. Small angle neutron scattering (SANS) is a widely used tool to characterize samples (with thicknesses around 1 mm for hydrogenated samples and 2 mm for deuterated samples) in the nanoscale range (few Angstrom to micrometer sizes) such as polymers, micelles, biological systems. Samples are liquid or solid contained or confined in quartz cells. SANS is particularly interesting for the study of polymer bulk. To characterize inhomogeneities and to investigate the structure of the objects (distribution size, the shape and characteristic distance) in the polymer film immersed or not in solvent/non-solvent mixtures, SANS is performed. Raw data gives the neutron intensity measured as a function of the momentum transfer Q ($Å^{-1}$) defined by the equation 2.11.

The q range is typically from 0.001 $Å^{-1}$ to 0.45 $Å^{-1}$ and is adjusted by changing the sample-to-detector distance and neutron wavelength.

The neutrons of the monochromatic beam are selected by a velocity selector. The collimation, a set of circular apertures converging in the detector direction, is performed by long adjustable flight paths. Varying the flight paths distance allows us to adjust the resolution and the intensity. Data is collected by the detector which is called neutron area detector. The detector resolution varies typically between 0.5 cm to 1 cm. Then, encoded 2D data are transmitted from the detector to the computer software. This software, called NoMAD at ILL, is also used to control the instrument parameters (motors, distance, samples change, etc.) throughout the experiment. One SANS measurement using cold neutrons can be a long experiment from few minutes to few hours as a function of the sample, the source and the parameters selected (low wavelength, sample-to-detector distance, resolution and flux).

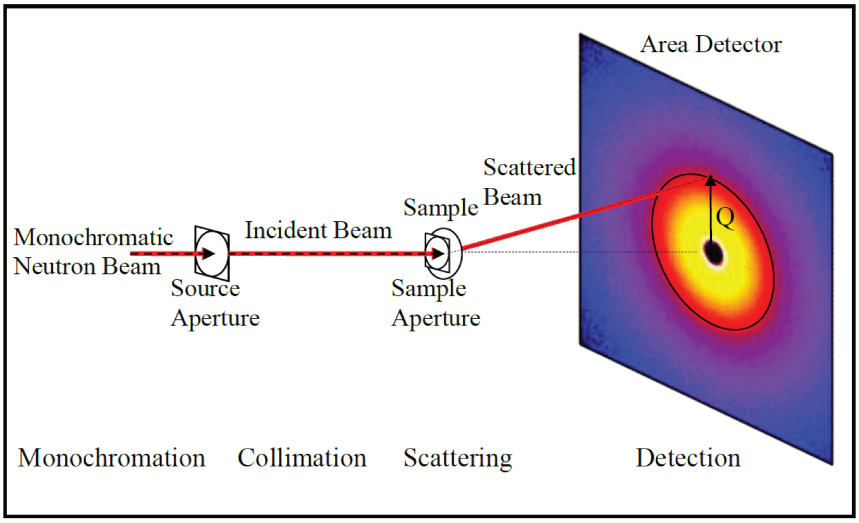

Figure 2.8 – Schematics representation of SANS technique from reference [63], not to scale (vertical sizes in cm and horizontal distances in m)

Such as neutron reflectivity, SANS is not a real space technique but operating in the reciprocal space (Fourier space). The absolute square of the scattering amplitude induces the loss of the phase in scattering. Before analysing the scattering data, one has to convert them in real space or to fit them following structural models. The different contrasts are to reduce the ambiguity in the real space model.

The possibility of changing the contrast and using deuterated labelling allows not only to monitor the density but also the composition of the sample in situ. In polymers, deuteration allows modeling the polymer chains conformation during the penetration of a solvent for example. This is why it is the selected method compared to X-rays (SAXS) which can only obtain

the electron density fluctuation.

Then, to obtain the characterization of the sample, the last step is to analyse data by dedicated software. They have to be reduced and plotted by linear curves and models such as Guinier, Porod, Zimm etc.

The power law is emerged from fractals of the particles (mass or surface) [90].

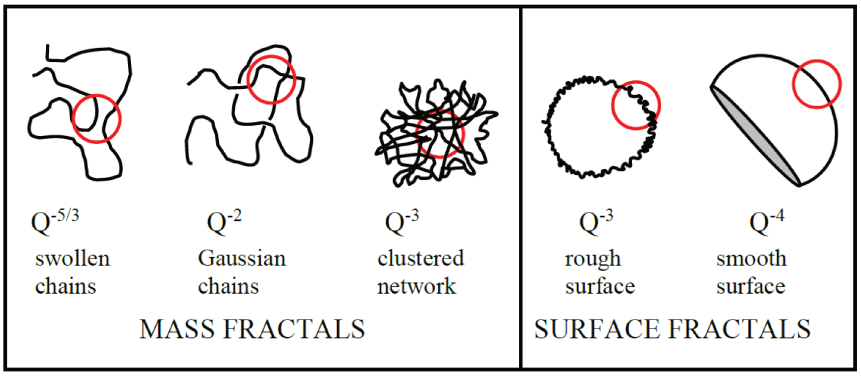

Figure 2.9 – Various fractal Porod exponents from reference [63]

The mass fractal D_m is equivalent to the Porod exponent. So the scattering intensity can be normalized for the mass fractal model and the asymptotic behavior of the curve depends of the Porod exponent (between D_m and D_m+1). To give an order of ideas, the Porod exponent is 5/3 for a scattering of a swollen polymer coil and 3 for a very rough surface.

Now, if one interests on surface fractal structure of a particle, the Power law scattering can be established (eq. 2.30).

The form factor including the fractal surface at *high-q* is:

$$\phi V_p P(q \to \infty) = \phi \pi \frac{S_p}{V_p} \Gamma(5 - D_s) sin\left[\frac{\pi(D_s - 1)}{2}\right] \frac{1}{q^{6-D_s}}, \tag{2.29}$$

where, D_s is the structure fractal.

For D_s = 2 and a *high-q*, the Porod law for smooth surface is:

$$P(q \to \infty) = \frac{3}{2{r_0}^3} \frac{S_p}{V_p} \frac{1}{q^4}, \tag{2.30}$$

where, S_p is the surface and V_p is the volume of the particle.

2.2 Polymers in solvent/non-solvent mixtures, swelling and dissolution

Basically, a polymer is a macromolecule consisting of repeated monomeric units joined together by covalent bonds. The simple image of a single-sequence polymer with only one repeated unit is that of a pearl necklace. The number of monomers (pearls) can vary from hundreds to thousands of units. They form long chains with a large number of segments which might be entangled with each other and form a matrix which could be compared to a spaghetti dish.

Polymers have a major place in the world, they are present in most everyday objects in the natural state (leather, animal tendons, wood, wool, etc.) or synthesized from petroleum chemistry (packaging, tires, paint, glue, PVC, polyesters, etc.). They are adaptable to the demand and very useful in numerous domains so industry is in need to improve new formulations to stay at the cutting edge of technology (synthetisizing of new polymers) and also concerning cost of manufacture and energy. And taking into account the current awareness of human pollution, we must seek for solutions to dissolve or recycle these different polymers. Polymers

are indispensable in industry and in applied fields like in art restoration where the constituent elements of paintings and products of restorations are mainly polymers. This section is based on the following references : [91] [92] [93] [94] [95] [96] and [97].

2.2.1 Mechanisms of dissolution and swelling

Swelling

The swelling process is the diffusion of the solvent into the polymer which undergoes a transition from glassy to rubbery state. It depends on several factors as the affinity of the polymer with the solvent or the molecular weight of the polymer to name a few. The solvent/polymer mixing process in a good solvent is explained by fundamental thermodynamics. During solution, there is a change in the Gibbs energy (eq. 2.39). This means, the solvent breaks its own interactions and its liquid cohesion in order to create the necessary space (entropy of mixing) for the incorporation of the polymer. In parallel, when the polymer/solvent interactions are stronger than the chain attraction forces, the polymer absorbs the liquid solvent in the empty spaces (enthalpy of mixing) which increases the total volume of the polymer matrix and changes the coils size. The swollen polymer film increases until a quasi-stationary state is reached. It is the 'swollen limit' of the polymer by the solvent (Ueberreiter, 1968 [98] [91]).

Dissolution of a rubbery polymer

The dissolution of the rubbery polymer by a 'good' solvent proceeds as follows:

- the solvent diffuses into the rubbery polymer (swelling of the polymer)
- the onset of dissolution in the diffusion boundary layer by chain disentanglement
- and, the free displacement of the disentangled chains into the solvent via Brownian motion in the solvent, leading to the complete dissolution of the rubbery polymer.

When the solvent concentration goes beyond a critical concentration in the polymer, it dissolves thanks to the disentanglement until the total disappearance of the glassy state. According the review of Koenig et al. [91], there are two kinds of dissolution: the 'normal dissolution' or the fast disappearance of the polymer due to the absence of gel layer creation. The dissolution depends on several parameters which can affect the dissolution process: 1) the temperature, 2) the molecular weight of the polymer, 3) the T_g of the polymer, 4) the polymer structure, composition and conformation; and 5) the type of solvent used

1) The dissolution in solvent has to happen above glass transition temperature. The gel layer thickness becomes weaker with decreasing temperature. Below a certain gel formation temperature, the polymer cracks leading to polymer fragmentation (Asmussen and Raptis, 1965 [91]).

2) The transition layer increases with the molecular weight of the polymer. A polymer at high molecular weight will be more difficult to dissolve than at low molecular weight by the same solvent.

3) when the T_g of the polymer is low, it is easier to dissolve the layer with a 'good solvent'.

4) As a function of the polymer chemistry, the polymer dissolves by swelling or by cracking (Ouano and Carothers, 1980 [99], [91].

5) The solubility rate depends on the chosen solvent. For example, a small amount of non-solvent mixed with a solvent, allows to slow down the dissolution rate of the polymer (Cooper *et al.* 1986 [100] [91]).

Brownian movement, displacement of solvent molecules in solvent/nonsolvent mixture

The Stokes-Einstein law describes the relationship between the speed of movement of molecules and their size. Thus, the larger the molecules, the lower the speed of their movement. The diffusion coefficient D of a solvent molecule in water is given by the following equation:

$$D = \frac{k_B * T}{6\pi\mu R}, \tag{2.31}$$

where, k_B is a Boltzmann constant (1.38 * 10^{-23} $m^2.kg.s^{-2}.K^{-1}$), T is the temperature in Kelvin, μ is the viscosity of the sample in Pa.s and R is the radius of a molecule of solvent.

And the diffusion time from a Benzyl alcohol molecule as function of the thickness of the nonsolvent has for equation:

$$t = \frac{e^2}{2D}, \tag{2.32}$$

where, e is the thickness and D is the diffusion.

In a solvent/non-solvent system applied on the polymer varnish film, one can ask what is the necessary time for a BA molecule to go to the surface of this film. A question which allows the restorers to predict how long the film should be in contact with the solvent/nonsolvent mixture to have the best result. Using the equations 2.31 and 2.32, the diffusion of a molecule in a nonsolvent can be calculated. The results are shown in the Fig. 2.10.

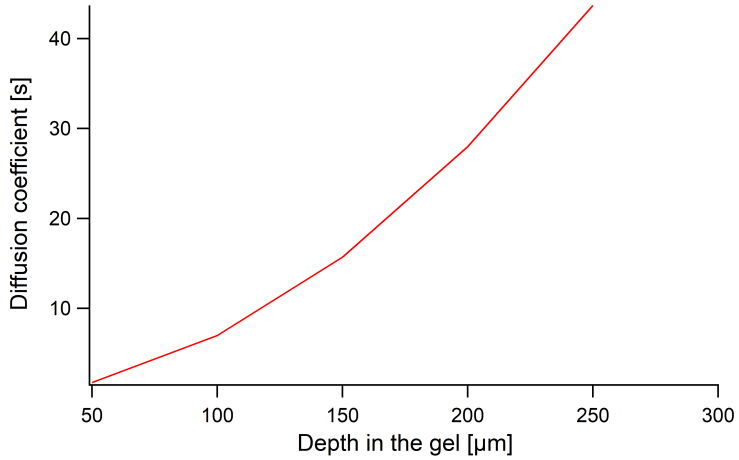

Figure 2.10 – Transfer of one molecule of solvent in a non-solvent

The diffusion time of the solvent is a function of the deposited thickness. This is the average time that molecules will need to travel a certain distance. The previous results are valid for solvent/water mixture. And the thicker the water layer, the longer the diffusion time.

Thus, two cases occur: a) case of the thin layer of water and b) case of thick layer of water.

a) In the case of a thin water thickness, for example 200 microns, on average, the solvent molecules will take less than 30 seconds to cover this distance, which is a very short. As a result, the molecules of the top of the solvent arrive almost at the same time as those which were already at the bottom of the gel. This time finally has so little effect that it is negligible compared to the penetration time in the varnish.

b) In the case of thick water thickness, for example 1200 microns, on average, the solvent molecules will take 1007 seconds or 17 minutes to cover this distance. Therefore, either if

the water is removed from the polymer film surface early (well before 17 minutes), the top of the solvent is useless because its molecules do not reach the varnish. If one abrades later, all molecules have time to arrive. In this case, the concentration of solvent molecules that will be in the varnish film depends on the waiting time. But the risk is that, while the last molecules arrive at the surface of the varnish, the first molecules will continue their progression in the varnish and could reach the pictorial layer. This will depend on the concentration of solvent at the start but also the thickness of the varnish and its capability to swell and dissolve.

Of course, these results only take into account the displacement of the solvent in the water, with the gel, the kinetics of displacement is a little different. The gel molecules delays the diffusion of the solvent in the solvent/gel layer. If the solvent passes through the varnish and reaches the paint layer, it may solubilize the components of the latter and change the structure. To avoid any damage, it is better to apply a thin gel layer. The solvent is thus diffused quickly and the varnish film can be lightened layer-by-layer. The paint layer is safe and the restorer can control its action.

2.2.2 Solutions of polymers in Good Solvent

To assess the size of a polymer molecule, we need to talk about the dimensions of Random-Walk chains and their End-to-End Distance and the Radius of Gyration in a linear chain consisting of N bonds of length b [91]. The end-to-end distance of the chain (root-mean-square end-to-end distance) is the root main square of the end-to-end vector R_f.

Considering the average end-to-end distance defined as R_f=$N^{1/2}b$ and the whole chain contains in a sphere of diameter R_f, the square of the root-mean-square radius of gyration ${R_g}^2$ is defined as the mean square distance between the monomers R_n and the center of the mass R_G. The radius of gyration R_g of a polymer chain [101] is the root-mean-square distance of the segments of the molecule from its center of gravity of the ideal chain is given in eq. 2.33:

$$2{R_g}^2 = \frac{1}{N}\sum_{n=1}^{N} < (R_n - R_g)^2 >, \tag{2.33}$$

Which give the information about the size of the random coil shape. For large N ideal chains ($N \gg 1$):

$${R_g}^2 = \frac{Nb^2}{6}, \tag{2.34}$$

where, the ratio of R_f and R_g is $6^{1/2}$.

Indeed, the Fourier Transform of the average density of segments of the chain, *g(q)* is given by the following equation:

$$g(q) = \int drg(r)exp(iq \bullet r) = \frac{1}{N}\sum_{n=1}^{N}\sum_{m=1}^{N} < exp[iq \bullet (R_m - R_n)] > . \tag{2.35}$$

When N tends to infinity in the ideal random walk, $g(q)_{gaussian}$ for a Gaussian ideal polymer coil was solved in 1946 by P. Debye and is the Debye equation:

$$g(q)_{gaussian} = \frac{2N}{Q^2}[Q - 1 + exp(-Q)], \tag{2.36}$$

where, $q = (qR_g)^2$.

For polymer coil in solution in long range interactions, the ideal and Gaussian chain exists only at the theta point. Outside this special condition, the random walk disappears in favor of a self-avoiding walk model.

2.2.3 Effect of the Temperature on the Solvent Goodness

The solvent power can be changed by changing the temperature. It affects the coil size. When the temperature reaches the good solvent regime, the size of the coil increases. At the theta temperature θ (a very narrow temperature), the coil is Gaussian. Each polymer/solvent couple has its own θ-temperature value. It is the Flory temperature. In the case of temperature below the θ-temperature, the homogeneous mixture becomes unstable, the coils of the polymer collapse (phase separation) and form a precipitate.

2.2.4 Flory-Huggins Theory applied to bulk mixtures

Considering polymer chains as random walks on a lattice, Flory and Huggins assumed that the solvent and the polymer monomers are able to rearrange arbitrary themselves in this lattice model [92]. Each monomer occupies a specific site and the solvent molecules are in the free space which are not already occupied by the polymer. It is assumed that the free volume of each molecule or monomer is the same for all. Φ is the fraction of sites occupied by monomers and depends on the monomers concentration per cm^3: $\Phi = ca^3$, where a^3 is the volume of the cubic site in the lattice [97].

P.J. Flory [93] described the entropy of mixing ΔS for three-component mixture (nonsolvent (1), solvent (2) and polymer (3)) as:

$$\Delta S = -R(n_1 ln\phi_1 + n_2 ln\phi_2 + n_3 ln\phi_3), \tag{2.37}$$

where, n_i is the number of moles and ϕ_i is the volume fraction and R is the gas constant.

And the equation of the enthalpy of mixingΔH is:

$$\Delta H = -RT(\chi_{13}\phi_1\phi_3 + \chi_{12}\phi_1\phi_2 + \chi_{23}\phi_2\phi_3)(m_1n_1 + m_2n_2 + m_3n_3), \tag{2.38}$$

where, χ_{ij} is the Flory interaction parameter and m_i is the ratio of the molar volume.

According to De Gennes [92], χ is dimensionless and it depends on several external parameters such as temperature and pressure. By its value, χ differentiates good solvents (*low* χ) from bad solvents (*high* χ) . When the free energy originates only from the entropy of mixing, the solvent interaction is close to the polymer and χ = 0. When the solvent is very good, temperature has no impact on the solvent/polymer interaction. The solvent is then called athermal. However, most of the time the interactions between polymer/solvent, polymer/nonsolvent and solvent/nonsolvent is mainly Van der Waals attraction and the Flory interaction parameter is positive and χ is not independent of the temperature.

A solvent with $\chi \ll 1/2$ including negative χ, is considering as a 'good' solvent. And conversely, a solvent with $\chi > 1/2$ is a 'bad' or 'poor' solvent. The higher the $\chi_{solvent}$, less the solvent is able to dissolve the polymer. A solvent is called nonsolvent when it is unable to dissolve the polymer.

The free Gibbs energy depends on two factors, the strength of the intermolecular interactions which corresponds to the enthalpy of mixing ΔH (eq. 2.38) and the driving force at a given temperature which corresponds to the entropy of mixing ΔS (eq. 2.37):

$$\Delta G = \Delta H - T\Delta S. \tag{2.39}$$

And the chemical potential μ_i is:

$$\Delta\frac{\mu_i}{RT} = (\frac{dG}{dn_i})_{T,P,n}. \tag{2.40}$$

2.2.5 Interaction parameter in the Phase Diagram for a solvent/nonsolvent/polymer mixture

A Phase Diagram is a representation of the physical states of a single or of mixed substances including polymer. It demonstrates the equilibrium and non-equilibrium phases of this system. To estimate regions where the interactions parameters are favorable or unfavorable, we have to find the Flory-Huggins parameters assuming the mixing of polymer/solvent such as the effect of both enthalpy of mixing and entropy of mixing described by the free Gibbs energy of mixing, given then by:

$$\frac{\Delta G_M}{RT} = n_1 ln\phi_1 + n_2 ln\phi_2 + n_3 ln\phi_3 + g_{12}(u_2)n_1\phi_2 + \chi_{13}n_1\phi_3 + \chi_{23}n_2\phi_3, \tag{2.41}$$

where, g_{ij} is the concentration-dependent interaction parameters and u_2=ϕ_2/(ϕ_1+ϕ_2).

2.2.6 Rupture, Dewetting and Drop Formation of thin polymer films

Dewetting is the processes of the transformation of a homogeneous film into droplets (rupture). The film becomes unstable and leads to dewetting of the film. Reiter et al. [102] proposed four stages of dewetting: rupture of the film, size change and coalescence of holes, disappearance of polymer ridges (Rayleigh instability); and instability of hole rims on low wettability coatings.

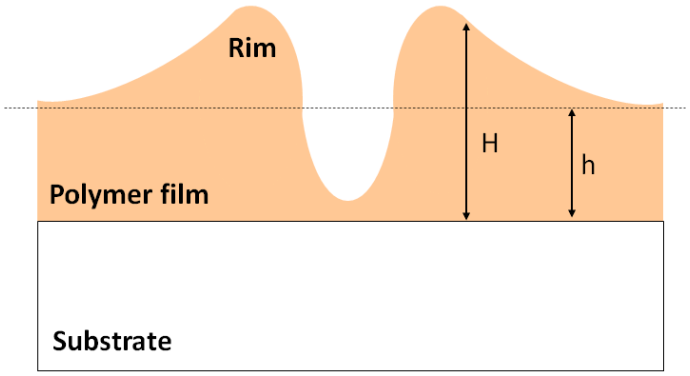

Figure 2.11 – Schematic of the hole and rim in a thin polymer film on a substrate

Dewetting stages and its theory are well described by several references [103] [104] [105] [106] and more particularly by Reiter et al. in the three references already mentioned [107] [102] [108]. According to Reiter et al. [102], the film becomes unstable due to a negative disjoining pressure given by attractive intermolecular interactions.

Spinodal decomposition or nucleation of the film irremediably change the initial smooth surface of the film by hole formation. Holes grown up and slowly expend with a constant velocity until the coalescence. The system tends always to minimize its total free energy. This expansion is due to the conjoining pressure near the interface polymer/substrate and the tension force of the surface which comes from to the circumferential curvature. Eventually, a thick polymer rim forms around the hole, because the flow imposes a viscous resistance on the polymer which varies as μH^{-3} with H is the local thickness of the deformed film. However, the surface tension force limits the growth of the rim. And, its expansion velocity depends of the initial thickness of the film. The hole/rim formation is faster for a thick film. Eventually, the rims of the holes can touch each other leading to coalescence. In this case, they form fluid pockets by capillarity instability comparable to the instability of Rayleigh. The last step is the formation of a pattern of droplets on the substrate by static ribbons forming the polygons of the rim movement at the edges of the holes (Rayleigh instabilities). The average distance between

the holes is proportional to the square of the film thickness. Furthermore, the size of the holes does not depend on the interfacial energy of the interface of the substrate-film.

The dewetting of ultra-thin films of polystyrene (Ps) deposited onto silicon wafers was studied by Sharma and Reiter in 1996 [102], by Xie et al. [106] and by Reiter in 2001 [108]. Holes on the film surface were observed with an asymmetric rim and the inside wall of the hole is very steep unlike the outer part. The rim appears progressively. The number density of holes is given by Reiter [107] as $r \sim h^{-4}$ where h is the film thickness. To improve the understanding of the dewetting, a theoretical model to explain the difference between the rim outside and inside the hole was proposed by de Gennes et al. in 2002 [109]. They demonstrated that the size of the holes and the rims depend on the initial film thickness and also the experimental time.

Then,inspired by the work of Reiter and Sharma [108], Seemann and al.[110] proposed a new theoretical view of the study of dewetting of thin polymer films on a hydrophobic substrate by the use of a 2-D form of the lubrication model. They investigated the evolution of perturbations in the dewetting process at different boundary conditions (mainly no-slip and Navier slip conditions) at the liquid/solid interface. They showed that no-slip and slip-dominated cases lead to different rim profiles.

More recently, Pahlavan et al. [111] have proposed a new model to explore the partial-dewetting regime for thin liquid films on solid substrates by a thermodynamic framework.

2.3 Rheology and viscosity measurement

2.3.1 Theory

Rheology is the study of deformations and flows of material (gas or fluid), as a function of the forces applied on it. It applies to complex fluids, viscoelastic material, liquids and solids. Thus, it covers a wide range of products and materials as well as many fields (cosmetics, agri-food, material resistance, etc.).

The deformation depends on the material. Solid bodies can be deformed elastically (perfect solids). The energy required for the deformation is equal to the energy recovered after the applied stresses. For liquids and gases, the deformation is irreversible (ideal fluids) so the deformation energy is converted into heat in the fluid and cannot be recovered as such [112].

The relationship between applied stress and the resulting shear rate is called viscosity. Its influence was demonstrated as early as 1687 by Isaac Newton thanks to a simple shear experiment (Figure 2.12) between 2 plates, one fixed and the other with a translational movement under the action of an force $\overrightarrow{F}$, a pasty, molten liquid material. Leading to Newton's law which defines shear stress as the dynamic viscosity multiplied by the shear rate. Newton's experience has been redesigned and improved with the use of other geometries for viscosity measurements to adapt to any type of material but it is a model that is still valid nowadays and its law too [113].

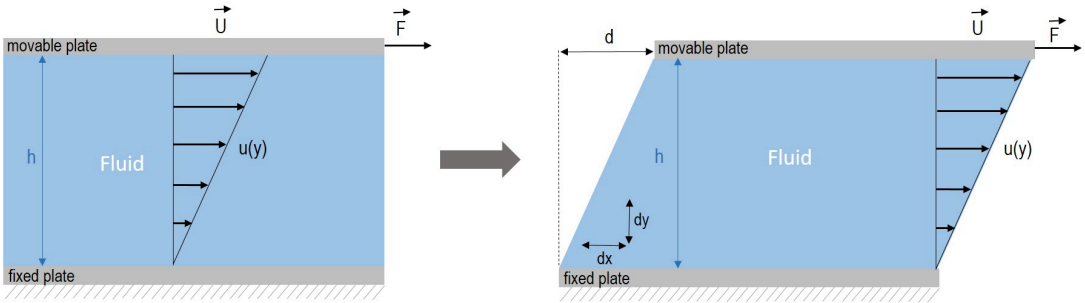

Figure 2.12 – 2-D representation of Newton experiment at a speed U and a force F

The dynamic viscosity μ (Table 2.2), in Pascal seconds or g.cm^{-1}.s^{-1}, can be defined as the resistance to laminar flow of incompressible matter. It corresponds to the coefficient of the shear stress τ (Pa) necessary to obtain a gradient of flow velocity also called shear rate $\dot{\gamma}$ (s^{-1}). The shear stress, in Pascal Pa, is the force F applied on the surface S of the sample, $\tau = \frac{F}{S}$ with F in Newton and S in m^2. The shear rate is the temporal derivative of the deformation, $\dot{\gamma} = \frac{d\gamma}{dt}$.

In Newtonian fluids (constant viscosity whatever the stress or the shear rate), the kinematic viscosity can be define as the ratio of dynamic (absolute) viscosity to density. It can be obtained by dividing the absolute viscosity of a fluid:

$$\upsilon = \frac{\mu}{\rho}, \tag{2.42}$$

with the fluid mass density ρ in g/m^3 and dynamic viscosity μ in g.cm^{-1}.s^{-1} (or Pa.s).

Table 2.2 – Some dynamic and kinematic viscosity values for some materials at atmospheric pressure.

material	μ (Pa.s)	υ (St)
Air (0°C)	1.7x10^{-5}	1.7x10^{-8}
water (20°C)	1.0x10^{-3}	1.0x10^{-6}
oil	10^{-2} to 1	10^{-5} to 10^{-3}
molter polymer	10^{2} to 10^{4}	10^{-1} to 10

In order to analyse the rheological properties of the fluids, it is possible to measure the viscosity during shear deformation stress; this is rheometry. In addition to the shear rate effect on viscosity, some other factors influence the fluid behavior such as the pressure and mainly the temperature. In the case of a liquid, an increase in temperature leads to a separation of molecules and reduces their mutual attractions, which reduces viscosity. An increased pressure does the opposite.

Fluids can be Newtonian or non-Newtonian. The non-Newtonian fluids [113] [114] are much more numerous and they correspond to all the fluids whose viscous stress is not proportional with the applied shear gradient.

Unlike Newtonian fluids (water and some mineral oils), the viscosity of non-Newtonian fluids does not remain constant but depends on the shear rate or applied stress. The viscosity of shear-thinning liquids change according to the shear rate following the Oswald model is given by :

$$\mu(\dot{\gamma}) = K|\dot{\gamma}|^{m-1}, \tag{2.43}$$

with K, a constant representing the consistency of the liquid and m, the fluid index of pseudo plasticity ($m \leq 1$). If $m = 1$, the behavior is Newtonian, if $m = 0$, then the behavior is plastic.

The law of power (eq. 2.44) and the Herschel-Buckeley's law (eq. 2.45), an generalization of Bingham's law (eq. 2.3.1) makes it possible to describe the behavior of non-Newtonian fluids even if it is not the only model.

$$\tau = K\dot{\gamma}^n. \tag{2.44}$$

$$\tau = \tau_0 + K\dot{\gamma}^n, \tag{2.45}$$

where, n is the flow index.

There are 3 types of behavior in the family of non-Newtonian fluids (Figure 2.13: shear-thinning (or pseudo-plastics), shear-thickening and yield stress fluids.

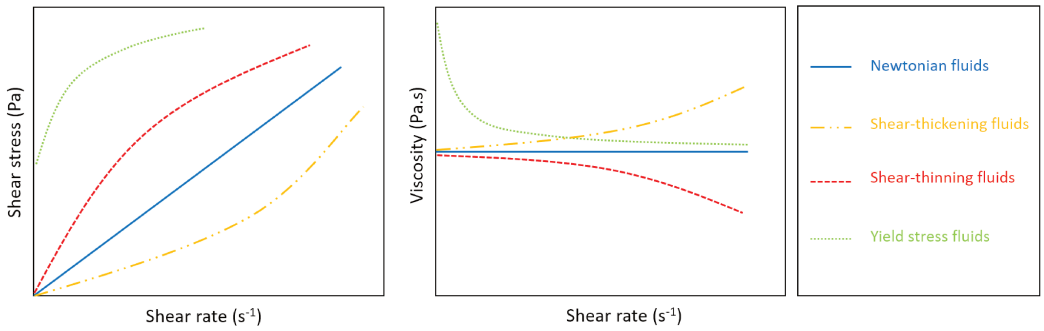

Figure 2.13 – The different fluids ranked according to their rheological behavior with, on the left, the flow curve and on the right, the viscosity curve

- Rheo-thinning fluids exhibit viscosity which decreases when the applied shear gradient increases. They are widely used in industry and are found in the products of everyday life and particularly in food, cosmetics and hygiene products [115].
- Rheo-thickening fluids have the viscosity which increases when the applied shear gradient increases. They are rather rare and are used in specific areas such as shock-absorptive skis, the impregnation of woven kevlar® fabric [116] and bulletproof protection [117].
- Yield stress fluids flow (Fig. 2.14) at a certain shear value reached. It cannot flow below a certain value. Beyond this value, the behavior is that of a viscous fluid. The Bingham law describes this rheological behavior at steady state (eq.2.3.1):

$$\dot{\gamma} = 0 \quad when \quad \tau < \tau_s \qquad and \qquad \dot{\gamma} = \frac{\tau - \tau_s}{\mu_p} \quad when \quad \tau > \tau_s, \tag{2.46}$$

where, μ_p is the plastic viscosity.

An alternative is the Casson model describes by Fung et al. in 1993 and which is used to model blood [118]. A comparison of these two models is showed in Fig. 2.14.

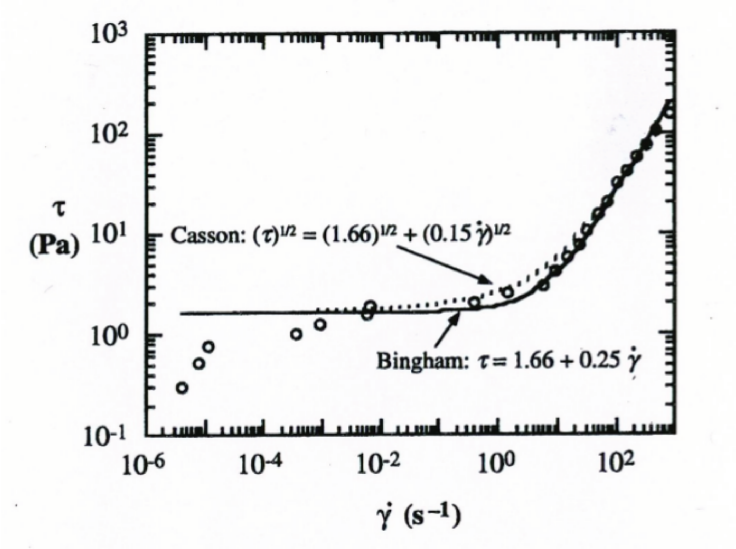

Figure 2.14 – Comparison of Bingham and Casson laws for an iron oxide suspension. Example of Threshold Fluid from reference [118]

2.3.2 Rotary rheometry

Rotary rheometry can be performed by using two geometries, cylinder-cylinder and cone-plane. The use of one or the other depends on the type of sample and the viscosity. The cone-plane geometry (Figure 2.15) is the most appropriate to use for this study because it allows a constant shear rate to be maintained in the space between the cone and the plane, whatever the angle θ and the radius R of the plane. The viscosity measurement is made by measuring torque as a function of deformation or vice-versa. For this, one of the two is imposed. It depends on the rheometer. For this project, the rheometer chosen imposed the stress thanks to a rotary motor. The material is then deformed and its displacement and the resulting torque is recorded and processed by the software.

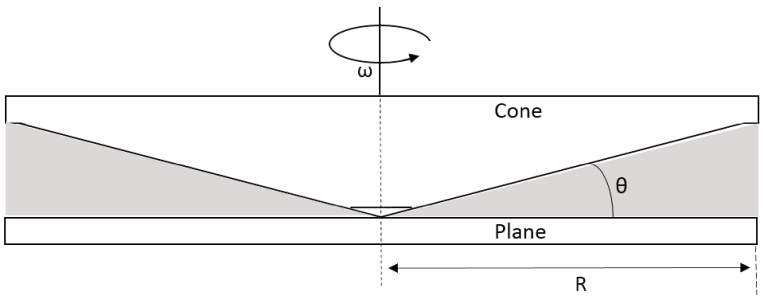

Figure 2.15 – Geometry cone-plane (according to [113])

2.3.3 Capillary rheometry

The viscosity can also be obtained with a capillary rheometer which operates according to the principle of Poiseuille flow in a cylinder. It is the flow of an incompressible viscous fluid between two fixed walls as in a cylindrical tube with a radius R (chosen according to the viscosity η) and a length L (z-axis flow is considered invariant if L is sufficiently large) defined in the figure 2.16. A constant pressure $\Delta P = P_0$ - P_L is imposed between the two ends of the tube. Considering laminar flow, the only non-zero component of the speed is υ_z and if the z-axis flow

is invariant, the Navier-Stokes formula in cylindrical coordinates (r, theta, z) becomes:

$$-\frac{\delta P}{\delta z}+\eta\frac{1}{r}\frac{d}{dr}(r\frac{d\upsilon_z}{dr})=0. \tag{2.47}$$

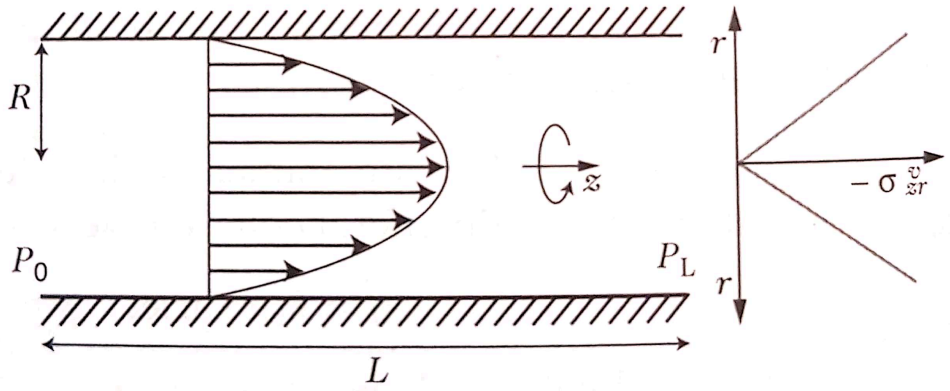

Figure 2.16 – Poiseuille flow in a cylindrical capillary with its velocity profile and its viscous stress σ_{zr}^{υ} (in module) from reference [113]

The velocity profile is parabolic and the viscous stress σ_{zr}^{υ} is maximum on the surface of the tube and decreases linearly towards the center of the tube so the shear is not constant.

The average flow of the fluid is proportional to the pressure gradient and inversely proportional to the fluid viscosity. It is given by the Poiseuille law which gives the flow Q and the average speed $\langle\eta_z\rangle$ of the fluid in the tube:

$$Q=\pi R^2\langle\eta_z\rangle=\frac{\pi(\Delta P)R^4}{8\eta L}. \tag{2.48}$$

CHAPTER 3
EXPERIMENTAL

In this chapter, the methods and the instruments chosen in order to perform this PhD project will be explained.

3.1 Materials

3.1.1 Synthetic polymers used in art restoration

Laropal®A81 (LA) is a resin increasingly used by conservators because of its superior properties compare to other resin. It is also a synthetic polymer that is not very sensitive to water, ideal for studying a solvent/nonsolvent model. For these reasons, it seemed the best choice of resin for this study.

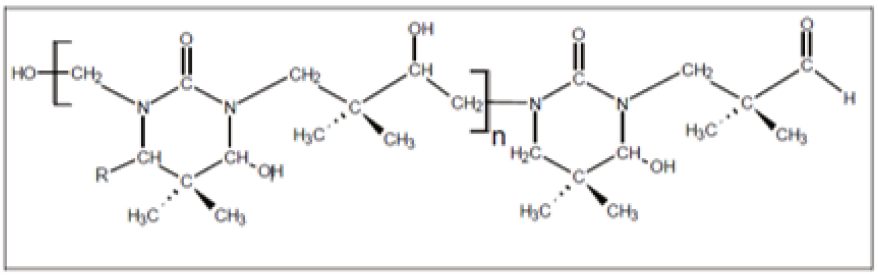

Figure 3.1 – Laropal®A81 formula from references [119] and [120]

Laropal®A81 is a synthetic thermoplastic polymer synthesized from urea, isobutyraldehyde, and formaldehyde. Size-exclusion chromatography (SEC) evaluated its weight-average molecular weight (Mw) as 3640 Da, its number-average molecular weight (Mn) as 1266 Da [28]. Its molecular structure was characterized by Bonaduce et al. using flow injection analysis coupled to electrospray ionization and quadrupole time-of-flight mass spectrometry (FIA-ESI-Q-ToF) and gel chromatography (GC). They concluded that Laropal®A81 is a product of the reactions between 4-hydroxy-6-isopropyl-5,5-dimethyl-tetrahydropyrimidin-2(1*H*)-one and aldehydic compounds. Futhermore, they showed that the hydroxyl groups have a strong effect on the physical properties of the film [95]. This resin is often used by art restorers to make the varnish layers and as a correction material for pictorial retouching [32]. The Laropal®A81 used in this study was produced by BASF [121] and purchased from C.T.S France [122]. It is sold in the form of pellets (solid non-volatile). Its T_g was measured as part of this study through Differential scanning calorimetry (DSC), its value is 47 °C (Fig. 3.35). The softening point indicated by the manufacturer is 80-95°C. Its density is 1,1 g/cm^3 at 20°C. It can be dissolved in aprotic and dipolar solvents to form a non-Newtonian shear thinning fluid and it is insoluble in water.

3.1.2 Solvents / nonsolvent

Used of Toluene for polymer solution mixture

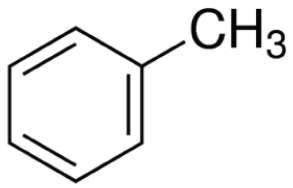

Figure 3.2 – Toluene structure from Sigma-Aldrich

Toluene C_7H_8 from Sigma-Aldrich was used, mixed with Laropal®A81 polymer resin, to make ultrathin, thin and thick polymer films by spin coating. Physical information are in table 3.1.

Table 3.1 – Physical properties of Toluene

Formula	C_7H_8
Molecular weight	92.14 g/mol
Density	0.867
Flash point	4˚C
Boiling point	110.6˚C
Melting point	-95˚C

Used of Benzyl alcohol to remove the layer

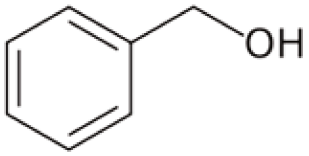

Figure 3.3 – Benzyl alcohol structure from Sigma-Aldrich

Benzyl alcohol anhydrous 99,8 % from Sigma-Aldrich was used in this study such as the solvent of reference to remove a polymer varnish layer on Si substrate. It was used only in small concentration (0 to 0.7 %) in D_2O. Physical informations are in table 3.2. Benzyl alcohol is chemically stable without oxygen and slowly oxidizes in its presence. It can explose in the presence of strong oxidants.

Table 3.2 – Physical properties of Benzyl alcohol

Formula	C_7H_8O
Molecular weight	108.14 g/mol
Density	1.045
Flash point	100.5˚C
Boiling point	205.3˚C
Melting point	-15.3˚C

Water

Deuterated water D_2O from Eurisotop (ref D214L) at 99,9 % D was used for NR, Optical microscopy, AFM and QCMD experiments. MilliQ water (resistance >18MΩcm) was used for all others complementary experiments.

3.1.3 Substrates

Single crystal Silicon wafers of (100) orientation and 8x5x1 cm^3 and 5x5x1 cm^3 Single crystal Silicon blocks of (111) orientation (Fig. 3.4) from Sil'Tronix France were used to perform NR and SANS experiments (for thin and thick films by spin coating). Quartz cells were also used for SANS experiments (for thick films by deep coating).

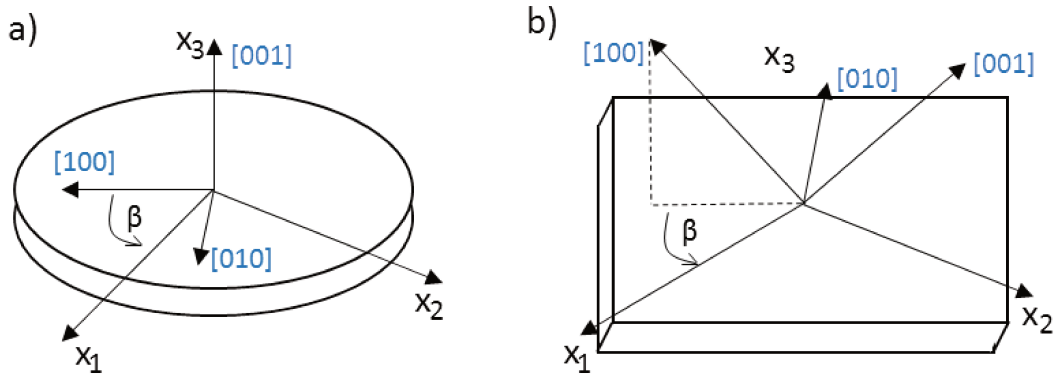

Figure 3.4 – Geometry a) (100) wafer, b) (111) block

3.1.4 Gel of Pemulen TR-2

Material

Pemulens are primary emulsifier and viscosity-enhancing agent. There exist two types of Pemulens: TR-1 and TR-2, and the difference between them resides in their ability to emulsify the oil phase. The TR-2 is more hydrophobic than the TR-1 [123]. Pemulen TR-2 commercialized by Lubrizol is a oil-in-water emulsifier with a high molecular weight. It is a polymerized acrylic acid which forms a macromolecule of a polyacrylic acid -$[CH_2$-CH-(COOH)-$]_n$- (Fig. 3.6). When Pemulen TR-2 in its aqueous form comes into contact with a base, the macromolecules ionize, i.e. the (-COOH) groups release a H^+ proton and form carboxylates ($-COO^-$). This chemical reaction leads to the creation of salt. The macromolecule, initially in the form of a pellet, takes place by electrostatic repulsion inducing swelling of the matrix and an increase in viscosity.

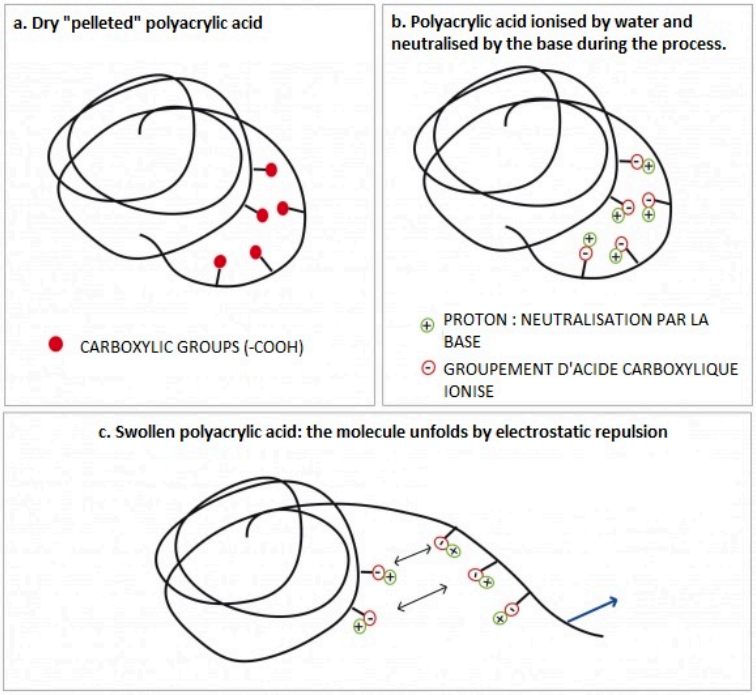

Figure 3.5 – Polyacrylic acid during the process of swelling (from an image by Claire Dupuy [124]

It can stabilize until a high oil concentration (50wt % of oil) that is to say, much more than the majority of surfactants. Pemulen TR-2 (PTR2) was used for cleaning painted surfaces at these high concentrations to form an emulsion [47] [123] [125]. It can form stable o/w emulsions even with low emulsifier concentrations (0.15 %) 3.11 and also at high concentrations. According to N. Ravenel, the conservation lab at Shelburne Museum use Pemulen TR-2 in a 1 % concentration in the gel since R. Wolbers introduced them to this gel in 2007 [126]. Wolbers proposed to use the triethanolamine (TEA) to neutralize the Pemulen TR-2 and the water/Pemulen TR-2/TEA mixture has quickly become the standard mixture among restaurateurs. Physical informations of TEA are in table 3.3.

Table 3.3 – Physical properties of triethanolamine

Formula	$C_6H_15NO_3$
Molecular weight	149.19 g/mol
Density	1.124
Flash point	21.6˚C
Boiling point	335.4˚C

Rheology of the gel

Informations about the rheometer used in this study and the method of analysis are presented later in the section 3.3.8.

The more PTR2 in the Pemulen/water mixture, the more viscous the gel is (Fig.3.8 and Fig.3.9). By increasing the pH (stable between pH 3 and pH 9) with for example some triethanolamine or sodium hydroxide NaCl, the gel becomes more viscous (Fig.3.10). The presence of a small amount of BA (between 0 % and 1 % BA) slightly decreases the viscosity of

the Pemulen TR-2 gel at fixed pH (Fig.3.12). The flow behavior index n from the law of power equation 2.44 corresponding of the slope of the rheology curves (Shear stress as function of shear rate) in the Fig. 3.9 and Fig. 3.12 are ~ 0.5, so less than 1 which is characteristic of pseudoplastic behavior (viscosity decreases as shear rate increases) of this gel. It is consistent because most non-Newtonian fluids are pseudoplastic. Moreover, the flow behavior index is higher with the increasing concentration of PTR2. The gel has a very slight slip behavior which means the adhesion to the interface of the cone-plane/gel and gel/support is good (Fig. 3.13). So, the rheology of Pemulen TR-2 samples show a non-newtonian shear thinning behavior with a slight thixotropy (apparent viscosity decreases over time under constant stress). The gel with and without BA appeared physically stable, even after several weeks at room temperature. The apparent viscosity depends on the concentration of Pemulen TR-2 and the amount of BA contained. It is also sensitive to the temperature. Its behavior and its formulation are close to those of the Carbopol® resins. Pemulen TR-2 gel is a crosslinked copolymer of acrylic acid and a hydrophobic *C10-C30* alkyl acrylate co-monomer (Fig.3.6) [127].

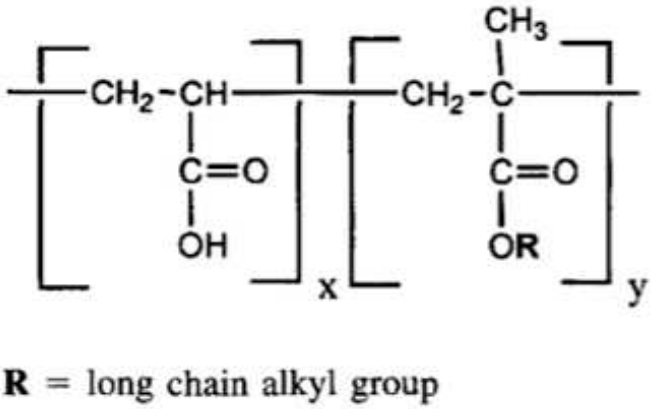

Figure 3.6 – Formula of Acrylate / C10-30 Acryl Acrylate Crosspolymer (Goddard et al. 1999)

Groups R (lipophilic part) is able to absorb at the o/w interface and the acrylic acid (hydrophilic portion) swells in contact with the water to form a gel network. This network contains numerous stables oil droplets. Unlike other emulsifiers where droplets are stabilized by phospholipids, droplets formed in the Pemulen TR-2 gel keep their spherical shape thanks to the repulsive force between hydrophilic and lipophilic regions (Fig. 3.7). It allows us to obtain an O/W emulsion gel with a great stability.

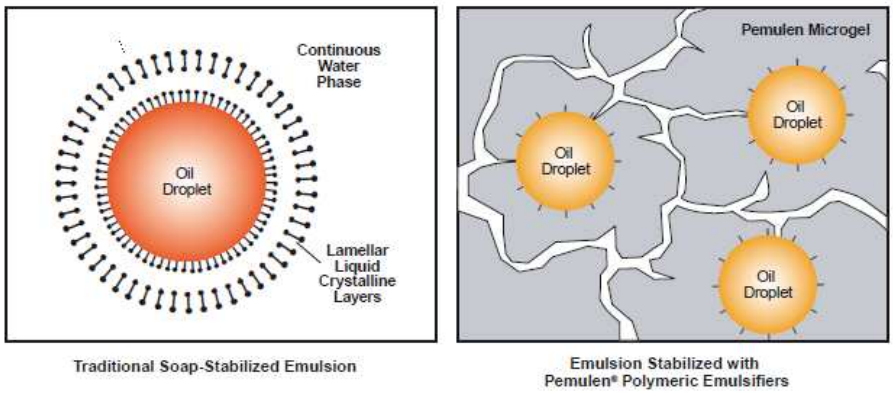

Figure 3.7 – The repulsive force due to the aqueous gel layers that surround each droplet of oil, keep the o/w emulsion in a state of great stability (Lubrizol-Technical data sheet. 2007)

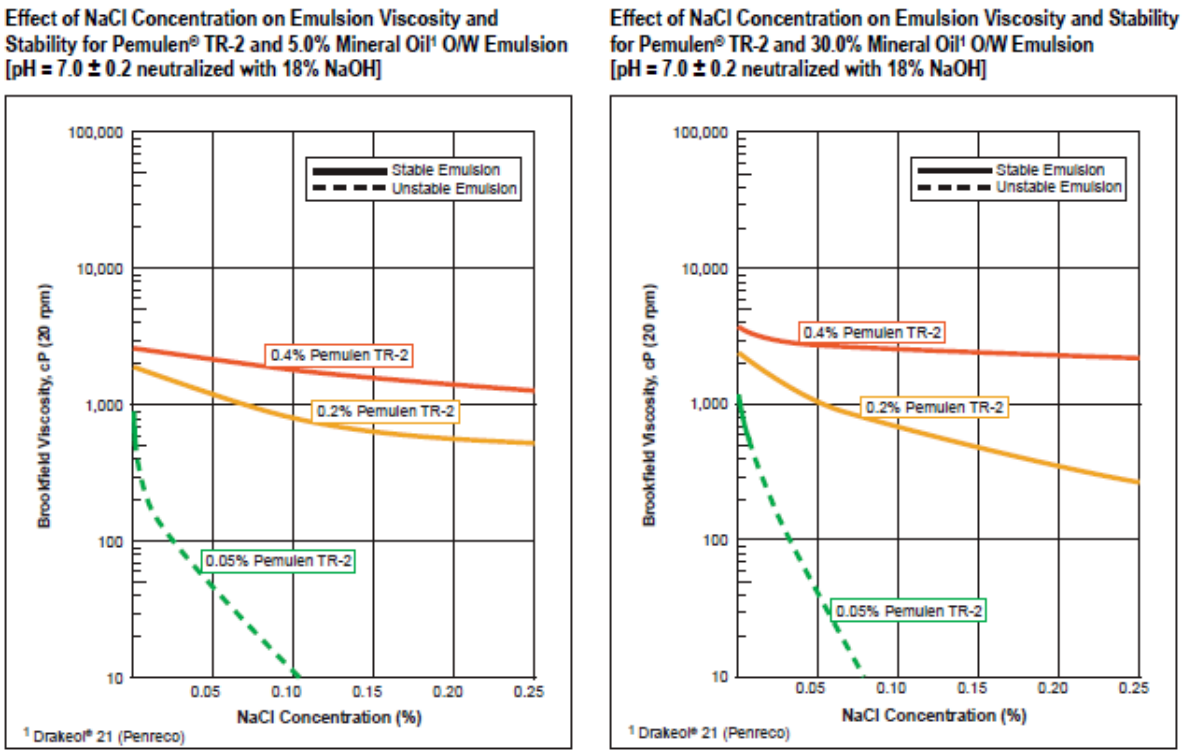

Figure 3.8 – Effect of NaCl concentration on the viscosity of Pemulen TR-2 with 5 % and 30 % Mineral Oil and at pH 7± 0.2 neutralized with 18 % NaOH (Lubrizol-Technical data sheet. 2007)

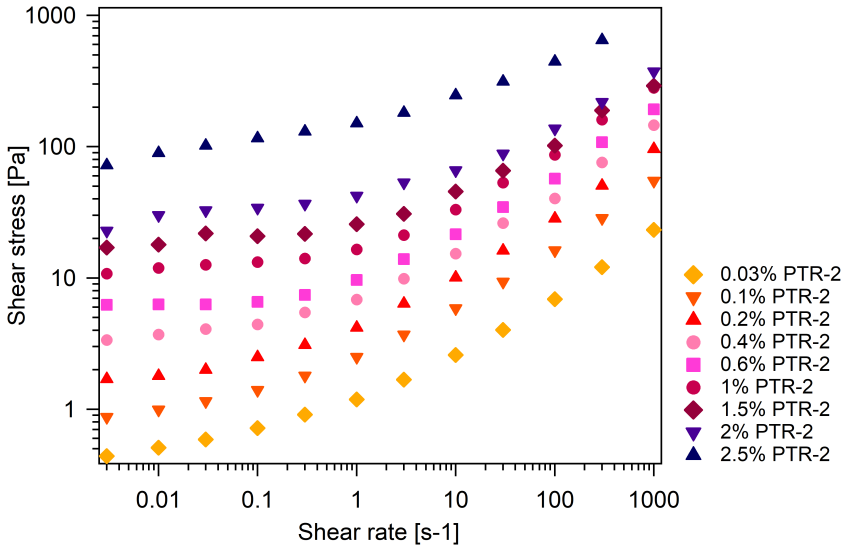

Figure 3.9 – Shear stress [Pa] of a Gel at different concentration of Pemulen TR-2 (0.03 % to 2.5 %) at fixed ph $\sim$ 7 as function of shear rate [s^{-1}] at room temperature and obtained by rheology measurements at the LRP. The higher the concentration, the more the gel is viscous and difficult to shear.

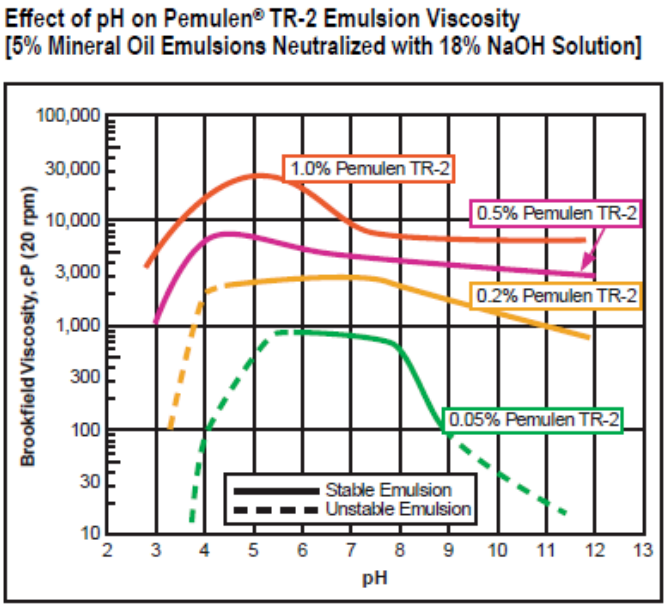

Figure 3.10 – Effect of pH on the viscosity of Pemulen TR-2 with 5 % Mineral Oil (Lubrizol-Technical data sheet. 2007)

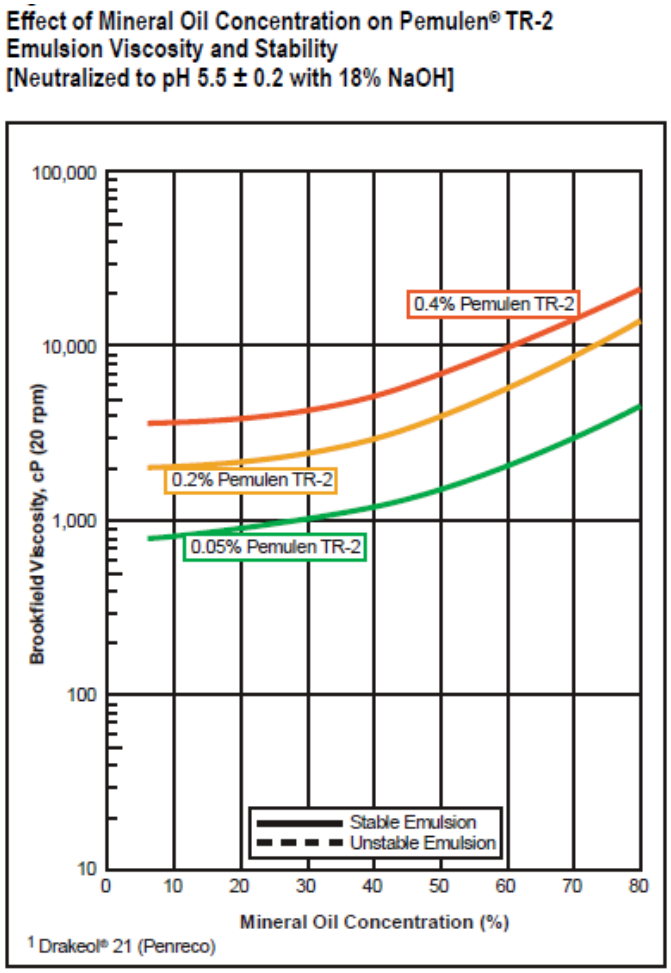

Figure 3.11 – Effect of Mineral Oil concentration on the viscosity of Pemulen TR-2 at pH 5.5± 0.2 neutralized with 18 % NaOH (Lubrizol-Technical data sheet. 2007)

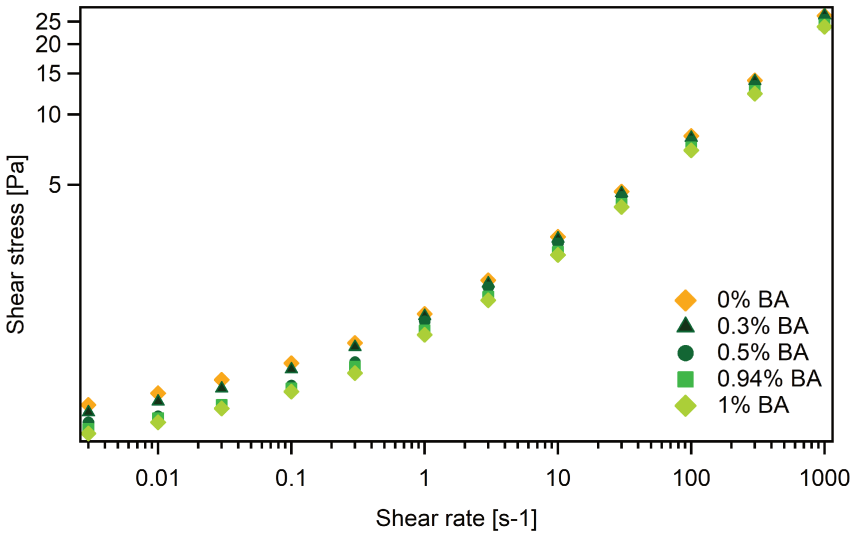

Figure 3.12 – Shear stress [Pa] of a Gel of Pemulen TR-2 at 0.03 % at fixed ph $\sim$ 7 and with an increasing concentration of BA as function of shear rate [s^{-1}] at room temperature and obtained by rheology measurements at the LRP. BA slightly decreases the viscosity of the gel.

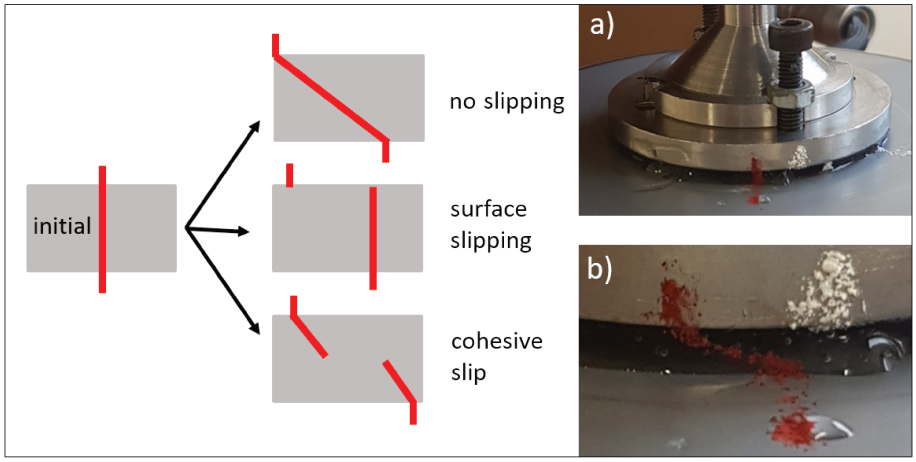

Figure 3.13 – Observation of the slip of the gel by a marking during a very slow shear at room temperature. The gel exhibits no slippage.

Rheology measurements were performed to characterize the Pemulen TR-2 gel with and without BA. For these measurements, several Pemulen TR-2 gel mixtures were made at fixed pH $\sim$ 7 with different concentrations homogenized with a rotary rheometer with blades (Fig. 3.14):

- Pemulen TR-2 in water (between 0.03 % and 2.5 % PTR2). The results are shown in Fig. 3.9.
- BA inside the gel at 0.03 % PTR2 (between 0 % and 1 % BA). The results are shown in Fig. 3.12.

Figure 3.14 – Mixing and homogenization of the PTR2 gel sample by slow rotations with a rotary rheometer with blades.

3.2 Preparation of samples and measurement of thickness

Film preparation can be made using several methods such as spin coating, dip coating, spray-coating, casting or flow coating methods but the first one is most widely used for depositing thin polymer layers on flat solid substrates [128]. Spin coating method is mainly used because of its simplicity of use and the repeatability of the samples [129]. It quickly became an indispensable tool for industrial application and scientific research. However, this is not a suitable technique to make thick layers, in which case, the method by dip coating is preferred and allows us to obtain homogeneous thick films.

3.2.1 Thin and Thick Films formation by spin coating for NR and SANS

Ultrathin film ($\sim$ 100 nm) and thin film (between 200 nm and 500 nm) are obtained by spin coating which is a common reproducible techniques for applying uniform thin and ultrathin films of few nanometres to a few microns thicknesses on plane surfaces of substrates by spreading a polymer liquid solution on a horizontal rotating substrate. The polymer solution is previously achieved by polymer solubilization in a solvent. Then, the polymer fluid is deposited on the wafer which spreads by high speed rotation evenly across the surface of the substrate. At the end, the aim is to obtain a uniform film layer with the thickness previously chosen.

Cleaning of wafers and blocks

Before spin-coating the polymer solution, substrates and single crystal silicon blocks were rigorously cleaned subsequently 15 min sonication in water/Decon 90 (1 drop) mixture, ethanol, acetone, chloroform and ending with clean water and dried with filtered nitrogen at room temperature. Then, the thickness of the SiO_2 layer was determined by ellipsometry (3.2.3).

Ultrathin and thin films by Spin-coating

Predicting thicknesses and homogenize the layer on the flat substrates is a challenging task which depends on several factors (the polymer concentration and viscosity in liquid state in solvent, the evaporation rate of solvent, the angular velocity, the rotation time and the substrate roughness) not governed by fixed rules but based on empirical models. These factors impact the surface state and are at the origin of common spin coating defects (air bubbles, comets, streaks of flares, swirl pattern, center circle, uncoated areas and pinholes) which are described and analysed in reference [130]. A simple model of spin coating as a function of the polymer concentration, the polymer viscosity and the spin speed was proposed by Bornside, Macosko and Scriven in 1989 [131]. This study was completed by Hall, Underhill and Torkelson in 1998 [129] by carrying out a study on the thickness of the PS and PMMA films obtained by spin coating as a function of the spin speed (Fig. 3.16) and by showing the impact of a highly volatile or low volatile solvent on the thickness of the film.

Taking into account these factors and the studies of the review [128], thin films of Laropal®A81 at ∼100 nm (Fig. 3.19), ∼200 nm, ∼300 nm and ∼500 nm were achieved by spin coating for neutron reflectometry and SANS studies on the SÜSS MicroTec Lithograhy GmbH (Ak-200609) shown in Fig. 3.15.

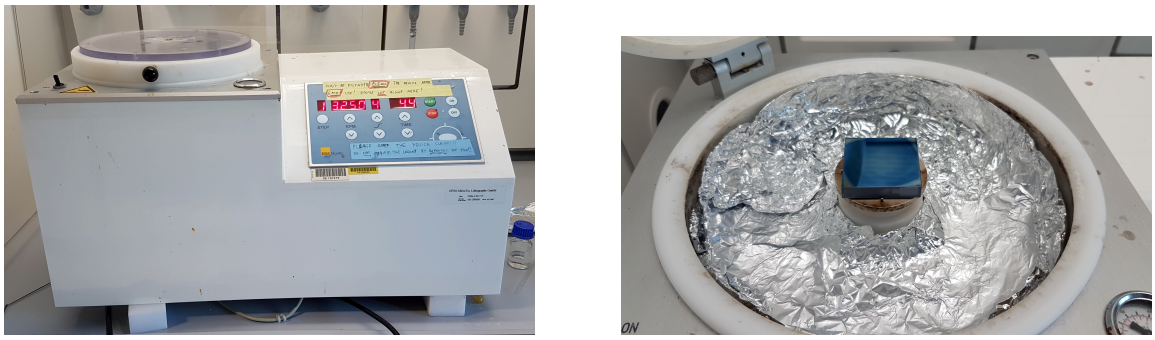

Figure 3.15 – Spin coater (left) used for the deposition of polymer film on Si substrate. Rotating support with a sample of LA film after spin coating (right).

The spin coating method was always the same: pure toluene was deposited and spread by high speed rotation. Then, LA polymer resin diluted in toluene of a certain concentration was deposited on the center of the substrate. The solution was spread on the substrate by high speed rotation. Then, the excess solution was ejected from the substrate. After solvent evaporation, a thin film was formed on the substrate. Films thicknesses were measured by ellipsometry (3.2.3).

To find the best parameters to obtain homogeneous ultrathin films, first a test with different spin speed (500 RPM to 3000 RPM) at 20 g/L LA and 40 g/L LA on silicon wafers was done. The density (1.11 g/cm^3) and the chemistry of LA are similar to PS (1.04 g/cm^3) and PMMA (1.18 g/cm^3). As only a few data are present in the scientific literature for LA, PS and PMMA polymers was chosen such as references because of their chemical similarities with LA. In order to approach 100 nm thick films, LA concentrations were chosen following the PS and PMMA spin-coating investigation (fig. [129]) from Hall et al. in the reference [129]. Between 1200 RPM and 3000 RPM, ultrathin films of 43 nm (2 %) and 90 nm (4 %) homogeneous films were obtained. For spin speed, numerous defects on LA films were observed, such as streaks, center circle or swirl pattern and the thickness varied too much on the film and it was difficult to obtain a real value by ellipsometry.

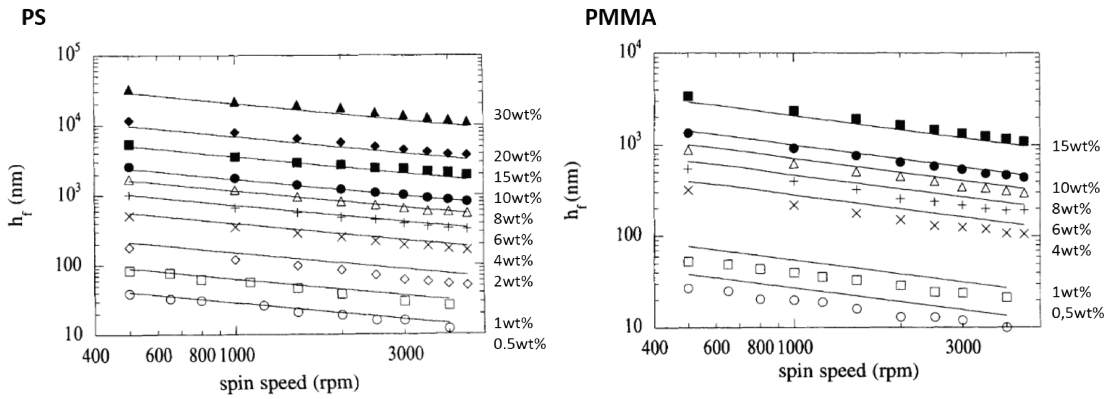

Figure 3.16 – Film thicknesses h_f as a function of spin speed and initial polymer solution concentration for PS and PMMA in Toluene (Hall et al. 1998)

The second step was to vary the LA concentration (between 20 g/L to 200 g/L) at the same spin speed on Si wafers and Si crystal blocks (Fig. 3.18). A program of 1250 RPM for 44 seconds was chosen. Several thicknesses according to these concentrations were obtained. The film thickness changes with the LA concentration in the liquid solution but not only that, it changes also with the substrate (wafer or block). On silicon blocks, it needed less LA resin on silicon wafers (Fig. 3.18) to obtain the same film thickness. It is true that the chemistry of the two is very similar but the geometry change (Fig.3.4), however that does not explain such a difference on the substrates. One can explain it by a different mass between the wafer ($\sim$ 10g) and the block ($\sim$ 100g) which can impact the inertia of the speed rotation. The inertia of the silicon block is significantly higher than that of the silicon wafer. It also showed that the higher the LA concentration, the less the film is homogeneous at a fixed RPM. Moreover, the film thickness homogeneity was worse on the silicon blocks as seen by an inhomogenous color distribution visible by eye.

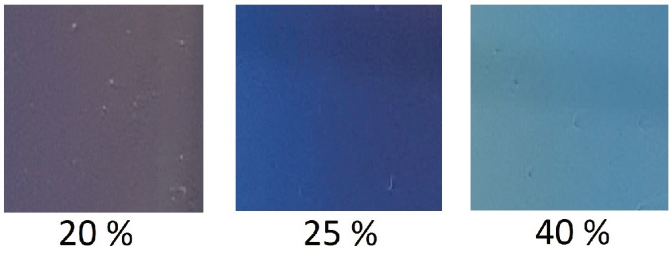

Figure 3.17 – Surface of LA thin films on Si Crystal Blocks obtained by spin coating using three concentrations of LA in toluene, 20 %, 25 % and 40 % LA, spread on substrates at 1250 RPM for 44 seconds, highlighting the apparent colors as function of the thickness of the film

This work made it possible to guide the realisation of the rest of the samples. It was therefore sufficient to slightly adjust the parameters concentration, RPM to obtain the most homogeneous films possible for the thickness chosen.

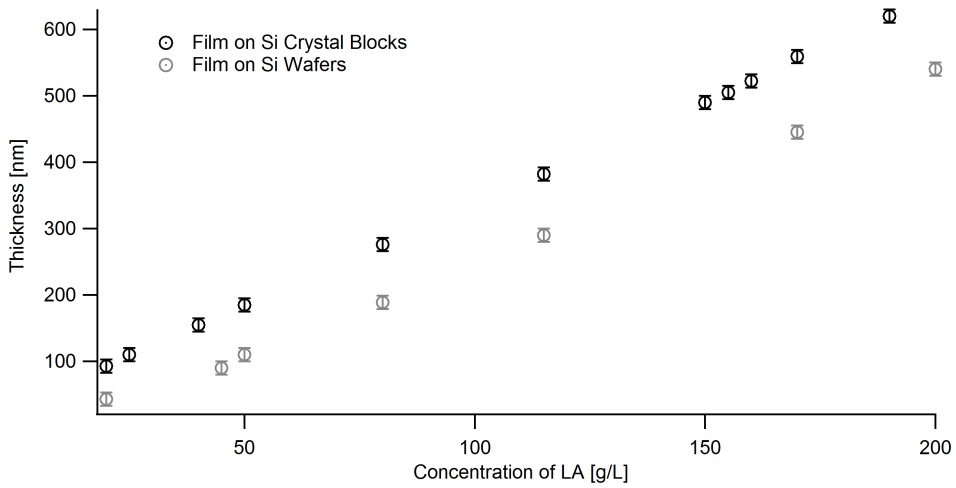

Figure 3.18 – Thickness of LA thin film on Si Crystal Blocks (black) and on Si Wafers (grey) substrates obtained by spin coating method at 1250 RPM for 44 seconds as function of the concentration of LA in toluene

A program in two steps was used on the spin coater. The first step was set to 300 rpm for 2 s. The second step was set to 3000 rpm for 44 s. This program was carried out first with only toluene, then with the polymer solution. The thickness of the films is given the table 3.4). Thicknesses are measured by ellipsometry (3.2.3). An example of 100 nm sample is shown in Fig. 3.19.

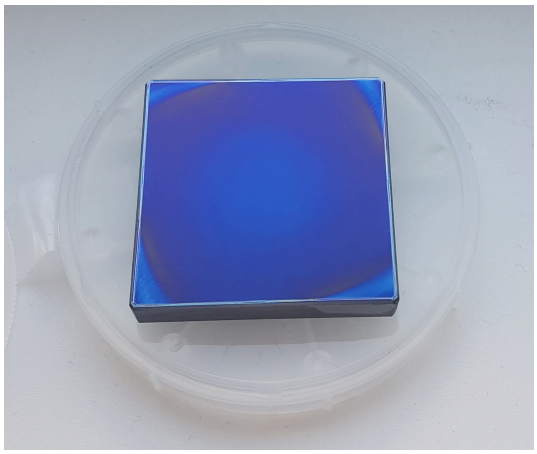

Figure 3.19 – Sample of 100 nm LA thin film on Si crystal block

Table 3.4 – thickness of films according to the concentrations of LA in toluene at 3000 rpm/44s spin coating program

Film thickness	LA concentration
$\sim$ 100 nm	30 g/L
$\sim$ 200 nm	80 g/L
$\sim$ 500 nm	190 g/L

3.2.2 Thick films by dip coating for SANS

Principle

Dip Coating is the process which involves the deposition of a liquid film on a substrate by soaking. To obtain reproducible samples with the same thickness and homogeneity, numerous parameters have to be controlled: temperature, speed of soak, immersion time and sample output speed. It implies 4 steps: 1. the immersion of the substrate, 2. the period of time, 3. the withdrawal [132] and 4. the film formation by drying.

1. The substrate is immersed into the polymer solution at a constant speed.

2. The substrate remains in the solution for some time previously defined.

3. The substrate is withdrawn at a constant speed. Two forces interact during this step : draining forces (drawing the liquid away from substrate) and entraining forces (retain fluid onto the substrate). The combination of the two defines the thickness of the film. Withdrawal speed affects the thickness and the homogeneities of the film (Fig. 3.20) [133]. The faster the removal of the substrate from the solution, the thinner the film. The slower it is, the more the film may be unevenly distributed due to different immersion times on the substrate. 4 regions can exist on the film during the withdrawal period: (a) the wetting zone (wet film), (b) the constant thickness area (wet film at a constant thickness), (c) the dynamic meniscus (draining forces and entraining forces are equilibrium) and (d) the static meniscus (immersion zone where the meniscus shape depends on the hydrostatic and capillary pressures) showed in the Fig. 3.21.

4. By solvent evaporation, the film dries in the air.

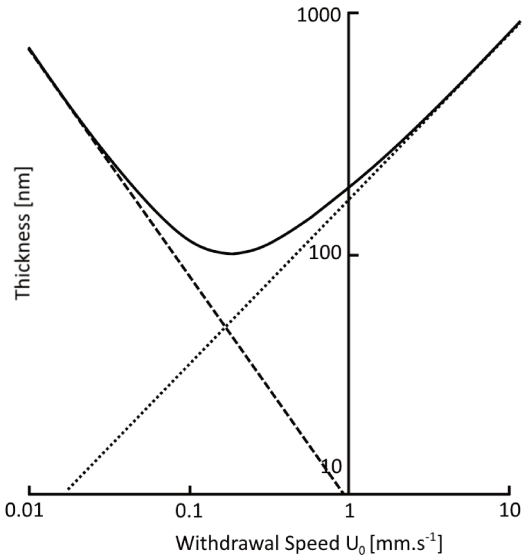

Figure 3.20 – Thickness as a function of the withdrawal speed U_0 for the dip coating process. The minimum is achieved at the crossover between these two coating regimes. (Faustini et al. 2010)

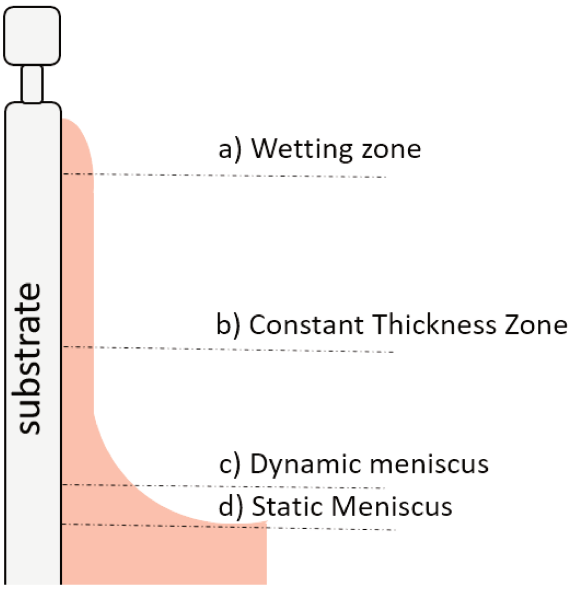

Figure 3.21 – Schematic representation of the 4 regions during the withdrawal of the film by dipping. These regions are the wetting zone (a), the constant thickness area (b), the dynamic meniscus (c) and the static meniscus (d)

Sample

For SANS experiments, thick films prepared by dipping were deposited by an automated robot on which the substrates were fixed perpendicular to the y-axis in the z direction and then a displacement was made on the z-axis according to the parameters previously chosen: speed of displacement in mm/s and distance to be traveled.

Quartz cells of 4.6 x 1.25 x 0,3 cm^3 were cleaned subsequently in water, ethanol, acetone, chloroform and water, immersed and sonicated 15 minutes for all solvents. Cell substrates were immersed during 10 min in 400 g/L of the LA in toluene mixture. The dipping program was the same for all samples. A thickness film of approximately 1.5 µm was obtained on each face of the cell substrate so 3 µm in total thickness. Then, all samples, except one, were annealed at 114˚C during 30 min in a vaccum oven. The aim of the un-annealed film was to know if the penetration and dissolution are different with and without annealing time for thick films.

Figure 3.22 – Dip coating, immersion stage (left) and drying stage (right)

Immersion in BA/water

Afterwards, samples were put in vats of 4.6x2.5x0.5 cm^3 containing different concentrations of benzyl alcohol in D_2O (0 %; 0.6 % and 0.7 %) in order to observe the kinetic of swelling or/and dissolution of the polymer film by Small angle scattering (SANS).

3.2.3 Ellipsometry measurement for ultrathin and thin films

Ellipsometry is a specular optical and non-destructive technique suited for the investigation of the thickness and the optical properties of thin and ultrathin films on silicon substrates by measuring the change of parallel and perpendicular polarization upon reflection of collimated light from the sample. The analysis of this polarization change between incident light and reflected light R (eq. 3.1) can reveal the thickness and refractive index of the film by using a stratified layer model (no roughness) and calculating the corresponding polarization changes via Fresnel theory [134] [135].

$$R = \frac{r_p}{r_s} = tan(\Psi)e^{i\Delta}, \tag{3.1}$$

where Ψ is the amplitude and Δ is the phase difference.

Ellispometry measurements were performed on Beaglehole Picometer Light Ellipsometer (Fig. 3.23 using a monochromatic He-Ne laser beam (λ = 633 nm). An angle scan between 35°and 70°, was chosen for every measurement. The Igor Pro 6 software (WaveMetrics) is used on this instrument to evaluate the multi-layer model's data with the sequence Si, SiO_2, LA and air ; including the refractive indices of the materials (n_{si} = 3.882, n_{siO_2} = 1.457, n_{LA} = 1.5 and n_{air} = 1) corresponding to the wavelength used.

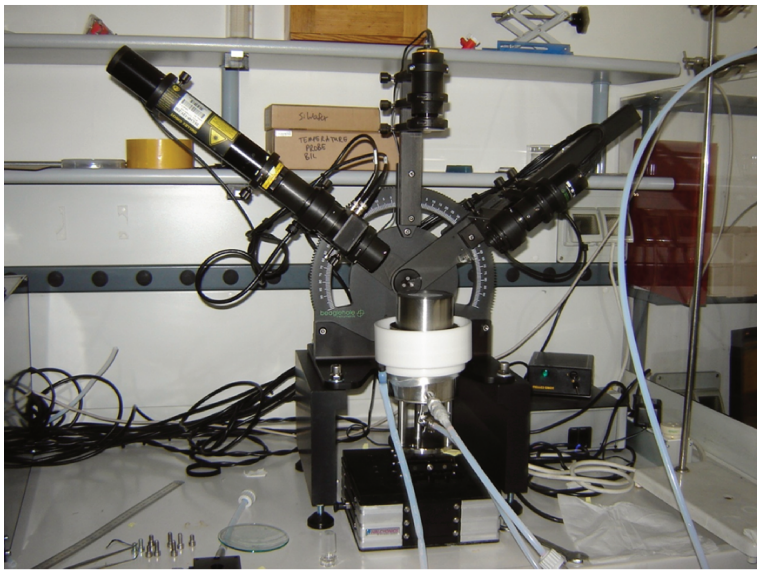

Figure 3.23 – Beaglehole Picometer Light Ellipsometer of ILL

3.2.4 Immersion of samples in BA/water and BA/gel

For NR experiments, ultrathin and thin films were immersed in different concentrations of BA in D_2O (0 %, 0.05 %, 0.1 %, 0.15 %, 0.2 %, 0.25 %, 0.3 %, 0.35 %, 0.4 % and 0.5 %) in situ the NR reflectometer at room temperature (beamtime 1) and in different concentrations of BA in a gel of D_2O (0 %, 0.3 %, 0.5 %, 0.6 %, 0.65 %, 0.7 %) in situ the NR reflectometer at an increasing temperature (16.5 to 75°C) (beamtime 2). For SANS beamtime, thin sample coatings were immersed in different concentrations of benzyl alcohol in D_2O (0 %, 0.2 %, 0.4 %, 0.6 % and

0.7 %) or D_2O+H_2O (0.6 %). The time of immersion of thin films was 2h. To avoid evaporation of solvent after immersion, two polymers wafers were joined, film by film, to form a single film of 1000 nm film. The system was closed with a parafilm film on the joint.

3.3 Instruments and methods of analysis

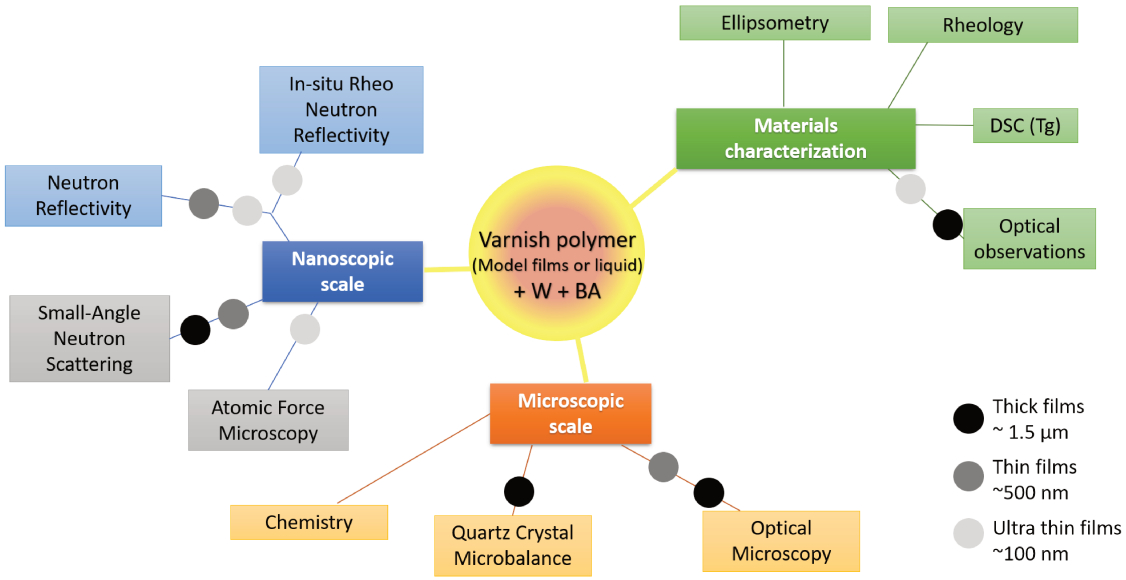

Figure 3.24 – Overall organization chart of project experiences

3.3.1 Neutron scattering measurements on Figaro and N-REX

NR scattering experiments (reflectometry and SANS) were achieved at two neutron institutions : mainly at Institut Laue-Langevin (ILL) [72] (Grenoble, France) but also at Forschungs-Neutronenquelle Heinz Maier-Leibnitz (FRMII) [136] (Garching, Germany) for one beamtime experiment.

FIGARO at ILL

For the study of horizontal surfaces solid/air or solid/liquid interfaces, the majority of NR experiments were performed on FIGARO (Fluid Interfaces Gazing Angles ReflectOmeter) at the ILL showing in the Fig. 3.25. Three experiments were performed on FIGARO between 2016 and 2019. On the time-of-flight (ToF) reflectometer FIGARO[137] at ILL with horizontal sample geometry a wavelength band between 2 Å and 20 Å was used with a relative wavelength resolution of 0.82 % (FWHM). The two dimensional multitube detector allows the measurement of specular and off-specular reflectivity simultaneously. The detector has a size of 25 x 48 cm^2 and a resolution of 2.2 x 4.8 mm^2 (FWHM) at a distance of 2.8 m from the sample. Two reflection angles were used to cover the full q-range: 0.622 and 2.622 degrees. The collimation slits were set to ensure a constant relative angular resolution of $\Delta\theta/\theta = 2\,\%$ and the footprint on the sample was 40x40 mm^2. The raw data was converted to absolute reflectivities as a function of momentum transfer by using the data reduction software COSMOS [83].

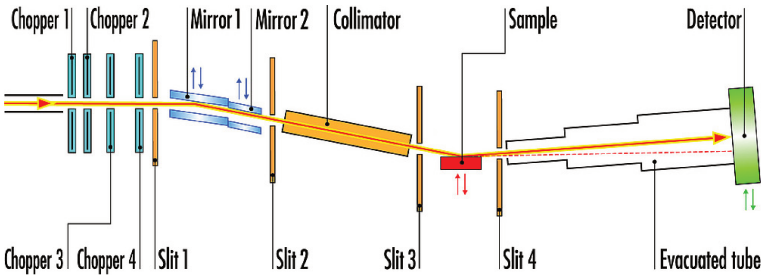

Figure 3.25 – Schematic layout of the FIGARO reflectometer from [72]

Two types of experiments were achieved. The first one, was to investigated polymer films with BA/water in a closed system in situ the instrument. The second was performed to study polymer films with BA/gel of water in situ FIGARO in a closed system (Fig. 3.26) to study the effect of the temperature on the films, and in situ rheo-reflectometry on FIGARO (Fig. 3.27) to study the impact of shear rate on the films removal.

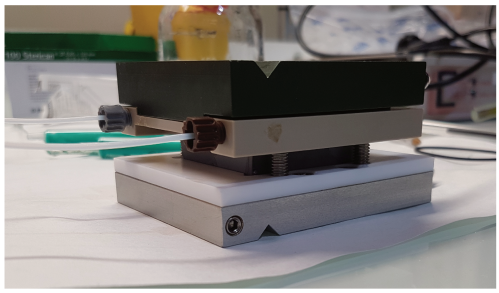

Figure 3.26 – Assembly for the NR study of polymer film in contact with a solution or a gel

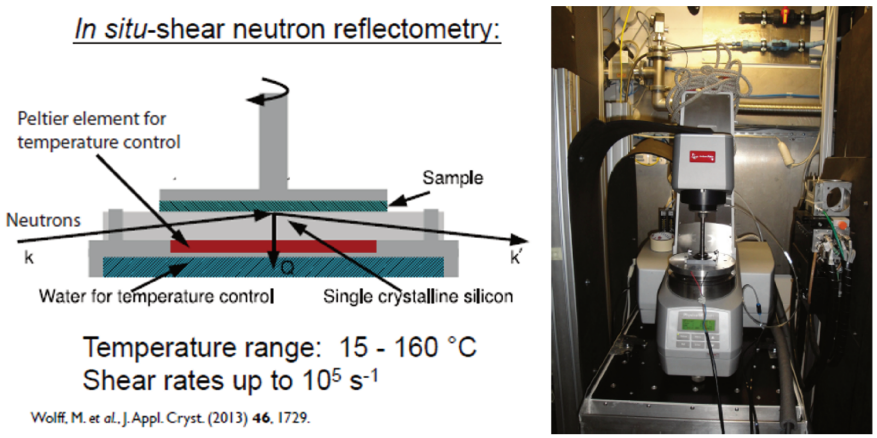

Figure 3.27 – In situ Rheo-reflectometry on FIGARO from reference [138]

N-REX+ at FRMII

N-REX+ [139] (Neutron Reflectometer with X-ray option) at FRMII shown in the Fig. 3.28, is an angle dispersive fixed wavelength (4.4 Å, resolution 3 %) reflectometer with horizontal sample geometry. A 20 x 20 cm^2 position sensitive detector was used allowing for specular and off-specular reflectivity measurements although only the specular data was analyzed here.

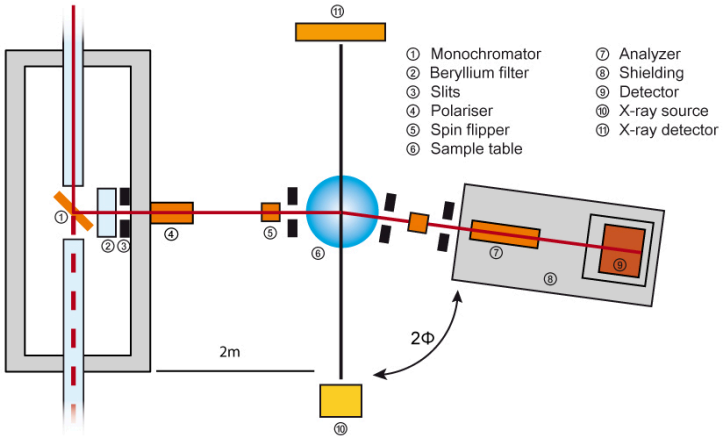

Figure 3.28 – Schematic layout of the N-REX+ reflectometer from [136]

3.3.2 Neutron scattering data analysis

Following the model previously explained in the section 2.1.5 and analysing with MOTOFIT on IGOR Pro 6, NR curves were fitted to find each structural parameter: thickness, SLD and roughness of the layers. The SLDs of silicon dioxide and silicon are given in the literature but SLDs of the LA and water were fitted. The SLDs for the materials used in this study are given in table 6.1.

Table 3.5 – Scattering length densities of the materials used in this study. For LA and D_2O the range of measured values during different experiments is given. In case of BA, silicon and silicon dioxide the literature values are given assuming the chemical composition to be C_7H_8O, Si and SiO_2 with densities of 1.02 g/cm^3, 2.33 g/cm^3 and 2.2 g/cm^3, respectively.

Material	bulk SLD [10^{-6}Å^{-2}]
D_2O	6.1 - 6.25
BA	1.298 (literature value)
Silicon	2.07 (literature value)
Silicon dioxide	3.47 (literature value)
Laropal®A81	0.9 ± 0.1

Instead of the fitted SLD values of the polymer layer the total excess volume fractions of BA ϕ_{BA} and that of D_2O ϕ_{D_2O} inside the varnish layer are reported by applying the following boundary conditions, which assumes constant density and mass conservation of the varnish, obviously only applicable before dissolution of the film:

$$\begin{aligned} &1 + \phi_{D_2O} + \phi_{BA} = \frac{d}{d_{dry}} \\ &\frac{d}{d_{dry}} * SLD = \phi_{D_2O} * SLD_{D_2O} + \phi_{BA} * SLD_{BA} \\ &+\left(\frac{d}{d_{dry}} - \phi_{D_2O} - \phi_{BA}\right) * SLD_{LA}, \end{aligned} \tag{3.2}$$

where, d and d_{dry} are the swollen and dry layer thicknesses, respectively, and SLD_{D_2O}, SLD_{BA} and SLD_{LA} are the swollen SLD and the bulk SLDs of D_2O, BA and LA, respectively.

The total swelling ratios r of the whole film is defined by the layer thickness:

$$r = d/d_{dry}. \tag{3.3}$$

As shown in table 6.1 the SLD contrast between heavy water and all other components is significantly higher than between BA and the polymer. This will dictate the sensitivity of the

measurements mainly towards the distribution of D_2O in this system. This can be readily seen in Fig. 5 in the chapter 4 where a typical NR curve is shown from a 70 nm LA layer in contact with a solution containing 0.2 % BA in heavy water (circles). Clearly visible are the oscillations in the reflectivity profile coming from the total thickness of the polymer film. This curve can be fitted by assuming a molecular smooth interface between the varnish and the liquid as can be seen by the blue line, corresponding to a total roughness of only 0.2 nm. If the roughness of the D_2O profile is only marginally increased to 1 nm the resulting profile shows a significantly worse fit to the data as shown by the broken red line. Also assuming an only 0.5 nm thick D_2O layer between the silicon substrate and the polymer layer leads to a significantly worse fit as can be seen by the green dotted-broken line. This testifies the high sensitivity of this technique to the concentration profile of D_2O inside the layer, significantly better than 1 nm. Concerning the distribution of BA, however, the situation is different. Due to the low SLD contrast it is possible to fit a rather broad interface region inside the polymer penetrated by only BA to the data as can be seen from the black line corresponding to a BA profile roughness of 5 nm keeping the D_2O roughness at 0.2 nm, which is practically indistinguishable from the blue line corresponding to a sharp BA interface. Therefore, the resolution concerning the concentration profile of BA is estimated to be around 10 nm.

The width of the reflected beam was also extracted from the COSMOS data reduction software in order to monitor any broadening coming from buckling of the layer on a length scale of mm or cm [140] or from increased OSS due to in-plane inhomogeneities.

3.3.3 Small angle Scattering measurements on D11

Small Angle Neutron Scattering measures diffracted neutrons at small angles. For it, on D11 at ILL the sample is placed far away the high flow reactor ($\sim$ 140 m) which allows to work at different detector/sample distance (between 1.2 m and 39 m). To investigate the LA polymer film samples of this study, two detector distances were chosen, (a) 8 m and (b) 40 m with a collimation of 8 for (a) and 4 for (b) and a wavelength of 0.6 nm. The scattered intensity is collected by a 2D detector and subsequently transformed to scattered intensity as a function of the q diffusion in $Å^{-1}$. Then, 2D data was normalized by the thickness and the incoherent scattering of D_2O with the software LAMP.

The spectra of the intensity as function of q for each measurement were fitted with a power law $y_0 + Ax^{pow}$, where A is the intensity and x the q, assuming $y_0 = 0$ and pow is between -1 and -4. This makes it possible to trace the intensity A and the q as function of $\Phi_{BA/LA}$.

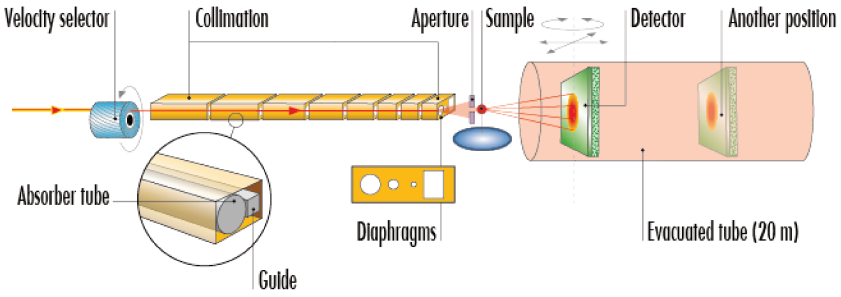

Figure 3.29 – Schematic layout of the SANS reflectometer from [72]

3.3.4 Optical microscopy measurements

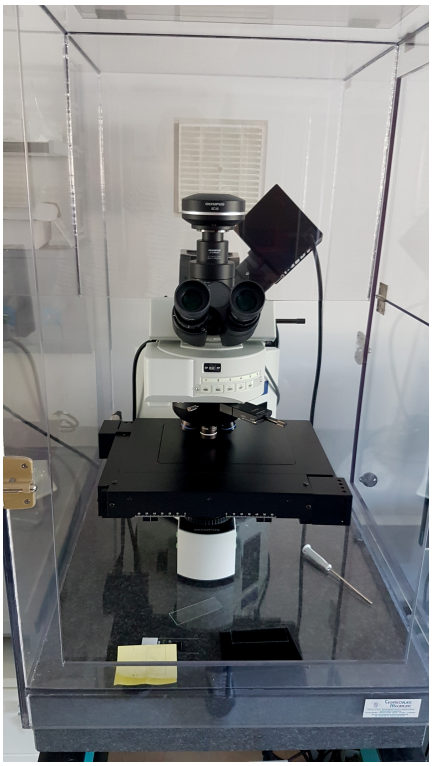

Figure 3.30 – Microscope Olympus BX61 of ESRF at Grenoble

Optical microscopy use visible light to captures photographic images of LA films surfaces before and after immersion by normal light-sensitive cameras on the micrometer scale. After immersion in 0.3 % and 0.5 % BA, ultrathin films was observed by optical microscopy with the Microscope Olympus BX61 of ESRF at Grenoble (Fig. 3.30) at several magnifications (10x, 20x, 50x and 100x) and its associated software. Samples comes from NR experiments.

3.3.5 AFM measurements

Atomic force microscopy (AFM) [141] is used to investigate the dewetting on LA films after its swelling by BA/W mixture. This powerful imaging technique is able to scan the surface of a film by using a sharp tip (< 10 nm) at the end of a cantilever (around 100-500 µm in length). It allows to obtain topographical images of the surface and of the objects or alterations that are on it. The resolution is highly accurate with a scale of the order of a nanometer (Fig. 3.32).

Informations from the surface film is obtained thanks to the electronic attraction and repulsion forces (Van der Waals and steric interactions), generated between the sample and the tip. The tip scans and maps the sample during its displacement in the x, y, z direction. Thanks to piezoelectric actuators, the movement of the sample is very precise. Similarly, the cantilever is fixed at a piezoelectric driver to oscillate at its resonance and its resonant frequency. The cantilever behaves as a damped spring. For soft material structure, the tapping mode is chosen. This mode does an intermittent contact and a high amplitude oscillation which prevents the tip from making a frictional force on the material surface and damaging the sample. The operation of the AFM for the investigation of a polymer film on a Si wafer is shown in the Fig.3.31.

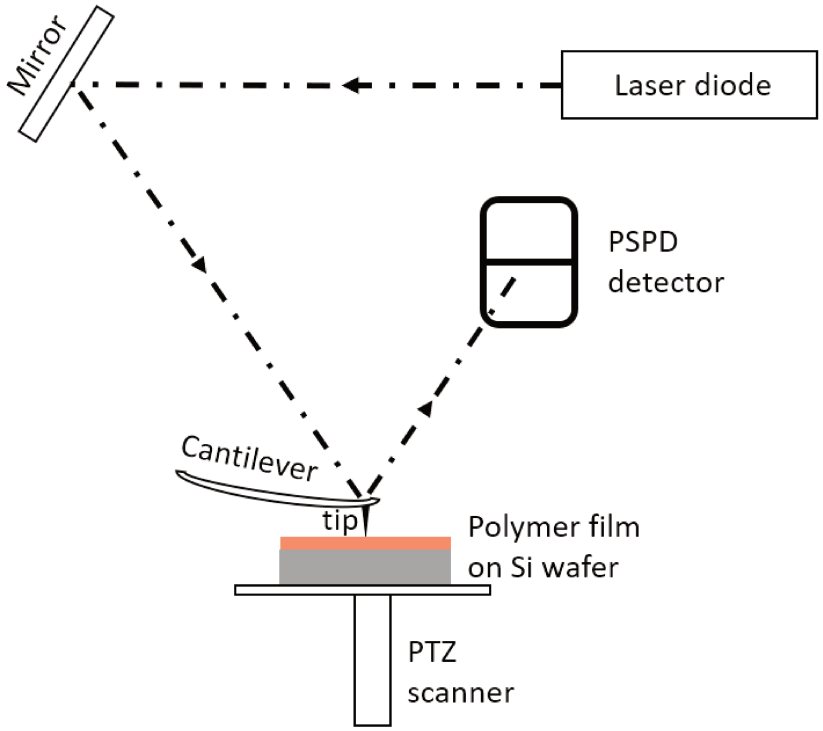

Figure 3.31 – Schematic of AFM, not to scale (according to a figure from [142])

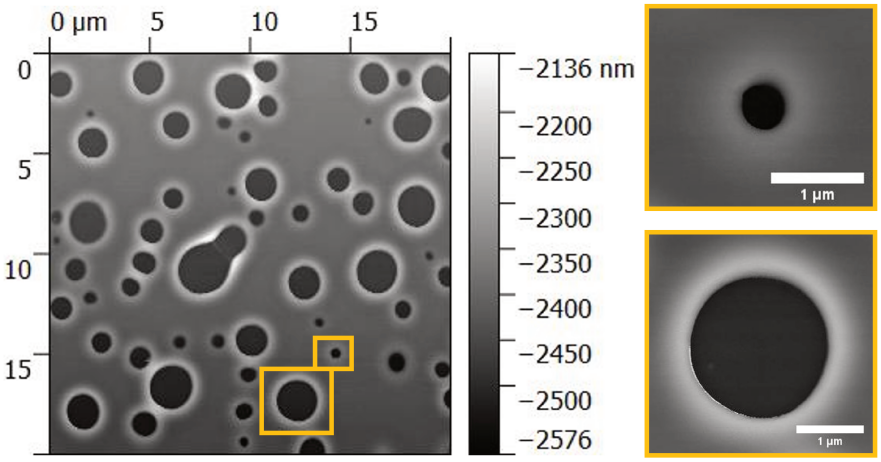

Figure 3.32 – Examples of AFM images of LA polymer surface immersed 19 hours in 0.3 % BA in D_2O obtained by tapping mode

The Veeco Dimension 3100 is an Atomic Force Microscope (AFM) of the ESRF (Grenoble). It was used for the characterization of LA polymer films on Si blocks. This samples were very similar (material, thickness, conditions) to the samples used for NR experiment. LA films of 100 nm were spin coated on 5x5x1 cm^3 Si blocks. One film was immersed in 0.3 % BA in D_2O for 19 hours and the second film was immersed 1 hour in several solutions: deionized water, D_2O, 0.1 % BA, 0.2 % BA and 0.3 % in D_2O. These films were dried by a nitrogen stream just before the measurement. Then, the topological images of the surface of these thin films were achieved in air by tapping mode. It was obtained surface images and profiles of film instabilities (holes) observed on the surface of LA films after immersion few hours in BA/W mixture.

3.3.6 QCM-D measurements

The piezoelectric effect was discovered by the Curie brothers in 1880. A few years after, in 1959, Sauerbrey [143] brought to light the relation between the mass per unit area loaded on a quartz crystal surface and the resonance frequency shift (eq. 3.4) and laid the foundations of QCM for the study of a rigid film in a liquid. The theory and application of quartz crystal microbalance (QCM) is described in the review by Xiaoxi Qiao et al. in 2016 [144].

Quartz Crystal Microbalance, a nondestructive technique, is a sensitive mass balance which allows us to measure the mass per unit area of a material (nanogram to microgram) by oscillation frequency measurement on quartz crystal chips with two electrode sensors and an AT-cut quartz crystal (Fig. 3.33). QCM is based on the piezoelectric effect [145] [146] of 'acentric' materials class crystals of which Quartz is part. By application of a driving voltage between the two electrodes sensors, the quartz crystal is deformed in thickness-shear-mode.

$$\Delta m_f = -C' * \frac{1}{n} * \Delta f, \tag{3.4}$$

where, Δm_f is the mass change, Δf is the frequency change, C' is a constant depending of the crystal used (for a 5 MHz-AT cut quartz crystal at room temperature, $C' \sim 17.7$ ng /(cm^2.Hz)) and is the overtone number.

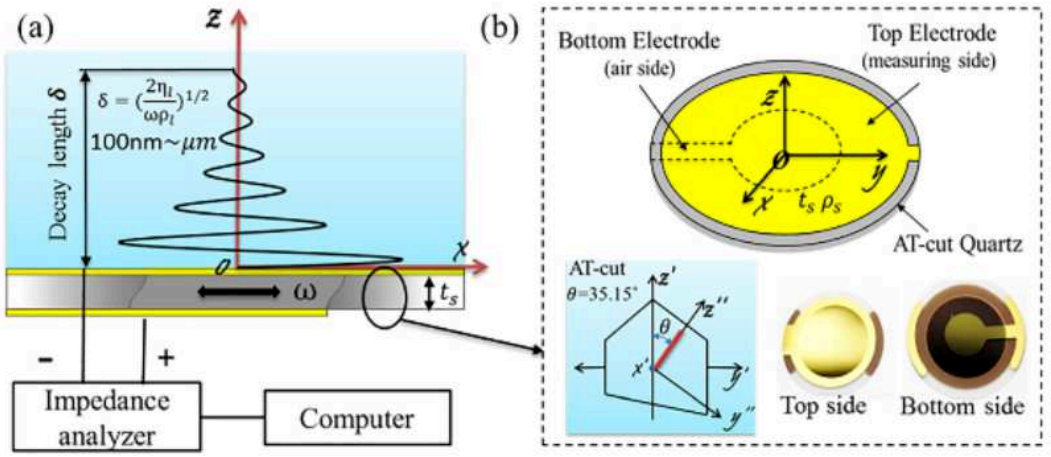

Figure 3.33 – Schematic illustration of (a) the work principle of QCM and (b) the quartz crystal ship from reference [144]

LA films of 500 nm were deposited on the quartz crystal surface by spin coating taking care of previously protect the At-cur Quartz (Fig. 3.34). Samples were annealed 30 min at 114°C being careful not to shock the fragile sensor thermally. Frequencies change of LA films in an increasing BA/D_2O concentrations were monitored for a few hours on the QCM-D.

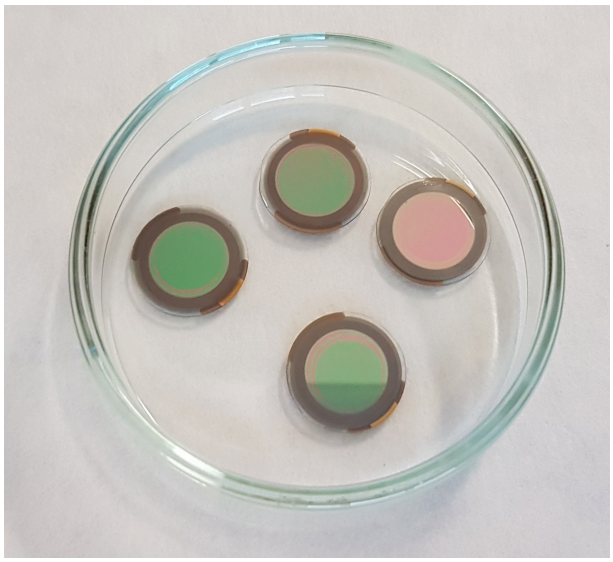

Figure 3.34 – QCM Samples

3.3.7 DSC measurements

The DSC (Differential scanning calorimeter) is a thermal analysis tool to investigate the amorphous and crystalline behaviour of materials such as polymers, food products, nanomaterials and other industries by temperature change.

Some pellets of LA81 resin was previously placed in contact of a small concentration of BA (0 %, 0.4 %, 0.6 %, 0.8 % and 1 %) in D_2O. 4 mg of LA81 samples resin, with and without immersion in BA solutions (0.3 %, 0.5 % and 0.7 %), were loaded into aluminium capsules previously weighed which are then sealed. One by one, a sample and an empty closed aluminium reference capsule were placed in a DSC instrument at room temperature. The samples were heated between 0˚C to 130˚C at a rate of 10˚C/min in four separate runs. The glass transition temperature (T_g) was obtained from the average of the second, third and fourth runs using TA Instruments Thermal Advantage (Fig. 3.35).

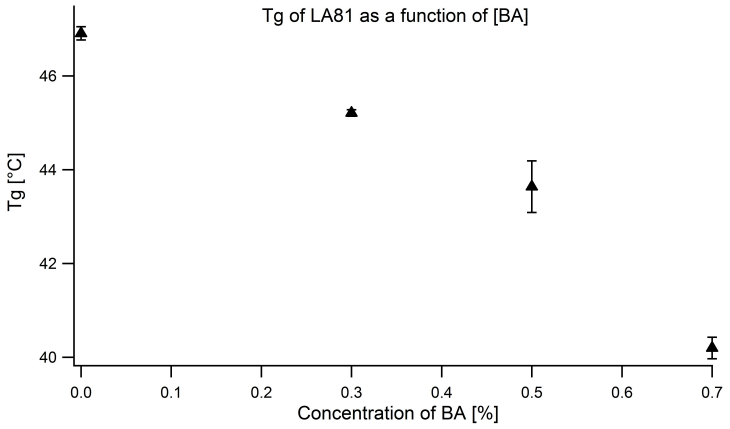

Figure 3.35 – Tg of LA81 before and after immersion in a small quantity of BA (0 %, 0.4 %, 0.6 %, 0.8 % and 1 %) in D20

3.3.8 Rheometer measurements

Rotary rheometer

The characterization of the gel was made on the rheometer AR-G2 by TA Instruments from the Laboratoire de Rhéologie et Procédés, Grenoble. It was chosen to use the geometry cone-plane (Fig. 2.15).

Rotary rheometry is most used for measuring the viscosity of the material studied (gel, polymer, etc.). It allows to make a relation between the stress and the deformation. It presents mainly two geometries, cylinder-cylinder and cone-plane. The use of one or the other depends of the type of sample and the viscosity expected by eyes. The cone-plane geometry (Figure 2.15) is the most appropriate to use for this study because it allows a constant shear rate to be maintained in the space between the cone and the plane, whatever the angle θ and the radius R of the plane.The viscosity measurement is done by measuring the combined amount of the couple γ and the rotation speed ω. For this, one of the two is imposed. It depends of the rheometer. The theory of rheology was previously exposed in 2.3. For this project, the rheometer chosen imposed the stress via the geometry cone-plane (Fig. 2.15) and thanks to a rotary motor. The material is then deformed and its displacement or the resulting torque is recorded and processed by the software.

Capillary rheometer

Theory of capillary rheometry is given in the part 2.3. In order to propose a ternary phase diagram model, the three Flory-Huggins interaction parameters in LA(3)/BA(2)/W(1) systems is determined by combining both viscosity measurement with a capillary rheometer and Flory-Huggins energy calculation. Viscosity of a homogeneous solution of LA/BA at very low polymer concentration (0.1 %, 0.2 %, 0.4 %, 0.6 %, 0.8 % and 1 % LA) is obtained by capillarity measurements at 25.2°C $\pm$ 0.1°C allowing the calculation of the intrinsic viscosity of LA as function of the concentration of LA in BA showing in Fig. 3.37. A Ubbelohde capillary rheometer n°538-20 of the LRP was used. Its range was from 4 to 6 mm^2/s which corresponds to a capillary tube of 0.70 mm.

The Ubbelohde capillary rheometer consists mainly of three tubular parts. The main one is the capillary tube (on the right in the Fig. 3.36) because it is the part where the measurements of the fluid travel time are made between the marks A and B. A liquid is placed into the sphere of the pre-flows above the mark A. Once the pressure is removed, the fluid begins its descent towards the capillary tube (down), subjected to gravity. The measurement begins at the moment where the fluid passes the mark A. The time taken for the liquid to travel from mark A to mark B is recorded with a ViscoClock, an electronic timer for determining absolute and relative viscosity which automatically measures the flow time through the viscometer of the liquid at a fixed temperature with a high resolution of 0.01 second. The kinematic viscosity is deduced from the measured passage time following this formula $\upsilon = K(t - \delta)$ with K = 0.1, the constant relating to the capillary used and δ = 0.12, the kinematic energy correction which is function of the passage time.

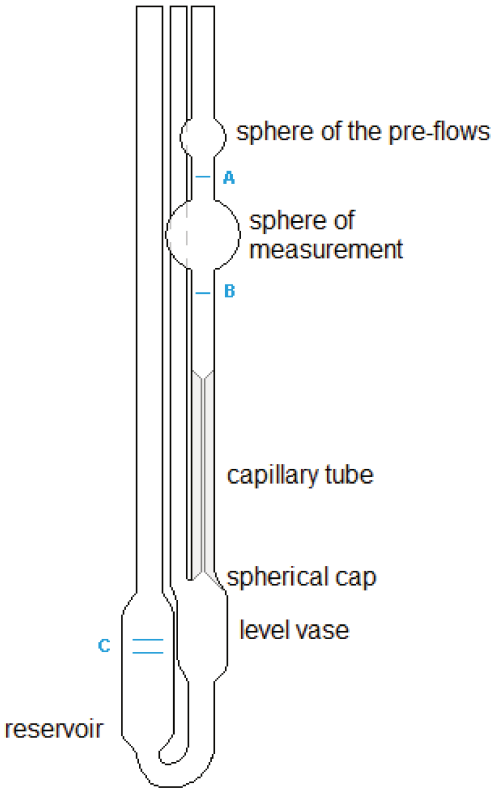

Figure 3.36 – Schema of Ubbelohde Viscosimeter with A and B the upper and lower measurement marks and C the limit of the reservoir

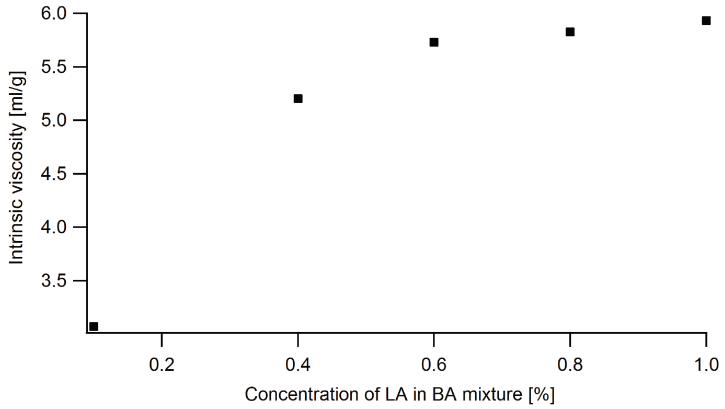

Figure 3.37 – Intrinsic viscosity of LA as a function of LA concentration in BA mixture.

CHAPTER 4
SWELLING, DEWETTING AND BREAKUP IN THIN POLYMER FILMS FOR CULTURAL HERITAGE

This chapter is focused on the first paper of this project which was submitted the 2 October 2019, accepted the 25th November 2019 and published the 13th January 2020 in Soft Matter in the issue 16 on pages 1485 - 1497 [13]. In addition, this paper gave rise to a web story on the ILL page, an article in the Sunday Telegraph by Dalya Alberge on March 15, 2020 and on the website, an article in the Picture Perfect of the Laboratory News on may, 2020 (pages 20-21), an article entitled "Gentle approach to the restoration of valuable paintings" in the Farbe und Lack and an article online entitled "Protecting works of art with neutrons" in the pro-physik.de website.

The aim is to understand the macroscopic and nanoscopic behaviors of a film of a polymer (Laropal®A81) currently used in the Cultural Heritage and more particularly as a varnish coating on paint layers. Ultrathin films were observed in different conditions: annealed a few minutes, immersed in water and the most important result, immersed in BA/water mixture. It represents a long research work and leads in particular to the analysis of the reflectivity data. It also shows the use of a large number of techniques and materials (NR, DSC, low viscosity polymer viscosity measurement, Optical Microscope and AFM) leading to exploitable results and consistent discussion about the kinetics of swelling of the film and the distribution profiles of solvent (BA) and nonsolvent (heavy water) inside the polymer.

This work reveals at a certain BA concentration the apparition of holes with a significant bump on the polymer films models and that after immersion few hours in BA/water. These holes was observed by Optical microscope and AFM. Holes with bump is characteristic of a dewetting process of thin polymer film.

Soft Matter

ARTICLE TYPE

Cite this: DOI: 10.1039/xxxxxxxxxx

Swelling, Dewetting and Breakup in thin polymer films for cultural heritage

Amélie Castel[1,3], Philipp Gutfreund[1*], Bernard Cabane[2] and Yahya Rharbi[3*]

Received Date
Accepted Date

DOI: 10.1039/xxxxxxxxxx

www.rsc.org/journalname

The removal of ultrathin amorphous polymer films in contact with nonsolvent/solvent binary mixtures is addressed by means of neutron reflectometry and atomic force microscopy. The high resolution of neutron scattering makes it possible to resolve the distribution profiles of heavy water and benzyl alcohol inside Laropal®A81, often employed as a protective varnish layer for Culture Heritage in restoration of easel paintings. The swelling kinetics and distribution profiles were recorded as a function of time and increasing benzyl alcohol concentration in water. The varnish film swells by penetration of the good solvent. At higher concentrations water-filled cavities appear inside the varnish and grow with time. Contrary to homogeneous dissolution dewetting is observed at late stages of exposure to the liquid which leads to the Breakup of the film. The high resolution measurements are compared to bulk behaviour characterized by the ternary phase diagram and the Flory-Huggins interaction parameters are calculated and used to predict the swelling and solvent partition in the films. Distinct differences of the thin film to bulk behaviour are found. The expectations made previously for the behaviour of solvent/non-solvent mixtures on the removal of thin layers in the restoration of easel paintings should be revised in view of surface interactions.

Keywords: Art restoration; Diffusion; Laropal®A81; Neutron reflectivity; Polymer; Solvents; Swelling; Ternary Phase Diagram; Thin film

1 Introduction

Thin films of glassy polymers or varnishes are frequently used to protect a substrate from physical or chemical agents. They can be deposited through a variety of techniques, usually involving a liquid to solid transition of a solution of the polymer in a volatile solvent.[1] It appears that the removal of such thin films has not been studied as extensively as their deposition, although there exists a detailed review of polymer dissolution.[2] Yet there are many fields where a better control of polymer dissolution and removal is highly desirable: industrial applications[3] such as the fabrication of microchips, the recycling of plastics and the manufacturing of polymer membranes, and also biomedical applications such as the tissue regeneration and drug delivery.[4]

A particularly demanding field is the restoration of works of art[5 6 7 8], particularly old paintings that have been altered by exposure to ambient conditions (urban air, humidity) over very long periods of time. Indeed, the varnish layers that ancient painters have applied originally to protect the paintings may deteriorate in many ways: capture of airborne particles[9], formation of microcracks or change in color and acidification[5] just to name a few. The classic restoration treatment consists in removing most of the old varnish layers and replacing them with a fresh varnish, which will restore the protective and aesthetic functions. The removal of the old varnish is achieved through the addition of solvents, which enter the solid varnish and transform it into a liquid polymer solution. A condition for safe removal of the old varnish is that it should have no effect on the pictorial layer. This raises a question regarding the depth of penetration of the solvent that has been applied to the film. The quantity of solvent applied by the restorer is adjusted to liquefy a certain number of varnish layers, but not all of them; however, controlling the quantity of solvent does not imply that the penetration depth is controlled.[7 8 10] A safe varnish removal would have full respect for the integrity of the innermost varnish layer, which means that the solvent would never reach it. At present, they are few studies that give indications of whether or not this condition is met.[5 11 12 13]

In recent years, restorers have employed two approaches to this problem: On the one hand, they have tried to decrease the chem-

[1] *Institut Laue Langevin, Grenoble, France.*
[2] *ESPCI ParisTech, Paris, France.*
[3] *Laboratoire de Rhéologie et Procédés, Grenoble, France. (a) Univ.Grenoble Alpes – LRP, F-38041 Grenoble, FRANCE (b) CNRS, LRP , F-38041 Grenoble, FRANCE*
∗ gutfreund@ill.fr, rharbi@ujf-grenoble.fr

ical potential of the solvent, and thus make it less aggressive to the inner layers of the painting. Accordingly, the restorer may dilute the solvent with a bad-solvent for the varnish [14] and, by trial and error, determine which compositions and volumes of solvent mixtures appear to be harmless to the pictorial layer at the time of observation. [15,16] On the other hand, some restorers are using delivery systems for the solvent, such as hydrogels, sponges or nonwoven fabrics that contain the solvent. Several studies propose to use a solvent/water system to reduce the toxicity of the process to the operators. [17] However, the effects of a solvent/nonsolvent mixture may not be extrapolated from those of a solvent alone, especially when the nonsolvent is water. In order to understand and model these phenomena, it is necessary to use a technique that makes it possible to measure the depth of solvent and nonsolvent penetration in the films with a high special resolution. Ultimately, it should be possible to construct a model that takes into account the relative locations of all molecules in the films and their interactions, and makes it possible to predict the spatial and temporal features of the dissolution process. For very thick films, the imaging of the film during dissolution through Fourier Transform Infra-Red spectroscopy (FTIR) has produced spectacular maps showing the locations of macromolecules and of the solvent and nonsolvent molecules in the films. These maps have revealed different patterns of dissolution depending on the solvent/nonsolvent composition [18]; they also show that dissolution/condensation processes have a large effect on the dissolution rates. [18,19] However, the experiments by FTIR imaging have a limited spatial resolution and, in addition, the films ($\sim$ 150 nm) were sandwiched between two salt plates, which is far from the coating procedure employed in varnishes. Usually varnish films are deposited through classical coatings techniques.

Neutron reflectometry (NR) is a technique that yields both structural and chemical information thanks to targeted hydrogen/deuterium (H/D) labeling. It is an ideal tool to observe the solvent penetration in real time and has already proven this in similar experiments. [6,20,21] It is a non-destructive and non-invasive technique for the investigation of thin polymer films. It is a powerful technique for the study of liquid/solid and liquid/liquid interfaces with a resolution of a few ÅngstrÃ¶ms. For aqueous systems the replacement of water with heavy water can yield an excellent contrast. In addition, NR makes it possible to record the kinetics of the transformations that take place between the initial and the final state of the films. To complement the NR results optical and atomic force microscopy (AFM) is also used in this study together with thermodynamic calculations based on the bulk ternary phase diagram. Note that while NR gives a statistically averaged concentration depth profile over a large area AFM gives a local snap-shoot of the surface morphology. Therefor NR is essential for a complete view of the system.

What we would like to obtain from the NR is the concentration profiles of solvent and nonsolvent, and a detailed picture of the solid-liquid transition in the varnish layer as a function of solvent uptake. This transition may be quite different from the solid-liquid transitions of non-polymeric materials. Unlike non-polymeric materials, polymers do not dissolve instantaneously and the classic dissolution process of a polymer involves transport processes, namely solvent diffusion and disentanglement of the polymer chains. [1] The first stage is penetration of a few solvent molecules that plasticize the polymer. As a result, the macromolecules can cross the polymer/solvent interface. If the molecular weight of the polymer is high enough, they will form a gel layer at the surface of the film. The next stage is the disentanglement of the macromolecules and their escape from the gel layer into the solvent. But there are also cases where the polymer cracks before any gel layer is formed. At present, we do not know which is the dissolution process (i.e. with or without a gel layer) of thin and ultrathin varnish films.

Motivated by new emerging technologies the physics of swelling and dissolution of thin polymer films has been the subject of several literature reports. [2,18,19] It involves the synergy between several interconnected phenomena: solvent/polymer interaction, polymer dynamics, molecular and macromolecular diffusion in glassy material and the physics of the glass transition in the presence of solvent moieties. This problem becomes even more intriguing in ultrathin films because of the dimensional reduction, the confinement and the surface/polymer interactions. Because there are several indications that confinement in ultrathin films induces deviation of several polymer properties (glass transition, polymer dynamics, thermal expansion) one might question how confinement affects swelling and dissolution. The behavior of the varnish in dissolution largely depends on the polymer mobility inside the films. Initially the varnish polymers are in an amorphous glassy state where the glassy dynamic inhibit chain mobility and the amorphous structure leads to a good transparency. The glassy state is characterized by a glass transition temperature (T_g). The intrusion of small solvent molecules with a low T_g will eventually reduce the T_g of the system below ambient temperature. When this happens the varnish polymer will cross to a gel or liquid state with substantial chain mobility. In the vicinity of non-adsorbing interfaces, the glass transition temperature is lower than in the bulk and therefore ultrathin polymer films may cross the solid-liquid transition earlier than thick films. [22,23,24,25] There remains some controversy on the variation of T_g as a function of distance to the interface in ultrathin polymer films. [26,27,28] There may also be an effect of the Van der Waals attractions between the film and its substrate. [29,30,31] If a binary solvent is used the situation becomes even more diverse because of three-body interactions in such confined systems.

Here we present a quantitative characterization of the swelling and dissolution mechanisms of supported ultrathin films of the amorphous glassy polymer by solvent/nonsolvent mixtures. This work is carried out on a glassy amorphous varnish Laropal®A81 (LA) to address the scientific aspect of varnish removal from easel paintings which is one of the most destructive treatments in the field of art restoration. We use time-resolved neutron reflectometry to probe the swelling kinetics of supported thin LA films (70 - 200 nm) on silicon substrates by mixtures of benzyl alcohol (BA) and deuterated water (W). The quantitative analysis of the NR spectra reveals two very distinct swelling regimes at low and intermediate solvent concentrations: At low solvent concentrations the varnish is penetrated by the good solvent (BA) and exhibits only swelling perpendicular to the interface followed by a verti-

cal swelling at higher BA concentrations. At these stages no water penetration is visible. The delay in vertical swelling is explained by swelling asymmetry induced by polymer adsorption to the substrate by van der Waals (VdW) forces.

At higher BA concentrations instead of a continued swelling and dissolution a dewetting type process starts leading to the appearance of holes in the polymer film filled with water. These holes grow with time and/or BA concentration and eventually the bulk of the film departs into the liquid phase leaving only some islands or droplets on the subtrate.

2 Experimental

2.1 Materials

The Laropal®A81 polymer (LA) from (BASF)[32] is a synthetic thermoplastic polymer synthesized from urea, isobutyraldehyde, and formaldehyde. Size-exclusion chromatography (SEC) analysis of this polymer yield Mw = 3640, and Mn = 1266 Da.[33] Its molecular structure was detailed in reference.[34] The T_g measurement was carried out on a Mettler-Toledo DSC823 apparatus in Nitrogen gas environment in the heating mode. This yields a T_g value of 47 °C. The LA density is 1,1 g/cm^3 at 20°C. Its reflective index is 1.503.[35,36] As solvents, Benzyl alcohol (Sigma-Aldrich, 99.8 %), deuterated water (Eurisotop ref D214L, 99,9 % D) and doubly deionized water were used in these experiments.

2.2 Thin film preparation and characterization

Laropal®A81 thin films were prepared by spin-coating using Delta 6 RC TT (SÜSS MicroTec Lithography GmbH).[37] The substrates (Sil'Tronix France) 8x5x1 cm^3 and 5x5x1 cm^3 single crystal silicon blocks (Si) were rigorously cleaned before spin-coating subsequently sonicate in water plus one drop on Decon 90 mixture, clean water, ethanol, acetone, chloroform and ending with clean water during 15 min for each products and dried at room temperature. The LA/toluene solutions at 30g/L and 80g/L were spin-coated at 2250 rpm for 44 seconds at room temperature (21°C).[38] Film thicknesses were measured using a Beaglehole Picometer Light Ellipsometer with a monochromatic laser beam. Note that the final film thickness prepared from the same solution on a 2 inch wafer of 0.7 mm thickness was not the same as the one prepared on a 10 mm thick silicon block. Therefore the size of the substrate clearly has an influence on the spin-coated polymer film. In the following only results obtained on 10 mm thick Si blocks are shown. The film thickness was found to be uniform (<10 % thickness variation over the whole film), this yields two set of films with thicknesses ∼ 70 nm and ∼ 230 nm. Given the commercial origin of the polymer the sample preparation is delicate. A large number of samples was prepared in advance of neutrons experiments and only samples that showed a homogeneous dry layer in water were used in this study.

2.3 Neutron Reflectometry

In NR a collimated neutron beam (incident beam) is directed at the Si/LA/W interfaces through the Si block, which is practically transparent for neutrons, with an incident angle θ and the reflectivity profile of the reflected beam at an exit angle $\theta_f = \theta$ equal to the incident angle is measured as a function of the momentum change perpendicular to the polymer film surface (see Fig. 1). As can be seen in the figure the difference in momentum normal to the surface before (k_i) and after (k_f) neutron reflection can be defined:

$$q_z = \frac{4\pi}{\lambda} * \sin(\theta). \quad (1)$$

A range of q_z values can be obtained either by varying the neutron wavelength λ (time-of-flight (ToF) method) or by varying the incident angle θ at constant wavelength (monochromatic method). NR experiments were performed on FIGARO at the Institut Laue-Langevin (ILL), Grenoble, France, and on N-Rex$^+$ at the Forschungs-Neutronenquelle Heinz Maier-Leibnitz (FR rching, Germany. On the ToF reflectometer FIGARO[39] with horizontal sample geometry, a wavelength band between 2 Å and 20 Å was used with a relative wavelength resolution of 2.1 % (FWHM). The two dimensional multitube detector allows the measurement of specular and off-specular reflectivity simultaneously. The detector has a size of 25 x 48 cm^2 and a resolution of 2.2 x 4.8 mm^2 (FWHM) at a distance of 2.8 m from the sample. Two reflection angles were used to cover the full q-range: 0.622 and 2.622 degrees. The collimation slits were set to ensure a constant relative angular resolution of $\Delta\theta/\theta = 2\,\%$ and the footprint on the sample was 40x40 mm^2. The raw data was converted to absolute reflectivities as a function of momentum transfer by using the data reduction software COSMOS.[40] N-REX+[41] at FRM2 is an angle dispersive fixed wavelength (4.4 Å, resolution 3 %) reflectometer with horizontal sample geometry. A 20 x 20 cm^2 position sensitive detector was used allowing for specular and off-specular reflectivity measurements although only the specular data was analyzed here.

LA Films on silicon blocks were first measured in air and then in D_2O. Subsequently, the LA films were measured in solutions of D_2O containing an increasing BA concentration ϕ_{BA-W} (0 %, 0.05 %, 0.1 %, 0.15 %, 0.2 %, 0.25 %, 0.3 %, 0.35 %, 0.4 % and 0.5 %). All NR samples were measured at room temperature (21 °C). Time resolved NR spectra were integrated over 5 min and the measurement repeated several times between 1 h and 12 h in total.

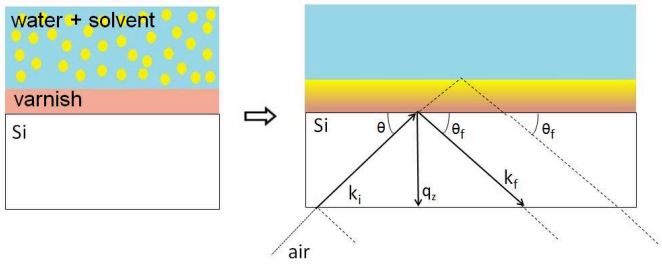

Fig. 1 Sketch of the specular reflection geometry at the water/polymer/Si substrate system. Note that the reflection angles are exaggerated for illustration, in a real experiment the neutron beam enters and leaves the silicon substrate from the sides rather than the bottom.

2.3.1 Analysis of specular reflectivity

The measured NR data is subsequently compared to simulated NR curves calculated by an optical matrix formalism from a slab

model[42] and the goodness of the fit is calculated. This least-squares fitting procedure is repeated until a convergence is found by using MOTOFIT.[43] The model used here to fit the NR curves consists of an infinitely thick single crystal silicon slab covered by a thin layer of silicon dioxide, which thickness varied between 1 nm and 2 nm among the samples, and a layer of swollen LA on top capped by an infinite layer of D_20/BA. The fitting model uses several fitting parameters, the BA and D_2O concentration profiles in LA, the thickness and the roughness of each layer. Several models can be chosen to describe the solvent profiles within the film: constant concentration , a linear, adsorbed or brush model.[44,45] In the first stage the constant profile model was used to quantify the average film thickness and concentrations and the interface roughness. Each of the layers was fitted by allowing its thickness and roughness to change until convergence was found. The SLDs of silicon dioxide and silicon were fixed at the corresponding literature values reported in table 1 and the SLDs of the swollen LA and D_20/BA phases were fitted. The thicknesses and the roughness of all layers were fitted as well. The silicon substrate and silicon dioxide were found to be atomically smooth (between 0.2 nm and 0.5 nm) and therefore are not discussed further. In an other set of analysis, a concentration profile of the solvent within the film was added to the three steps profile described above (Si/LA/W), including the roughness of the Si/LA and LA/W interfaces, and the resulting reflectively data was compared to the experimental one.

Table 1 Scattering length densities of the materials used in this study. For LA and D_2O the range of measured values during different experiments is given. In case of BA, silicon and silicon dioxide the literature values are given assuming the chemical composition to be C_7H_8O, Si and SiO_2 with densities of 1.02 g/cm^3, 2.33 g/cm^3 and 2.2 g/cm^3, respectively.

Material	bulk SLD [10^{-6}Å^{-2}]
D_2O	6.1 - 6.25
BA	1.298 (literature value)
Silicon	2.07 (literature value)
Silicon dioxide	3.47 (literature value)
Laropal®A81	0.9±0.1

From the combination of the fitted film thicknesses and SLD values, the volume fractions of BA ($\phi_{BA/LA}$) and D_20 ($\phi_{W/LA}$) are calculated assuming mass conservation of the polymer (equation 4). This assumption is obviously applicable only before film dissolution or breaking.

Starting from 0.3% of BA in water a single polymer layer model was not giving satisfactory fits to the NR data anymore. For higher concentrations the LA layer was split into three sub-layers with individual SLDs, roughness and thickness. In these cases the mass conservation of LA was not assumed anymore, but instead it was assumed that the polymer thickness swelling is solely due to BA uptake (no thickness swelling due to water).

The total vertical swelling ratios ϕ_{total} is calculated using the swollen and the non swollen film thicknesses:

$$\phi_{total} = h/h_0 \tag{2}$$

, h being the swollen film thickness and h_0 the initial dry thickness.

2.3.2 Off-Specular neutron reflectivity

As the neutron reflectivity spectra were recorded using 2D detectors the off specular neutron reflectivity (OSS) is also accessible.[46] The OSS intensity corresponds to the intensity scattered at a condition were $\theta_f \neq \theta$. In this case the total momentum transfer also comprises an in-plane component:

$$q_x = \frac{2\pi}{\lambda}(\cos\theta_f - \cos\theta). \tag{3}$$

This allows one to determine SLD variations parallel to the interface but due to the geometry the momentum transfers are typically two orders of magnitude smaller than in specular reflectometry and therefore the spatial resolution is much lower probing micrometer sized structures. The width of the reflected beam was also extracted from the COSMOS data reduction software in order to monitor any broadening coming from buckling of the layer on a length scale of mm or cm.[47]

2.4 Ternary phase Diagram

The LA/BA/W ternary phase diagram was measured using turbidity measurements at room temperature. LA/BA mixtures with different concentrations were prepared by dissolving LA pellets in BA solution between 10 % and 80 % LA under rigorous agitation for more than 48h. Hydrogenated water was added drop-wise to LA/BA solutions in a 15 mL clear Vial (2 cm in diameter and 7 cm in height) and the mixture was agitated and then left to rest for several hours. The turbidity of the solution is monitored for each step until turbidity appears. Because of the high viscosity above 55 % LA only samples below 50 % were considered in this study. The quantification of the second single phase in the water rich corner of the ternary phase diagram was carried out by dissolving aliquots of LA powder in BA/water solutions at 0.5 % and 0.1 % at room temperature. The limit of the binodal curve was taken as the solubility limit of LA in the BA/water.

2.5 Viscosity measurement

The simulation of the ternary phase diagram requires knowing the LA/BA Flory-Huggins (FH) interaction parameter χ_{LA-BA} which is calculated using the concentration dependence of the intrinsic viscosity and the method proposed in reference.[48] Viscosity of diluted LA in BA solution (0.1 %, 0.2 %, 0.4 %, 0.6 %, 0.8 % and 1 % LA) were measured in an Ubbelohde capillarity viscosimeter (n° 538-20) at room temperature. The flow time is measured automatically with a resolution of 10 ms. The kinematic viscosity is deduced from the measured passage time following this formula $\upsilon = K(t-\delta)$ with K = 0.1 and δ = 0.12.

2.6 Optical microscopy observations

After immersion in 0.3 % and 0.5 % BA, ultrathin films was observed by optical microscopy with the Microscope Olympus BX61 at several magnifications (10x, 20x, 50x and 100x) and its associated software.

2.7 Atomic Force Microscopy (AFM)

Similar to NR experiment, LA films of 100 nm were spin coated on 5x5 cm Si block and subsequently immersed in 0.3% BA in D_2O during 19 hours and finally dried by a nitrogen stream just before the measurement. Then, the surface of this thin film was investigated in air by a Veeco Dimension 3100 operated in tapping mode.

3 Results

3.1 Effect of thermal annealing

Ultrathin polymer films were deposited by spin-coating onto silicon single crystals. These films were then annealed at 114°C for 30 min. Optical microscopy observation shows that the films do not de-wet from the silicon substrates during annealing, despite the fact that they were in the fluid state, and regardless of their thickness, in the range between 50 - 1500 nm and therefore one can consider the thin LA films to be in thermodynamic equilibrium in air. Fig. 2 shows the NR data of a spin-coated thin film before and after annealing at 116°C for 30 min. No apparent dewetting[49] was noticed corroborating the optical microscopy observation. On the other hand the quantitative analysis of NR spectra for films between 70 and 232 nm reveals 14-16 % reduction of the film thickness of upon annealing. This could either be due to evaporation of entrapped solvent or due to a collapse of the out-of equilibrium structure induced by spin-coating.[50] However, mass density differences due to different chain conformations are unlikely to produce a 15 % difference. In fact, NR has shown that toluene retention in spin-coated amorphous polymers depends on both molecular structure and film thickness. For example, toluene retention in freshly spin-coated films was found to be few percent (<3 %) in polymethyl methacrylate (PMMA) and almost nothing in polystyrene (PS). The high toluene retention in LA films (14-16 %) compared to PMMA and PS, suggests a low toluene diffusion in LA. Indeed, making thick LA films by evaporation from toluene solution at room temperature was found to take more than a year, comforting the high toluene retention observed in the NR experiment. In the following all reflectivity experiments are carried out on pre-annealed films.

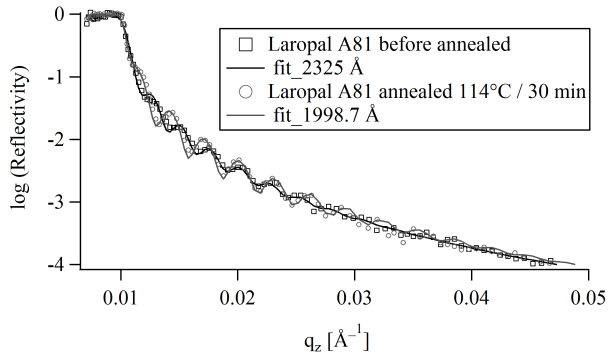

Fig. 2 Neutron Reflectivity from a polymer film of LA in air before and after annealing (114℃ /30 min). The modelling of the data (solid line) shows a reduction of film thickness from initially 232 nm to 200 nm.

3.2 Swelling in pure water

To understand the role of water in the swelling and dissolution of LA films, the reflectivity was first measured on films immersed in pure D_2O for a period ranging from 10 min to 12 h (Fig. 3). The analysis of the NR spectra shows that, upon immersion in D_2O, the fitted film thickness does not increase, within the detection limit of NR experiment, which in this case is about 0.5 % or 4 Å for a total film thickness of 70 nm. Moreover, the width of the reflected beam remained unchanged pointing to the absence of buckling, which again corroborates the observed absence of water swelling. The absence of any significant swelling after 12 h of immersion raises the question of whether this is an equilibrium or a kinetic property, resulting from slow diffusion of D_2O in the vitreous polymer. By taking a typical value of the diffusion coefficient of small molecules in a glassy polymer (10^{-12} m^2/s) and calculating the time necessary to reach equilibrium, a characteristic equilibrium time of 10 ms is obtained. This time is many orders of magnitude shorter than experimental times scales (5 min). Accordingly, the low water absorption by ultrathin films of LA must be due to unfavorable interactions between LA and water.

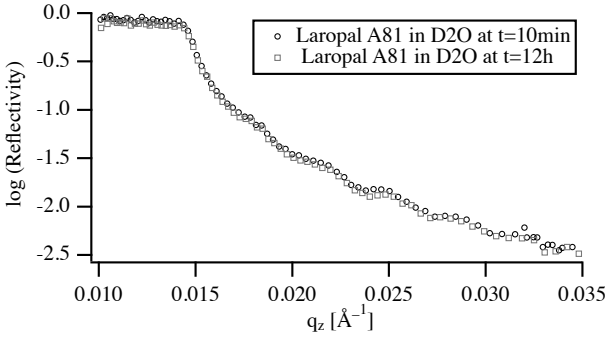

Fig. 3 Neutron reflectivity from a 200 nm polymer film of LA immersed in D_2O.

3.3 Swelling in binary W/BA mixture

In contrast to pure water, the features of the NR spectra of films immersed in W/BA solutions point to a significant swelling, which is clearly enhanced with increasing $\phi_{BA/W}$. A quantitative analysis of these spectra yields two distinct structural features of the swollen films: a) Vertical distribution profiles of all three species in the direction perpendicular to the interface, which is examined by the specular component of the NR spectra. And b) in-plane structure, parallel to the substrate, which is extracted from the full scattering pattern. The kinetic changes of these structural features are deduced from the time evolution of the NR spectra. From Fig. 4, the relative thickness change h/h_0 shows four swelling regimes depending on $\phi_{BA/W}$: onset of swelling at low BA concentration (below 0.1 % BA), intermediate regime (0.1-0.25 % BA), high concentration (0.25-0.5 % BA) and critical conditions (above 0.5 % BA).

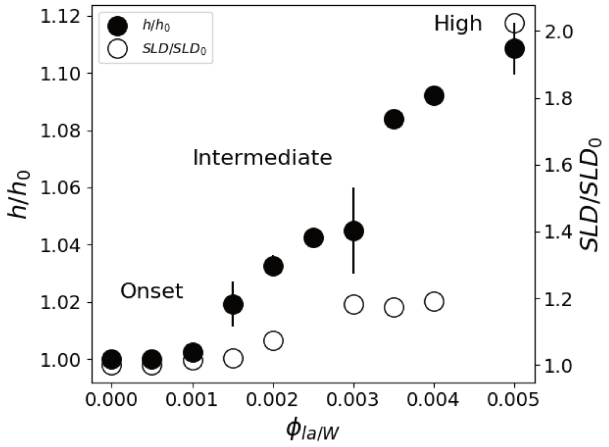

Fig. 4 The dependence of the total thickness swelling ratio h/h_0 and the SLD ratio (SLD/SLD_0) of a polymer film of LA in contact with aqueous solutions of BA in D_2O at different $\phi_{BA/W}$ as observed by neutron reflectometry using a one-layer model for interpretation of NR results.

One can rise the question about the detection limit of BA and D_2O from the NR analysis and the concentration profiles of these solvents within the films. The simulation of the NR spectra of the swollen film requires the simultaneous determination of BA and D_2O concentration profiles, the LA film thickness and the roughness of the Si and D_2O interfaces. Several shapes of the BA and D_2O profiles can be considered : constant, linear, adsorbed or brush.[44,45] As can be seen in table 1 the SLD contrast between heavy water and all other components is significantly higher than between BA and the polymer. This will dictate the sensitivity of the measurements mainly towards the distribution of D_2O in this system. This can be readily seen in Fig. 5, where a typical NR spectrum of a 70 nm LA film in 0.2 % BA in D_2O (circles) is simulated using various distribution profiles. Clearly visible are the oscillations in the reflectivity profile coming from the total thickness of the polymer film. This curve can only be fitted by molecularly smooth LA/Si (0.5 nm) and LA/D_2O (0.2 nm) interfaces as can be seen by the blue line in Fig. 5. Even slight deviations from these values lead to considerably worse fits to the data, which point out to the high sensitivity to the D_2O/LA surface roughness. The BA distribution profile is not finely resolved because of its low SLD. This can be seen from the black line corresponding to a BA profile roughness of 5 nm, which is practically indistinguishable from the blue line corresponding to a sharp BA interface. Therefore the estimated resolution concerning the concentration profile roughness of BA can be estimated to be around 10 nm. In addition to the "Gaussian" interface roughness a linear gradient in SLD spanning over the whole LA layer could be fitted to the reflectivity curves without worsening the fit quality. This profile corresponds to a 10% D_2O concentration difference between the two interfaces of the polymer layer. However, a completely flat SLD profile fits the data equally good for BA concentrations below 0.3% and therefore a constant profile for both BA and D_2O is used for the fits and the swollen thickness and the average concentrations are calculated. The second remark is whether the NR spectra can distinguish between a diffuse profile of water in the film or a (corrugated) rough film. Specular reflectometry cannot distinguish these two cases provided that the normal density profiles are the same.[51] On the other hand, if the characteristic length of the roughness is on the micrometer scale, off-specular scattering should be observed.[46]

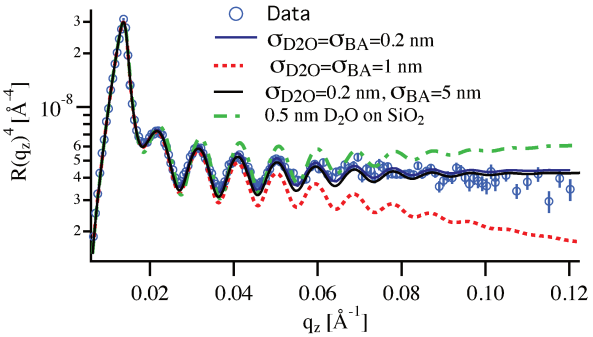

Fig. 5 Reflectivity multiplied by q_z^4 of a 70 nm LA film in contact with a solution of 0.2 % BA in D_2O (circles). The two solid lines are simulated reflectivities for a very sharp D_2O profile extending only 0.2 nm into the polymer, once with an evenly sharp BA profile (blue curve) and once with a rough BA profile extending 5 nm into the varnish (black line). The dotted red line shows the simulation assuming the D_2O profile extending 1 nm into LA. The dotted-broken green line corresponds to a 0.5 nm thick water layer between the silicon substrate and the polymer.

3.3.1 Onset of swelling

The fitted film thickness shows only a slight increase, by at most 0.1 % within the first regime ($\phi_{BA/W} < 0.1$ %) which is practically within the detection limit of NR. This infers that the extent of vertical swelling is very limited for low $\phi_{BA/W}$. The SLD is almost unchanged in this regime within the detection limit which infers that most of the detected swelling can safely be attributed to BA. The roughness at the polymer liquid interface stays molecularly smooth (less than 0.3 nm). The OSS intensity is very low pointing towards very little inhomogeneous water inclusions inside the layer. The width of the reflected beam on the detector shown in Fig. 6, however, shows a slight increase even at 0.05 % BA concentration pointing towards a slight buckling which probably results from the in-plane swelling of the thin films.[47]

3.3.2 Swelling at intermediate solvent concentration

Upon gradually increasing $\phi_{BA/W}$, a prompt change in the vertical swelling behavior takes place close to 0.1 % BA (Fig. 4). This can be clearly deduced from the prompt change of the h/h_0 dependence on $\phi_{BA/W}$. This swelling ratio was obtained within the first NR time frame, which is 5 min. This is expected since the estimated Fickian diffusion time of small molecules in a glassy thin films is less than 10 ms. The partial swelling in this regime can be attributed to BA solubilisation (see Fig. 13) because if water did penetrate the film, it would cause an increase in SLD that would be easily detected because of the high scattering contrast between D_2O and the non-deuterated materials.

Since the films do swell in presence of D_2O/BA mixtures, one may wonder what are the partial distribution profiles of these two solvents in ultrathin films, particularly because of the presence

of two interfaces: silicon crystal/polymer and polymer/aqueous solution. A possible cause of a gradient in the volume fraction of solvent in the film could be a Fickian diffusion process that would not have reached a steady state[2] or else a stratification of the equilibrium structure by the proximity of interfaces.[20] As discussed above, the diffusion of small molecules is expected to reach a steady state within the first 10 ms and if any BA concentration gradient higher than 10 nm were present it would show up in the SLD profile. Furthermore, the increase in the reflected beam width (Fig. 6) suggests an enhancement of film buckling which points to an increase in the in-plane swelling along with the vertical swelling. The careful analysis of off-specular data shows no increased intensity in this regime pointing towards the absence of significant in-plane water inhomogeneities throughout the film.

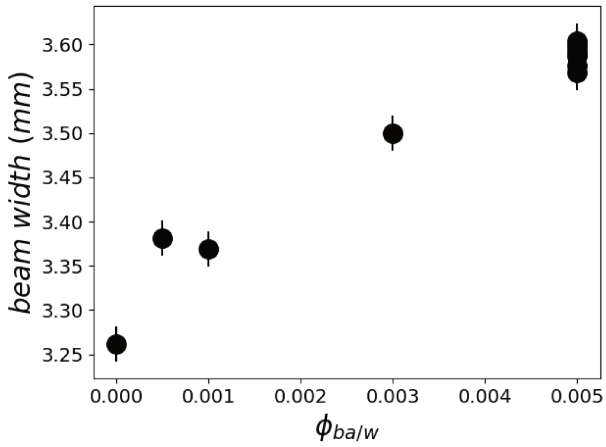

Fig. 6 Width of the reflected beam on the detector as a function of solvent concentration in water. The points gathered at 0.5 % BA correspond to the reflected beam width at several annealing times.

3.3.3 Swelling at high BA solvent concentrations (between 0.3% and 0.5 %)

Above $\phi_{BA/W}$ = 0.3 % , the vertical swelling deduced from film thickness continues to increase with increasing $\phi_{BA/W}$. However, the particularity of this regime is evidenced by the fast increase of SLD which could be interpreted as D_2O invasion of the film (Fig. 4). Indeed, while the total swelling follows a similar trend as in the previous regime, the SLD rises abruptly, suggesting that the D_2O is no longer excluded from the LA film for these compositions. The in-plane swelling seems to follow the same trend as in the previous regime, indicating a continued swelling by BA in the plane of the film as in the previous regime. The OSS intensity, on the other hand, increases significantly starting from $\phi_{BA/W}$ = 0.3 %. Its appearance is not instantaneous, though, contrary to the swelling by BA. As can be seen in Fig. 8 the OSS intensity increases slowly on an hour time scale.

3.3.4 Critical BA condition

Above $\phi_{BA/W}$ = 0.004, the equilibrated SLD significantly increases by more than 70 % while the total layer thickness only slightly increases by about 10 % (Fig. 4). Of course due to the high scattering length contrast of D_2O its influence on the increase in SLD is exaggerated but still the observed SLD increase in this regime cannot be explained by simple vertical swelling of the film by D_2O and BA, but has to be due to a significant increase in D_2O volume fraction, either on the expense of LA (breaking up of the layer) or by a decrease of molecular volume of the components (intercalation). At the same time a single polymer layer model does not fit the measured NR curves to a satisfactory level anymore. Clearly the thin film structure is significantly altered at these concentrations. This is evidenced also by a very slow thickness and SLD growth which took two hours to reach equilibrium (see Fig. 7).

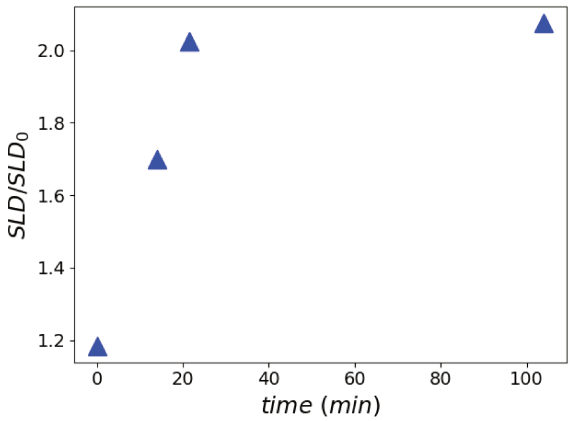

Fig. 7 Time evolution of the relative SLD change (SLD/SLD_0) of a LA film in contact with $\phi_{BA/W}$=0.003 mixtures as observed by NR. The SLD is deduced from fitting the time resolved NR spectra to the one polymer layer model. The film was first immersed in 0.0005 BA/D_2O prior to the experiment.

Moreover, this kinetic development is accompanied by an increased OSS scattering intensity close to the total reflection, which is known as the Yoneda peak.[52] This is an indication of enhanced concentration inhomogeneities of heavy water in the film or the adding of heavy water into existing inhomogeneities (See Fig. 8).

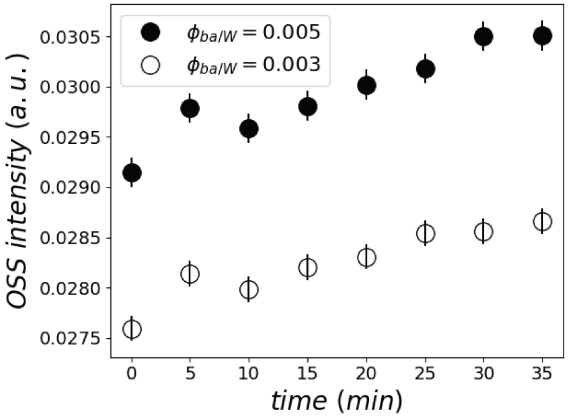

Fig. 8 Normalized Yoneda peak intensity as a function of time for the two samples at $\phi_{BA/W}$ = 0.005 (●) and 0.003 (○) calculated by integrating the off- specular peak intensity.

Looking on the buckling, on the other hand, one observes no significant changes of the reflected beam width on the detector in this regime of swelling. In Fig. 6, the points at 0.5% BA are all overlapping within experimental error, showing that there is no evolution of the surface buckling during this swelling process. This corroborates the finding that the solvent invasion in this regime is fundamentally different from the swelling at low BA concentrations.

To elucidate this stage of the film swelling optical and atomic force microscopy was performed on the same films in air after immersion for several days in the respective liquid mixtures. Typical micrographs can be seen in Fig. 9. The formation of holes with rims around is clearly visible, typical for the case of dewetting.

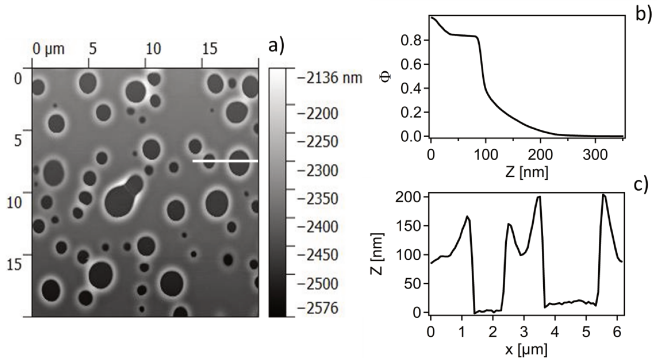

Fig. 9 a) Top of an ultrathin film at equilibrium state after immersion in 0.3 % BA in water observed by Atomic Force Microscopy (AFM). Without taking into account the white halos around the holes, the size of the biggest objects are 2.3 Âµm ± 0.03Âµm in diameter and holes cover 15.976 % of the area. b) Vertical density profile of the AFM image. c) Horizontal cut along the white line shown in a).

Inspired from the vertical density profiles obtained from AFM an adapted stratified SLD model was used to fit NR curves at 0.5% BA. In this case the polymer layer was split into three sublayers as can be seen in Fig.10.

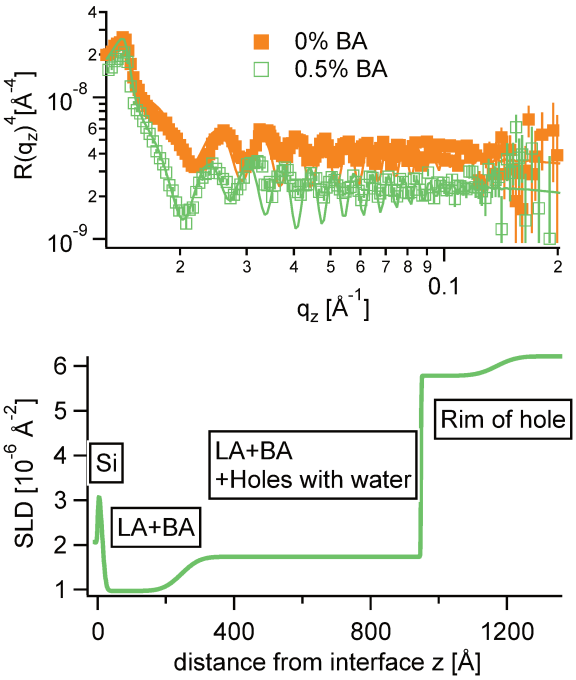

Fig. 10 Top: NR curves multiplied by q_z^{-4} of a pure D_2O/LA interface (orange closed squares) and a LA layer immersed in 0.5% of BA (green open squares). Bottom: The corresponding SLD profile for 0.5% BA.

In accordance with AFM the NR fits reveal a quasi water free wetting layer of 24 nm on top of the silicon followed by the main part of the LA film perforated by water filled holes and topped by a rim extending up to 30 nm in height for the chosen annealing time in NR. Note that the samples measured by AFM were annealed significantly longer, where the rim height extends up to 100 nm. Interestingly the water free wetting layer stays constant around 24 nm for all annealing times.

The last concentration tested was 0.7 % of BA. At this concentration, there is a radical rupture of the film. The NR result shows no residual film thickness, only a very rough layer with about 5 % volume fraction LA, probably some fragments (islands). Optical microscopy shows some residual droplets on the surface with very low surface coverage.

4 Discussion

4.1 Does water absorb in LA?

The combination of NR and optical as well as atomic force microscopy suggests that there is no significant water absorption into LA regardless the abundance of water surrounding the ultrathin film.

In order to estimate the effect of chemical potentials of the system BA/W/LA a ternary phase diagram was established and the three Flory-Huggins (FH) interaction parameters ($\chi_{W/BA}$, $\chi_{LA/BA}$ and $\chi_{LA/W}$) were calculated. The bulk ternary phase diagram was inferred from turbidity measurements and consists of two single-phase regions and is thus most likely to be of type II

(Fig. 11). The first region is located close to the LA/BA side. The second single-phase region is located near the W corner at W/BA < 0.96 and contains almost no LA polymer. For example the binodal line is located below $\phi_{LA/W} = 5{*}10^{-6}$ for $\phi_{BA/W} = 0.005$. All samples that have been made with compositions outside the single phase regions show the coexistence of these 2 phases in equilibrium, this coexistence is represented in the phase diagram by the tie-lines.

The $\chi_{LA/BA}$ in the limit of low LA concentrations is calculated following the method described in reference [53] using the intrinsic viscosity (equation 7 in the appendix). The viscosity at the θ condition was estimated from equation 14 by using a range of Kθ = $4.8{*}10^{-2}$ - $7.2{*}10^{-2}$ from reference [53] of amorphous PS and PMMA in θ solvents and an exponent $\alpha = 0.5$. In order to estimate k one can use the measured intrinsic viscosity in conjunction with using $\alpha = 0.7$ for a good solvent. Using these methods one can estimate $\chi_{LA/BA}$ to range from -0.05 to 0.17. At high LA concentrations a $\chi_{LA/BA}$ = -0.5 is found to be more compatible with the observed results.

$\chi_{W/BA}$, and $\chi_{LA/W}$ are deduced from fitting the binary and ternary phase diagrams using the FH model equations 5 and 6 [54 48 55 56 57 58 53] shown in the appendix. Following the methods described in reference [54], the binary line is computed by estimating the tie lines as the equality of the chemical potential between the BA rich phase in the right side of the phase diagram and the water rich phase in the left lower corner of the phase diagram (Fig. 11). The minimum least square method is used to minimize the chemical potential between two coexisting phases using the method described in reference [54]. The concentration dependence of $\chi_{W/BA}$ is calculated using the binary phase diagram of water/BA providing the measured solubility limits of BA in water of 0.1 and 0.96. An estimation of $\chi_{LA/W}$ of 4-5 in the vicinity of LA rich corner is deduced from the water solubility limit of LA of 0.001 (from NR). The $\chi_{LA/W}$ for $\phi_{LA/BA} < 0.5$ is estimated by fitting the binodal curve of the ternary phase diagram (●) in the Fig. 11) to the FH model and plotted vs. $\frac{\phi_{LA}}{\phi_{LA}+\phi_{BA}}$ (Fig. 12). $\chi_{LA/BA}$ is found to increase with increasing LA concentration from 2.6 to above 3 for $\chi_{LA/BA} < 0.5$ and if extrapolated to high LA concentration using a polynomial fit one can recover $\chi_{W/LA}$ of around 5 (Fig. 12), which is compatible to the estimated value using water solubility.

One might ask the question whether the LA film in the NR experiments should be swollen or completely dissolved in the W/BA mixture. Considering a 70 nm LA film immersed in a 1 mm thick liquid cell, a complete polymer dissolution would result in $\phi_{LA} = 10^{-4}$ which is much higher than the boundary line $5{*}10^{-6}$. This rejects the possibility of complete dissolution of the LA film in the conditions of the NR experiments and comforts the observed results of film swelling with BA and water.

In summary the estimations of chemical potentials and interaction parameters of bulk ternary phase diagrams corroborate the insignificant water absorption in thin LA films.

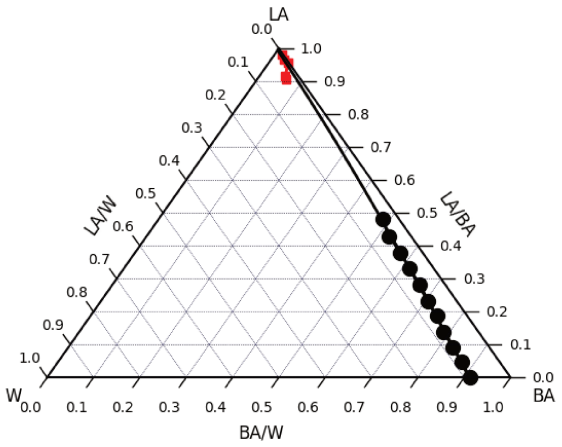

Fig. 11 Ternary BA/W/LA phase diagram of water (left) in benzyl alcohol (right) and Laropal®A81 (top) mixtures from turbidity measurements on bulk systems (●) and from NR experiments on ultra thin films (■). The binodal line from turbidity is obtained by dropwise adding water to a solution of LA/BA until turbidity traces appear. The binodal line from NR experiments is estimated by immersing 70 nm in water/BA solutions and measuring the partial fractions of BA and D_2O in LA. The experiments are carried out at room temperature. The experimental binodal curve is fitted to the FH model using the calculated $\chi_{W/BA}$ and $\chi_{LA/BA}$ and $\chi_{LA/W}$ as the fitting parameters (——).

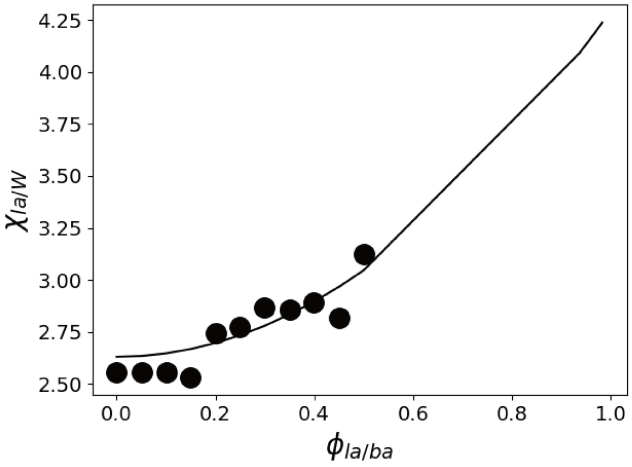

Fig. 12 Estimated LA/W FH parameter $\chi_{LA/W}$ by fitting the ternary phase diagram of Figure 11 to the FH model as a function of $\phi = \frac{\phi_{LA}}{\phi_{LA}+\phi_{BA}}$ (black circles). The values of $\chi_{W/BA}$ are estimated from fitting the water/BA binary system to the FH model and $\chi_{LA/BA}$ calculated from viscosity measurements. The black line is a guide to the eye.

4.1.1 Homogeneous swelling at low BA concentrations?

In the case of simple swelling of a single LA film by water and BA uptake, the fractions of BA and water $\phi_{BA/LA}$ and $\phi_{W/LA}$ can be calculated from (equation 4) if one assumes LA mass conserva-

tion:

$$1+\phi_{W/LA}+\phi_{BA/LA}=\frac{h}{h_0}$$
$$\frac{h}{h_0} * SLD = \phi_{W/LA} * SLD_{D_2O} + \phi_{BA/LA} * SLD_{BA} \quad (4)$$
$$+(\frac{h}{h_0}-\phi_{W/LA}-\phi_{BA/LA}) * SLD_{LA},$$

where h and h_0 are the swollen and dry layer thicknesses, respectively, and SLD, SLD_{D_2O}, SLD_{BA} and SLD_{LA} are the swollen SLD and the bulk SLDs of D_2O, BA and LA, respectively. The results of this model are shown in fig. 13. The blues points correspond to the volume fractions of water and show no significant absorption below 0.3% BA in water as stated above.

$\phi_{W/LA}$ as a function of $\phi_{BA/LA}$ can also be estimated from the ternary phase diagram by using the FH model using the χ parameters calculated above by assuming no LA dissolution in water and by minimizing the BA chemical potential between the two coexisting phases. This calculation leads to the blue line in Fig. 11. The estimated $\phi_{W/LA}$ is in accordance with the NR data up to $\phi_{BA/W}$ = 0.0025. This also confirms that water is unlikely to molecularly swell the LA film for this range of BA concentration.

The black triangles in fig. 13 depict the experimentally determined BA fractions in the LA films. At high BA concentrations in water they nicely follow the predictions of the FH model (black line) estimated from the bulk phase diagram. For concentrations below 0.15% the BA fractions are clearly overestimated by the (bulk) model. Whatever the exact dependence of the $\chi_{LA/W}$ is, the predicted BA swelling $\phi_{BA/LA}$ is linear with increasing $\phi_{BA/W}$. $\phi_{BA/LA}$ can also be calculated by considering BA partitioning between two incompatible mediums and estimated using the difference between the $\chi_{LA/BA}$ and $\chi_{W/BA}$ leading to the same linear dependence.[59] Yet, the linear dependence contradicts the experimental data, which show no vertical swelling up to $\phi_{BA/W}$ = 0.001 and then a sudden increase to reach the predicted linear swelling at about 0.2 %. On the other hand, the observed film buckling for $\phi_{BA/W}$ < 0.001 (Fig. 6) points out to lateral swelling even at low concentrations, as expected. This could be due to the particularities of swelling thin films where Van der Waals (VdW) forces on the polymer/substrate interface could act as linking points and leads to anisotropic swelling. Indeed vertical swelling requires a movement of the chains along the substrate and therefore polymers at the free surface are more likely to swell before their counterparts in vicinity of the substrate leading to anisotropic swelling and film buckling. For higher BA concentrations, both vertical and in plane swelling takes place. This implies that swelling is heterogeneous below $\phi_{BA/W}$ = 0.001 and becomes more homogeneous at intermediate BA concentrations (0.001-0.003). Another indication that VdW forces may introduce an inhomogeneitiy is the 24 nm wetting layer observed by NR and AFM for large holes. Clearly this layer is much larger than expected for a classical wetting layer due to dipolar forces, which should be a few nm thick only. Therefore this must arise due to VdW interactions originating from the high refractive index of LA of 1.5.

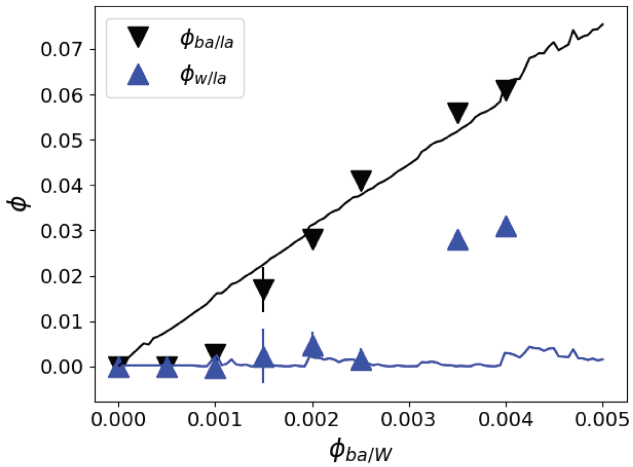

Fig. 13 Partial volume fractions of D_2O ($\phi_{w/La}$) (▲) and BA ($\phi_{BA/LA}$) (▼) in LA films calculated from NR analysis using the thickness and SLD variation upon swelling and assuming LA mass conservation. The estimated BA $\phi_{BA/LA}$ (——) and water volume fractions $\phi_{w/La}$ (——) from the FH model using $\chi_{LA/BA}$ = -0.5 and the tendency of $\chi_{LA/W}$ depicted in Fig. 12.

4.1.2 Heterogeneous water invasion (formation of cavities)

When immersed in solvent/nonsolvent systems above a BA concentration of 0.25% LA films apparently dewet creating holes which will be invaded by water. The tendency to de-wet is clearly set by the unstable nature of the system concenring short-range wetting forces: The SiO2 covered substrate is partially hydrophilic and it would be energetically more favorable to be covered by water rather than the hydrophobic LA. If the size of these defects is smaller than the in-plane neutron coherence length the NR spectra will still fit reasonably to a 3 slab polymer model but additionally diffuse scattering might appear if the SLD contrast and the surface coverage are big enough. Indeed microscopy images of film exposed to water and BA show holes with diameters between 0.5 and 3 Âµm, which is smaller than the estimated coherence length (2 - 10 Âµm), which explains the appearance of off-specular scattering at these BA concentrations (see Fig.8).

How these holes appear and evolve with time is a legitimate question because they are morphologically similar to those observed in early stages of thin film dewetting[60]. Dewetting can be attributed to capillary instabilities by thermal fluctuation, which is analyzed in analogy with spinodal decomposition of fluid mixtures[61] or homogeneous nucleation[60]. Therefore one can not exclude that thermal fluctuations and capillary instabilities as one of the precursors for film erosion.

Note that for the LA films studied here hole formation was only observed in films deposited on large Si blocks where the film thickness homogeneity was clearly worse than that of thin Si wafers, where no dewetting was observed for these BA concentrations. This would suggests that heterogeneous nucleation due to structural inhomogeneities of the films is more likely to induce the onset of these instabilities.

4.1.3 Shift of glass transition temperature?

One should not forget, however, that dewetting necessitates a structural reorganization of the polymer. Looking at Fig. 8 and Fig. 7 and explained in section 3.3.3, one clearly observes slow kinetics incompatible with Fickian diffusion meaning that these kinetics are controlled by the polymer dynamics in the bulk of the film or close to the surface. In the former case the dynamic acceleration would be due to the T_g reduction upon increasing BA. Using the T_g mixing model of a binary system $\frac{1}{T_g} = \frac{1-\phi_{BA}}{T_{g(LA)}} + \frac{\phi_{BA}}{T_{g(BA)}}$ and the $T_{g(BA)}$=168 K[62], with $T_{g(LA)}$=50°C and ϕ_{BA}=0.05, one recovers an average $T_{g(LA/BA)}$ value of around 35°C. This value is not far from room temperature especially taking into account the large polymer polydispersity leading probably to mobile parts at room temperature. Furthermore, there are several indications that amorphous confined polymers exhibit different behavior from bulk. For example, few aspect of the polymer dynamics in the glassy regime where found to be activated in confined geometry[63] which might accelerate the dynamics and enhance polymer reorganisation at room temperature. DSC measurements of the LA after prolongated contact with BA/Water mixtures showed, however, only very slight decrease in T_g far away from R.T. Also increasing temperature of the sample above T_g did not significantly accelerate the dewetting process.
Another reason for the dynamic acceleration could be breaking of surface/polymer links upon swelling. Indeed, one should not forget that the polymer/surface adsorption sites could act like grafting points or cross-links which could reduce the swelling and slow down the intrinsic polymer dynamics. Indeed, at low BA concentration no vertical swelling was observed while horizontal expansion was seen as buckling. This leads to a delayed onset of vertical swelling contrary to the predicted linear swelling as seen in Fig. 13. Breaking the links would allow certain inhibited chain movements, reduce the T_g and might accelerate the polymer dynamics.

4.1.4 Simple dewetting?

There are, however, at least two observations that point out that the here observed process is not a simple dewetting scenario. Firstly, in the AFM images it can be seen that only small holes actually perforate entirely the polymer film. As soon as the holes grow larger than about 1 micrometer in diameter an apparent wetting layer of about 24 nm thick LA is covering the substrate again. This thickness is obviously much larger than expected for a simple wetting layer due to dipolar forces, which should extend a few nm at most. Secondly, in contrast to simple dewetting, experiments at concentrations above 0.6% BA in water clearly show the disappearance of the bulk of the layer into the liquid phase, obviously violating the mass conservation of LA on top of the substrate. Even at 0.5% BA concentration NR shows a total LA mass decrease as function of time. We speculate about two possibilities, which would lead to the disappearance of the varnish above the critical concentration, namely emulsification or (heterogeneous) break up. Molecular dissolution of LA in water/BA can be excluded because control experiments have shown that the solubility limit of LA in water/BA mixtures of 0.5% BA is less than $5*10^{-6}$ while the NR cell had a total liquid volume leading to a total polymer concentration of 10^{-4} in the experiment. Continued breaking of polymer/surface links induce more in plane heterogeneities resulting in more holes and, finally, not enough links are left (critical BA concentration above 0.5%) leading to film break up by lifting and floating away. There is, however, a contradictory observations to this scenario: In no case during the film swelling/breakup a water enrichment was observed close to the Si substrate. This would have been apparent in NR due to the high contrast of heavy water (see broken green line in Fig. 5). On the contrary, a 24 nm water-free LA film was observed for sufficiently big holes as seen in Figs. 9 and 10 showing that the solid substrate is covered by LA just before the breakup.
An alternative pathway of the mechanism to remove the polymer from the substrate could be analogue to emulsification of swollen LA in water/BA because of the presence of polar species in the LA which could stabilize an emulsion in forms of small droplets by a reduction of surface tension similar to a surfactant.

5 Conclusion

The swelling and breakup of thin films of Laropal®A81, a synthetic varnish commonly used in art restoration, supported by silicon substrates exposed to a binary solvent/non-solvent mixture is studied here using a combination of neutron reflectoemtry, atomic force and optical microscopy as well as thermodynamic calculations based on turbidity measurements. The sample set-up follows a recent approach in art restoration to use a bad solvent as a matrix containing small amounts of (good) organic solvent in order to reduce the total amount of good solvent in the system limiting the risk of irreversible dissolution of all varnish and paint layers on easel paintings[14,17]. As solvent benzyl alcohol is chosen, which is dissolved in a matrix of water, a common system for art restoration.
The swelling and dissolution process of the thin films while increasing the good solvent concentration and/or increasing exposure time is found to happen sequentially following several regimes, which are distinct from the swelling and dissolution in bulk. At very low solvent concentrations an asymmetric swelling of the varnish by the good solvent is found: The swelling ratio parallel to the interface, observed as buckling, is instantly following the increased concentration of good solvent, while the out-of-plane thickness swelling is retarded and only happens at a sufficiently large solvent concentration ($\geq$ 0.1% BA in water). This phenomenon is explained by strong van der Waals forces acting like anchoring sites for the polymer close to the Si substrate. For higher solvent concentrations the vertical swelling catches up the behaviour predicted by bulk measurements. For concentrations below 0.3% BA no water absorption is observed into the hydrophobic varnish.
For larger solvent concentrations the behaviour changes drastically. Probably due to the solvent-weakened polymer structure heterogeneous nucleation of water-filled holes appears and those holes grow with time on an hour time scale ending in the loss of the film (>0.5 %). By hypothesis, we can surmise that the solvent weakens the film by homogeneous swelling which dynami-

cally activates the dewetting type process probably nucleated due to structural inhomogemneities of the film (either thickness variations or acidic group agglomerations).
In summary, this study shows unambiguously that the dilution of good solvent by a bad solvent can activate surface induced dewetting processes of thin polymer films due to the presence of the bad solvent that are not at all predicted in bulk systems. Therefore care has to be taken on this approach and surface energies (long and short-ranged) have to be taken into account.

Appendix

Flory-Huggins model equations for thermodynamic ternary phase diagram

The FH model can be extended empirically[54] so that the Gibbs free energy of mixing is given by:

$$\frac{\Delta G_M}{RT} = n_1 ln\phi_1 + n_2 ln\phi_2 + n_3 ln\phi_3 + g_{12}(u_2) n_1\phi_2 + \chi_{13} n_1\phi_3 + \chi_{23} n_2\phi_3 \quad (5)$$

where R is the universal gas constant, T is the temperature, g_{ij} is the concentration-dependent interaction parameters and $u_2 = \phi_2/(\phi_1+\phi_2)$. Subscripts refer to nonsolvent (1), solvent (2) and polymer (3) parameters.

This expressions can be obtained following the definition of the chemical potential:

$$\frac{\Delta\mu_i}{RT} = \frac{\partial}{\partial n_i} * (\frac{\Delta G_m}{RT})_{n_{j,j\neq i}} \quad (6)$$

The intrinsic viscosity is calculated using:

$$[\eta] = K M_n^{\alpha} \quad (7)$$

where M is the molecular weight in Da.

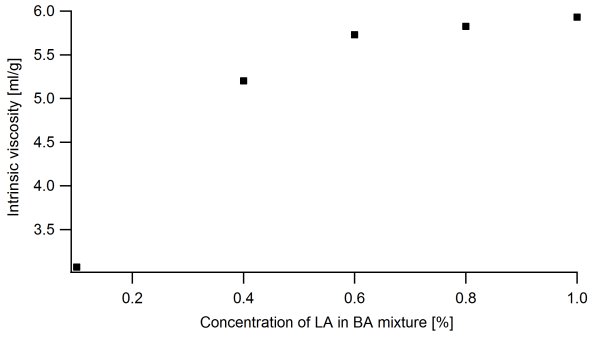

Fig. 14 Intrinsic viscosity of LA as a function of LA concentration in BA.

And the polymer/solvent interaction parameter χ_{23} can be obtain by:

$$\chi_{23} = 0.5 - A_2\rho_3^2 V_2 \quad (8)$$

where A_2 is the polymer-concentration-independent, ρ_3 is the polymer density and V_2 is the molar volume of the solvent.

Table 2 Data for χ calculation[54 48 55] where Mn is the molecular weight of LA, $[\eta]_\theta$ is intrinsic viscosity and c* is the critical concentration

Parameters	literature values
Mn of LA	1260 Da
k_θ	$4.8*10^{-2}$-$7.2*10^{-2}$
α	0.5

Acknowledgements

We thank the ILL for neutron beam time on FIGARO (doi:10.5291/ILL-DATA.1-03-34) and MLZ for neutron beam time on the N-Rex$^+$ instrument operated by MPG at the Heinz Maier-Leibnitz Zentrum (MLZ), Garching, Germany. We thank the Partnership for Soft Condensed Matter at ILL and ESRF for the use of complimentary techniques. We thank Alain Panzerella from the ESRF for performing the AFM measurements. The authors gratefully acknowledge the financial support provided by JCNS to perform the neutron scattering measurements at the Heinz Maier-Leibnitz Zentrum (MLZ), Garching, Germany. We acknowledge the help of Olaf Soltwedel during the NR measurements at MLZ. The Laboratoire Rhéologie et Procédés is part of the LabEx Tec 21 (Investissements d'Avenir - grant agreement n°ANR-11-LABX-0030) and of the PolyNat Carnot Institut (Investissements d'Avenir - grant agreement n°ANR-11-CARN-030-01). We acknowledge Dr. Hélène Galliard, Vincent Verdoot, Fréderic Hugenell for their technical support. We thank Michel Manu for fruitful discussions on the choice of the system to be used for this project. We acknowledge BASF for providing the varnish for this study.

References

1 A. Singh and R. Mukherjee, *Marcomolecules*, 2003, **36 (23)**, 8728–8731.
2 B.-A. Miller-chou and J.-L. Koenig, *Progress in Polymer science*, 2003, **28 (8)**, 1223–1270.
3 N. McCrum, C. Buckley and C. Bucknall, *Principles of polymer engineering*, 1997, vol. 49.
4 B. A. Miller-Chou and J. L. Koenig, *Progress in polymer science*, 2003, **28**, year.
5 E. D. la Rie and C. McGlinchey, *International Institute for Conservation of Historic and Artistic Works*, 1990, 168–173.
6 R.-L. Feller, N. Stolow and E.-H. Jones, *On picture varnishes and their solvents. Revised and enlarged edition*, 1971.
7 N. Stolow, *Some investigations of the action of solvents on drying oil films*, PhD Thesis, University of London, 1956.
8 N. Stolow, *Journal of the Oil and Colour Chemists' Association*, 1957, **40**, 488–499.
9 A. Phenix and A. Burnstock, *The United Kingdom Institute of Conservation*, 1990, 11–18.
10 A. Burnstock and R. White, *Studies in Conservation*, 1990, **28 (8)**, 1223–1270.
11 E. D. la Rie, S. Lomax, M. Palmer, L. Glinsman and A. Christopher, *Studies in Conservation*, 2000, **45:sup1**, 51–59.
12 K. Sutherland, *Studies in Conservation*, 2000, **45**, 54–62.
13 A. Phenix and K. Sutherland, *Studies in Conservation*, 2001,

46, 47–60.
14 A. Phenix, *The Building Conservation Directory*, 1997, 273–276.
15 L. Masschelein-Kleiner, *Les solvants*, 1994, vol. 2.
16 P. Cremonesi, *L'uso dei solventi organici nella pulitura di opere policrome*, 2004.
17 E. Carretti, M. Bonini, L. D. B.-H. Berrie, L.-V. Angelova, P. Baglioni and R.-G. Weiss, *Accounts of Chemical Research*, 2010, **43**, 751–760.
18 T. Ribar, R. Bhargava and J.-L. Koenig, *Macromolecules*, 2000, **33 (23)**, 8842–8849.
19 T. Ribar, J.-L. Koenig and R. Bhargava, *Macromolecules*, 2001, **34 (23)**, 8340–8346.
20 A. Diethert, E. Metwalli, R. Meier, Q. Zhong, R.-A. Campbell, R. Cubitt and P. Müller-Buschbaum, *Soft Matter*, 2011, **7 (2-3)**, 6648–6659.
21 S. Michalski, *Studies in Conservation*, 1990, **35:sup1**, 85–92.
22 J.-L. Keddie, R.-A.-L. Jones and R.-A. Cory, *Europhysics Letters*, 1994, **27(1)**, 59–64.
23 A. Knoll, R. Magerle and G. Krausch, *Macromolecules*, 2001, **34**, 4159–4165.
24 J.-A. Forrest and K. Dalnoki-Veress, *Advances in Colloid and Interface Science*, 2001, **94**, 167–195.
25 M. Alcoutlabi and G.-B. McKenna, *Journal of Physics-Condensed Matter*, 2005, **17**, R461–R524.
26 S. Ge, Y. Pu, M. Rafailovich, J. Sokolov, C. Buenviaje, R. Buckmaster and R.-M. Overney, *Physical review letters*, 2000, **85**, 2340.
27 K. Hyunjung, A. Rühm, L.-B. Lurio, J.-K. Basu, J. Lal, D. Lumma, S.-G.-J. Mochrie and S.-K. Sinha, *Physical review letters*, 2003, **90 (6)**, year.
28 C.-J. Ellison and J.-M. Torkelson, *Nature Materials*, 2003, **2(10)**, 695–701.
29 G. Reiter, *Langmuir*, 1993, **9**, 1344–1351.
30 A. Sharma and G. Reiter, *Journal of Colloid and Interface Science*, 1996, **178**, 383–399.
31 G. Reiter and P.-G. de Gennes, *The European Physical Journal*, 2001, **6 (1)**, 25–28.
32 https://www.basf.com.
33 C. A. Maines and E. R. de la Rie, *Progress in organic coatings*, 2005, **52**, 39–45.
34 I. Bonaduce, M. Colombini, I.Degano, F. D. Girolamo, J. L. Nasa, F. Modugno and S. Orsini, *Analytical and Bioanalytical Chemistry*, 2012, **405 (2-3)**, 1047–1065.
35 J. Arslanoglu and T. Learner, *The Conservator*, 2001, **25 (1)**, 62–72.
36 E. D. la Rie, *Studies in Conservation*, 1987, **32**, 1–13.
37 D. B. Hall, P. Underhill and J. M. Torkelson, *Polymer Engineering & Science*, 1998, **38**, 2039–2045.
38 P. U. D.B. Hall and J. Torkelson, *Polymer engineering and science*, 1998, **38**, 2039–2045.
39 R. A. Campbell, H. P. Wacklin, I. Sutton, R. Cubitt and G. Fragneto, *Eur. Phys. J. Plus*, 2011, **126**,.
40 P. Gutfreund, T. Saerbeck, M. A. Gonzalez, E. Pellegrini, M. Laver, C. Dewhurst and R. Cubitt, *Journal of Applied Crystallography*, 2018, **51**, 606–615.
41 http://www.mlz-garching.de/nrex.
42 F. Abelès, Annales de physique, 1950, pp. 596–640.
43 A. Nelson, *Journal of Applied Crystallography*, 2006, **39**, 273–276.
44 P. d. De Gennes, *Macromolecules*, 1981, **14**, 1637–1644.
45 S. T. Milner, T. Witten and M. Cates, *Macromolecules*, 1988, **21**, 2610–2619.
46 V. Lauter, H. Lauter, A. Glavic and B. Toperverg, *Reference module in materials science and materials engineering*, 2016.
47 C. M. Stafford, C. Harrison, K. L. Beers, A. Karim, E. J. Amis, M. R. VanLandingham, H.-C. Kim, W. Volksen, R. D. Miller and E. E. Simonyi, *Nature materials*, 2004, **3**, 545.
48 L. Xu and F. Qiu, *Polymer*, 2014, **55**, 6795–6802.
49 R. Mukherjee, D. Bandyopadhyaya and A. Sharma, *Soft Matter*, 2008, **4**, 2086–2097.
50 X. Zhang, K. G. Yager, S. Kang, N. J. Fredin, B. Akgun, S. Satija, J. F. Douglas, A. Karim and R. L. Jones, *Macromolecules*, 2009, **43**, 1117–1123.
51 J. Daillant and A. Gibaud, *X-ray and neutron reflectivity principles and applications*, Springer, Berlin New York, 1999, pp. 1 vol. (XXIII, 331 p.).
52 Y. Yoneda, *Physical review*, 1963, **131**, 2010.
53 C. M. Kok and A. Rudin, *Journal of Applied Polymer Science*, 1982, **27**, 353–362.
54 L. Yilmaz and A. McHugh, *Journal of applied polymer science*, 1986, **31**, 997–1018.
55 R. A. Orwoll and P. A. Arnold, *Physical properties of polymers handbook*, Springer, 2007, pp. 233–257.
56 Z. Li and C. Jiang, *Journal of Membrane Science*, 2000, **174**, 87–96.
57 H. Wang, Q. Wang, Z. Xiong and C. Chen, *Journal of Chemical & Engineering Data*, 2014, **59**, 2045–2053.
58 G. Ovejero, P. Perez, M. Romero, I. Guzman, E. Dı *et al.*, *European polymer journal*, 2007, **43**, 1444–1449.
59 R. Gavara, R.-. J. Hernandez and J. Giacin, *Journal of food science*, 1996, **61 (5)**, 947–952.
60 R. Seemann, S. Herminghaus, C. Neto, S. Schlagowski, D. Podzimek, R. Konrad, H. Mantz and K. Jacobs, *Journal of Physics: Condensed Matter*, 2005, **17**, S267–S290.
61 R. Xie, A. Karim, J. F. Douglas, C. C. Han and R. A. Weiss, *Physical Review Letters*, 1998, **81**, 1251.
62 M. Tylinski, Y. Chua, M. Beasley, C. Schick and M. Ediger, *The Journal of chemical physics*, 2016, **145**, 174506.
63 K. Paeng, S. F. Swallen and M. Ediger, *Journal of the American Chemical Society*, 2011, **133**, 8444–8447.

CHAPTER 5
STABILITY OF FLUID ULTRATHIN POLYMER FILMS IN CONTACT WITH SOLVENT-LOADED GELS FOR CULTURAL HERITAGE

This chapter is focused on the second paper of this project which is ready for submission and will be submitted in June or July 2020.

In the same line as the paper "Swelling, Dewetting and Breakup in thin polymer films for cultural heritage" (chapter 4) [13] , this second paper is part of the study of swelling and dissolution of ultra-thin films for Cultural Heritage using neutron reflectivity. Contrary to the first paper [13], this time, the solvent (BA) is not only mixed with water but is transferred to the film of polymer (Laropal®A81) by the use of a solvent-loaded gel (Pemulen TR-2).

For this experiment, ultrathin films of Laropal®A81 were made by spin-coating and then annealed for a few minutes following the same process as the first paper [13]. Then, films were studied in several conditions: in air, in contact with a solvent-loaded gel at room temperature, and with a successive increase in temperature and solvent concentration, using neutron reflectivity on the FIGARO instrument at ILL.

Results obtained by the solvent-gel mixture on the macroscopic and nanoscopic behaviour of ultrathin films were compared with those obtained by the solvent water mixture of the first paper [13]. Similar to the solvent/non-solvent mixtures, a dewetting-type process was observed in the system in the form of water-filled cavities. The dewetting kinetics are accelerated by an increasing concentration of BA contained in the gel. NR has also revealed differences between the dewetting observed on the film immersed in binary mixture and in the gel matrix such as the absence of rims in this second case. Then, the influence of the temperature on the solvent/gel/polymer system was shown. Above T_g, the kinetics of dewetting are not significantly accelerated but the combination of temperature with solvent influences the stability of the film.

Stability of fluid Ultrathin Polymer Films in contact with solvent-loaded Gels for Cultural Heritage

Amélie Castel,[†,‡] Philipp Gutfreund,[*,†] Bernard Cabane,[¶] and Yahya Rharbi[*,‡]

†*Large Scale Structure, Institut Laue-Langevin, Grenoble, France*

‡*Laboratoire de Rhéologie et Procédés, Grenoble, France*

¶*ESPCI Paris Tech, Paris, France*

E-mail: gutfreund@ill.fr; yahya.rharbi@univ-grenoble-alpes.fr

Abstract

The removal of ultrathin amorphous polymer films in contact with an aqueous gelled solution containing small amounts of good solvent is addressed by means of specular and off-specular neutron reflectometry. The distribution of heavy water and benzyl alcohol is revealed inside Laropal®A81, often employed as a protective varnish layer for Culture Heritage in restoration of easel paintings. The swelling kinetics, interface roughness and film morphologies were recorded as a function of temperature and increasing benzyl alcohol concentration in the dispersion of Pemulen TR-2, a hydrophobically modified acrylic acid copolymer. The addition of small amounts of good solvent results in the appearance of water-filled cavities inside the varnish, which grow with time. It is shown that while increasing the solvent concentration greatly enhances the hole growth kinetics an increase in temperature above the glass transition temperature has not such a big effect on the kinetics.

Introduction

Removing protecting thin glassy polymer films from a substrate is a critical step for numerous applications such as photonic band-gap materials,[1] microelectronics,[2] nanolithography[3] and lab-on-chip devices.[4] It is also a particularly crucial step in the restoration of easel paintings and the one bearing the highest risk. Indeed, all surfaces of old paintings and many surfaces of the contemporary paintings are covered by polymer films (varnish) which act as a protecting barrier for the pictorial layer against environmental exposure. However, due to natural ageing, external and environmental factors (dirt, light, humidity) these layers undergo irreversible changes over time. Consequently, the aesthetic and artistic aspects of the pieces of art change irreversibly due to (micro-)cracks, colour changes, oxidation, etc. Hence regular restoration of the altered varnish layer is needed. A Common restoration procedure consists of manually transferring a good solvent to soften the altered varnish layer and mechanically removing it by abrasion. During this process, the risk of irreversible damage of the pictorial layer underneath is very high because of two factors: 1) the solvent diffusion in thin layers is difficult to control, 2) collapsing the fragile granular structure of the pictorial layer under excessive stress during manual abrasion could also lead to non visual but irreversible structural damages affecting its stability.[5–10] Therefore there is an urgent need to conduct precise investigations of the physical mechanisms involved during the various restoration steps.[8,11,12]

In order to limit the amount of aggressive solvent in the cleaning process it was proposed to work in so-called 'mild conditions' by diluting the solvent by water.[13] However, the results preceding this work on such binary mixtures obtained by neutron reflectometry[14] showed that above a solvent fraction of 0.3% the water invades the whole film through a dewetting-type process destroying the entire varnish and exposing the underlying layer to the bare liquid. On the other hand, at the beginning of the 1990s, to reduce the capillary penetration and the concentration of liquid solvents on surfaces, Wolbers suggested to increase the viscosity of the products by using polymer solutions as a matrix for the cleaning agent,

so-called Wolbers gels.[15] The high viscosity of the gel and the low concentration of solvent allow to reduce significantly the action of the solvent such as its penetration power. Thanks to the increase in the retention time of the products/solvents maintained in the gel matrix, the product is slowly transferred and the restorer can adapt the gel/surface contact time. Quite quickly these gels were commonly employed in cultural heritage conservation.[16] Gels have been widely studied since because of their applications in numerous industries such as cosmetics, food, health and even in products for safety (bulletproof vests). New innovating gels appeared, which could be suitable in art restoration like tough-gels,[17] micro-emulsion gels,[18] emulsion-gels,[19] and nano-gels.[20] In two recent reviews Baglioni *et al.* emphasize chemically cross-linked gels as a promising tool for the conservation of cultural heritage.[21,22] In contrast to the here studied Wolbers gels, chemical gels do not need a subsequent cleaning after application to remove the gelling polymer residues from the surface. However, the application of gels in general and its effectiveness to remove non-original materials on a macroscopic scale are impressively demonstrated by visual images, the potential microscopic penetration of liquids into the original layers, and therefore potential irreversible changes are not investigated. In addition, after transferring a small amount of solvent by a gel into varnish, a mechanical action must follow to remove the swollen varnish. This step obviously bears risks on its own.

From a scientific viewpoint film removal seems straightforward in thick films where diffusion times and distances are macroscopic. Although the solid-to-liquid transition of polymers may be quite different from non-polymeric materials: Unlike non-polymeric materials, polymers do not dissolve instantaneously and the classic dissolution process of a polymer involves transport processes, namely solvent diffusion and disentanglement of the polymer chains.[23] The first stage is penetration of a few solvent molecules that plasticize the polymer. As a result, the macromolecules can cross the polymer/solvent interface. If the molecular weight of the polymer is high enough, they will form a gel layer at the surface of the film. The next stage is the disentanglement of the macromolecules and their escape from the gel layer

into the solvent. But there are also cases where the polymer cracks before any gel layer is formed.[24]

In the case of ultrathin films the situation is more complex as surface effects and reduced dimensionality may effect the physical properties of the polymer such as chain conformation, glass transition temperature and polymer dynamics.[25] Van der Waals interactions of the substrate may also play a role for these thin films.[26] And, last but not least, many films may become unstable below a certain threshold thickness leading to dewetting when heated close or above their glass transition temperature (T_g).[27] The phenomenon of dewetting is relatively well studied for unpolar polymer films[28] but systems with a significant amount of polar groups, as the case in the present study, may significantly alter the film stability.[29–31]

The use of a single solvent is the easiest case of polymer film dissolution. In this study, however, a binary solvent-non solvent mixture suspended in an emulsifier solution is used. The case of a binary solvent without the emulsifying co-polymer was already studied before[14] and revealed a dewetting-type polymer film removal due to the different surface affinities of the solvents. Using viscosity-enhancing emulsifiers to promote thin film removal, as studied here, generates new challenges in polymer physics and raises particularly one important question about the emulsification mechanisms in confined media. Due to the presence of the co-polymer, the matrix is now able to absorb the hydrophobic polymer layer in form of an emulsion.[32,33] This increases the diversity of chemical interactions in the system and may shift the solvent partitioning.

Similar to our previous study[14] we will determine the solvent penetration inside the polymer and follow the film break-up by using specular and off-specular neutron reflectometry (NR). NR was found an effective technique that yields both structural and chemical information thanks to targeted hydrogen/deuterium (H/D) labeling. It is an ideal tool to observe the solvent penetration in real time and has already proven this in similar experiments[14,34–36]. It is a non-destructive and non-invasive technique for the investigation of thin polymer films, liquid/solid and liquid/liquid interfaces with a resolution of a few Ångströms. In addition

NR can be linked to complex sample environment like cone/plate rheology[37] as was done here as well. In contrast to our previous study[14] we cannot easily complement NR by microscopy as the gel cannot be removed from the film after application without destroying the system.

As in our previous study[14] we will use ultrathin (∼100 nm) polymer films of Laropal®A81 (LA), a resin commonly used as varnish on paintings, in contact with a small quantity of benzyl alcohol (BA) dissolved in a bulk aqueous solution. In the preceding study we observed a swelling of the varnish layer by BA penetration at small BA quantities in the water matrix and a dewetting of the varnish by appearance of holes as depicted in Fig. 1 at BA concentration above 0.3% BA at room temperature (R.T.). The dewetting process, however, showed two remarkable differences when compared to the dewetting of polymer films from solids in air: a) The wetting layer underneath the holes was unusually thick (see Fig. 1) and b) clear loss of polymer at late stages of dewetting was observed. We identified the affinity of the water matrix to the hydrophilic substrate underneath the hydrophobic polymer to be the driving force for the film instability when in contact with the BA/water binary solution. The fact that the dewetting process started only above a threshold BA concentration in water lead us to speculate about the plasticizing effect of BA inside the polymer film reducing its glass transition temperature close to room temperature initiating polymer flow. In the present study we will vary the temperature significantly above T_g to test this hypothesis.

The second difference in the current study is the addition of a gelling agent to the aqueous phase: Pemulen TR-2 as proposed for varnish removal in art restoration. Unlike the earlier studied case of water/solvent mixtures the case of physical gels containing solvent is indeed used in Cultural Heritage, so the latter system is closer to the real application.

Finally, in order to go towards the abrasion of the swollen varnish, we will test the influence of gentle mechanical stress on the system by shearing the sample in a rheometer and watching it with NR *in situ*.[37]

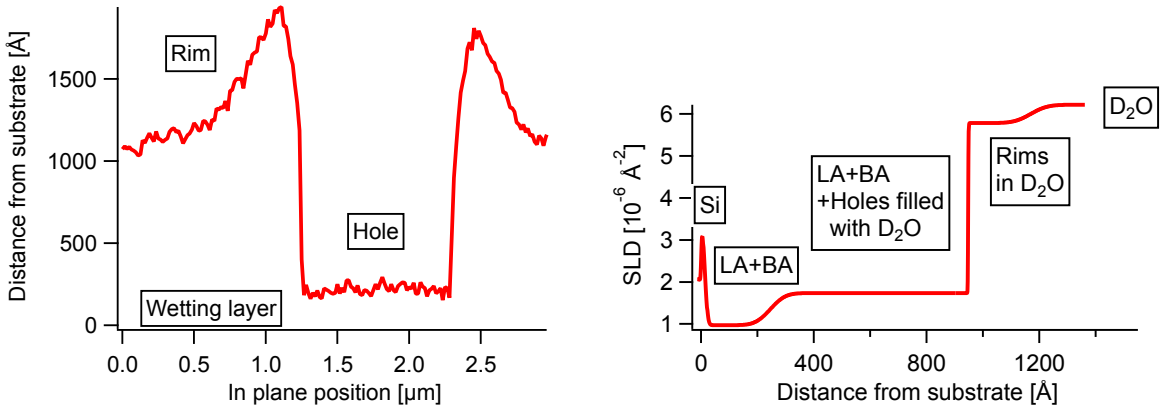

Figure 1: Left) Surface height versus in-plane position across a dewetting hole as seen by AFM in air of a LA film after prolonged exposure to a water/BA binary mixture. Right) Fitted SLD of a similar LA film in a BA/water mixture versus distance from the substrate. Note that the annealing time is longer for the AFM measurement leading to significantly larger holes and rims. This data is taken from Ref. [14].

Experimental

Materials

Laropal®A81 (LA) from BASF[38] is a synthetic polymer resin synthesized from an urea, isobutyraldehyde, and formaldehyde and is a reference varnish in cultural heritage because of its stability, its resistance and transparency.[39] The LA structure, was reported to consist of 4-hydroxy-6-isopropyl-5,5-dimethyl-tetrahydropyrimidin-2(1H)-one and aldehydic compounds.[40] LA is a small molecular weight polymer with a typical weight-average molecular weight (Mw) of 3640 Da and number-average molecular weight (Mn) of 1266 Da as deduced from gel chromatography (GC).[41] The T_g measured by differential scanning calorimetry (DSC) is 48 °C.[14] Benzyl alcohol (Sigma-Aldrich, 99.8 %), Deuterated water (D_2O, Eurisotop ref D214L, 99,9 % D), Pemulen TR2 (Lubrizol) and Triethanolamine (98%, CTS France[42]) were used as received. Pemulen TR-2 (PTR-2)[32,33,43,44] is an anionic polymeric emulsifier[33] made of a slightly crosslinked acrylic acid backbone (–[CH_2–CH–(COOH)–]$_n$–) and few hydrophobic pendent alkyl molecules, 10 to 30 carbons long. It is used as a primary emulsifier and a viscosity enhancing agent[45]. Triethanolamine (TEA) from CTS, a

ternary amine used in cosmetic and art restoration applications is used as buffering agent for Pemulen gel preparation.

Thin film preparation and characterization

In order to make ultrathin polymer films, LA/toluene mixtures of 20 g/L were deposited by spin coating using a Delta 6 RC TT (SÜSS MicroTec Lithography GmbH)[46] at 2500 RPM for 44 seconds onto silicon crystal blocks (5x5x1 cm^3 (111) from Sil'Tronix France or 7x7x1 cm^3 (100) from Crystec, Germany) rigorously cleaned following a precise protocol (20 min in deionized water, in acetone, in ethanol, in formalmyde and in water). These films were subsequently annealed at 114 °C for 30 minutes in a vacuum oven. During this heating process, all of the toluene is evaporated and an apparent homogeneous film of LA is observed. The film thickness measured by ellipsometry are $74\,nm \pm 1\,nm$. These films did not show any apparent dewetting by optical microscopy. The films were subsequently placed in contact with different concentrations of BA (0%, 0.3%, 0.5%, 0.6% and 0.7%) in D_2O with Pemulen TR-2 gel at pH 7 (adding TEA) and observed by NR as a function of shear, time and temperature.

Preparation of the gelly matrix

The LA film was studied in contact with a polymer solution of Pemulen TR-2 from CTS France (Lubrizol). This dispersion is prepared by following the suggestions from Stravroudis[44] at 0.1% of PTR-2 in D_2O at pH 7. First, 0.1w% dry powder of PTR-2 is mixed with water and dispersed by stirring it overnight to obtain an uniform mixture. Then, the final pH of the preparation is adjusted by adding some drops (about 0.1% in total volume) of TEA previously dissolved in D_2O to the PTR-2/D_2O mixture until reaching a homogeneous solution of pH 7 ± 0.2.[32,44] Then, a chosen amount of BA is added to the polymer solution, mixed 1 hour and left 48 hours at room temperature. At 0.1% PTR-2, the solution has a

low viscosity and it can flow through the tubing connected to the relfectometry cells.

NR experiments

Neutron reflectomery (NR) was performed to extract the vertical swelling of the polymer film by directing a collimated neutron beam at the Si/LA/W interfaces through the Si block, and measure the reflected intensity as a function of momentum transfer normal to the interface. For a short introduction of NR on the here studied system the reader is referred to our previous publication.[14]

NR experiments were performed on the time-of-flight (ToF) reflectometer FIGARO[47] at the Institut Laue-Langevin (ILL), Grenoble, France. The samples were either placed in air with the neutrons reflecting up to investigate the dry polymer layer or were contained in a heated solid/liquid cell with reflection down geometry to enable potential air bubbles to drift away from the interface (see Fig. 2 for a sketch of the experiment). Some measurements were performed inside a rheometer (Anton Paar MCR501) installed *in situ* on the beam line[37] to impose a shear stress on the LA film during the passage of the neutron beam. This was done in reflection down geometry, as well. In all cases a wavelength band between 2 Å and 20 Å was chosen with a relative wavelength resolution of 3.0 % (FWHM). The detector, which allows at the same time the specular and the off specular reflectivity to be measured, has a resolution of 2.2x4.8 mm^2 (FWHM) and a size of 25x48 cm^2 at a distance of 2.8 m from the sample. The full q-range was obtained with two reflection angles of 0.622 and 2.622 degrees. The beam footprint on the sample was set to 39x39 mm^2 for both reflection angles. The raw data was normalized to the incident beam spectrum by the data reduction software COSMOS.[48]

Ultrathin polymer films on silicon single crystals were first placed in contact with pure D_2O in order to have a reference state before swelling with BA. These films were then placed in contact with Pemulen/D_2O mixture containing various fractions of BA in a closed cell. Subsequently, the temperature was increased each 15 min until 70 °C and the structural

evolution of the films was observed by NR. Four BA concentrations were studied: 0.3 %, 0.5 %, 0.6 % and 0.7 % BA.

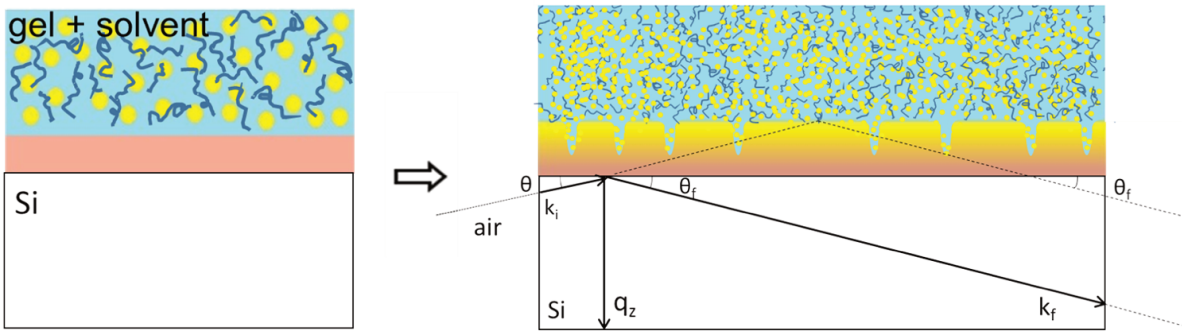

Figure 2: Sketch of the experiment. The yellow dots represent the solvent (BA) and the blue chains the Pemulen molecules. Note that the reflection angles are exaggerated for illustration. Also the lengths of the incoming (k_i) and outgoing (k_f) wave vectors are identical in elastic scattering. On the right hand side water-filled holes with finite depth inside the varnish are illustrated.

Specular NR analysis

The measured NR data is subsequently compared to simulated NR curves calculated by an optical matrix formalism from a slab model[49] and the goodness of the fit is calculated. This least-squares fitting procedure is repeated until a convergence is found by using MOTOFIT.[50] An alternative fitting program was based on a home modified Refl1D[51] program using python to take into account the relevance of the various parameters of the different models. The model used in all cases consists of an infinitely thick single crystal silicon slab covered by a thin layer of silicon dioxide, which thickness varied between 1 nm and 2 nm among the samples, and a layer (or sequence of layers) of swollen LA/D_20/BA on top capped by an infinite layer of D_20/BA/Pemulen/TEA. Each of the slabs has three fitting parameters, the thickness, the roughness and the scattering length density (SLD). The SLD is the number density of isotopes per unit volume multiplied by the corresponding scattering length for neutrons. It can be calculated by knowing the mass density of a material and its chemical sum formula. The SLD calculator from the NIST webpage was used here which uses tabulated values for

scattering lengths and isotope weights.[52] The SLDs and the corresponding chemical sum formulas used in this study can be found in Tab. S2 in the supporting information (SI). The thickness and the roughness of all layers were fitted as well. The silicon substrate and silicon dioxide were found to be atomically smooth (between 0.2 nm and 0.5 nm) and therefore are not discussed further.

Several morphological models were envisaged for the LA layer to fit the data including 1) A dewetting profile consisting of three sub-layers as shown in Fig. 1: Dry wetting layer, layer perforated by water-filled holes and a projected layer due to rims as used in our previous study about the same films in contact with BA/water,[14] 2) LA layers with holes that cross the films down to the substrate without a wetting nor a rim layer, 3) Similar to 2) but with limited depth holes (see Fig. 3 Bottom) and 4) a single homogeneously mixed layer consisting of LA/BA/water. Note, that models 2) and 4) cannot be distinguished by specular reflectometry alone, as for each of these models the SLD profile is estimated by in-plane averaging the LA and D_20 fractions. The NR spectra were calculated using Motofit or Refl1D with a modified model corresponding to the morphological case, and compared to the experimental spectra using a step by step least-squares fitting procedure. In order to justify the in-plane averaging of the SLDs, the size of the defects are supposed to be smaller than the in-plane neutron coherence length.

Note that the scaling of the fitted reflectivity curves was fixed to one in one set of analysis. The lower scaling of the measured curves at an advanced stage of layer destruction is due to enhanced off-specular scattering as explained in the Supplementary Information. In these cases the low q part of the NR curves was excluded from the fitting procedure. In another set of analysis the scaling factor was adjusted when the OSS becomes important and the low q part of the NR was also fitted. This analysis strategy lead to good fits as well, the resulting SLD values were not physically reasonable, though.

In order to extract quantitatively the partial volume fractions from the NR spectra two approaches were used: First the system was simplified into only two components: The polymer with a SLD_{LA} value of $0.9{*}10^{-6}$Å^{-2} and solvent with the fitted SLD_s values from the critical edge positions of the NR curves. From the fitted mean SLD values SLD and thicknesses h of the layer the resulting 'dry' volumes of the polymer v_{pol} (normalized to the dry LA volume) and solvent v_s fractions were extracted using the following formula:

$$\begin{aligned} v_{pol} &= \tfrac{h(SLD-SLD_s)}{h_0(SLD_{LA}-SLD_s)} \\ v_s &= \tfrac{h}{h_0} - v_{pol} \end{aligned} \tag{1}$$

Here h_0 is the dry thickness of the polymer. This approach does not assume mass conservation but can only extract two unknowns from the two measured values. Assuming conservation of the polymer mass ($v_{LA} = 1$) as done in our previous work for low BA concentrations[14] one can extract the BA (excess) volume fraction $\phi_{BA/LA}$ as well as the water fraction $\phi_{W/LA}$ inside the polymer layer from the following boundary conditions:

$$\begin{aligned} &1 + \phi_{W/LA} + \phi_{BA/LA} = \tfrac{h}{h_0} \\ &\\ &\tfrac{h}{h_0} * SLD = \phi_{W/LA} * SLD_w + \phi_{BA/LA} * SLD_{BA} \\ &+(\tfrac{h}{h_0} - \phi_{W/LA} - \phi_{BA/LA}) * SLD_{LA}, \end{aligned} \tag{2}$$

where SLD_{BA} is the bulk SLD of BA.

Off-Specular neutron reflectivity

As the neutron reflectivity spectra were recorded using 2D detectors the off specular neutron reflectivity (OSS) is also accessible.[53] The OSS intensity corresponds to the intensity scattered at a condition away from the mirror reflection (NR). In this case the total momentum transfer also comprises an in-plane component. This allows one to determine SLD

variations parallel to the interface but due to the geometry the momentum transfers are typically two orders of magnitude smaller than in specular reflectometry and therefore the spatial resolution is much lower probing micrometer sized structures. The 2D OSS patterns were simulated in wavelength vs. scattering angle space using the Distorted Wave Born Approximation (DWBA) assuming exponentially decaying in-plane correlation functions.[54] This gave access to one additional parameter, namely the mean size of in-plane inhomogeneities.

Results

Film morphology in contact with BA/TR2/water gel from specular NR analysis

A first-glance analysis of the NR spectra suggests a substantial LA film swelling in contact with BA/water/pemulen (Fig. 3). In accordance with the previous study which has shown that the LA thin film dewets the Si substrate when exposed to BA/water mixtures,[14] one could extrapolate this process to explain the NR data in contact with BA/water/pemulen as well. Dewetting leads to holes and rims and yields typically an averaged SLD profile as depicted in Fig. 1. When, however, the NR spectra of films exposed to BA/water/pemulen are fitted in terms of this dewetting induced SLD profile with various rim morphologies (height, width and fractions), the χ^2 values were found minimum for a rim fraction equal to 0 (Fig. 4). This strongly rejects rims as a potential morphology in the present case.

The second significant difference compared to LA films immersed in only solvent/non-solvent mixtures studied previously[14] is the absence of a well-defined wetting layer. Only models of constant SLD profile or SLD gradients over the entire layer (no sharp SLD step, see Fig. 3) lead to reasonable χ^2 values. In all cases the growth of the average SLD of LA exposed to BA/water/pemulen is apparent resulting either from holes that cross the film, non crossing

holes or heterogeneous zones of LA/BA/water/Pemulen inside the films. These models can all reasonably fit the specular NR spectra with small variation depending on the fraction of BA and temperature. The best goodness of fit for the 0.3% BA concentration with χ^2 values around 4 was achieved assuming a gradient in SLD across the whole layer starting with the SLD value of the polymer layer when in contact with pure D_2O close to the Si substrate and an increasing SLD towards the aqueous phase. This profile corresponds to a distribution of hole depths with only few reaching the Si substrate (penetrating the whole film). Typical reflectivity fits and SLD profiles using this model can be seen in Fig. 3. For higher BA concentrations, in addition to the gradient, the SLD of the LA in contact with Si had to be fitted as well to reach similar χ^2 values. This resulted in flat SLD profiles inside LA corresponding to water-filled holes crossing the whole film. A typical NR fit in this case can be seen in Fig. 4.

If the scaling factors of the NR data were adjusted in the fit, qualitatively similar results were obtained particularly for the total film thickness, however, the absolute SLD values gave nonphysical results.

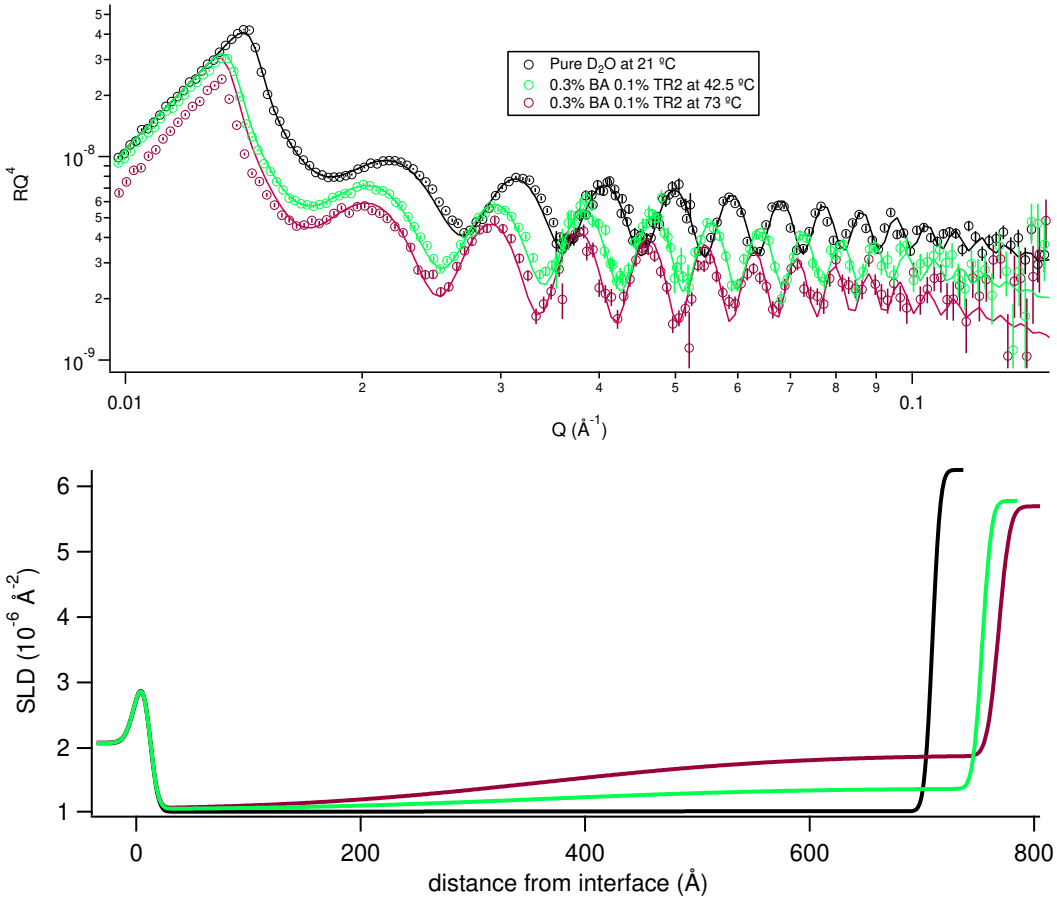

Figure 3: Top) Typical reflectively curves (multiplied by q_z^4) vs. momentum transfer q_z on a logarithmic scale for LA films in pure D_2O (black circles) and in aqueous solutions of 0.3% BA and 0.1% Pemulen at two different temperatures as depicted in the legend. The solid lines in the same color code are fits to the data. Bottom) The corresponding SLD profiles in the same color code.

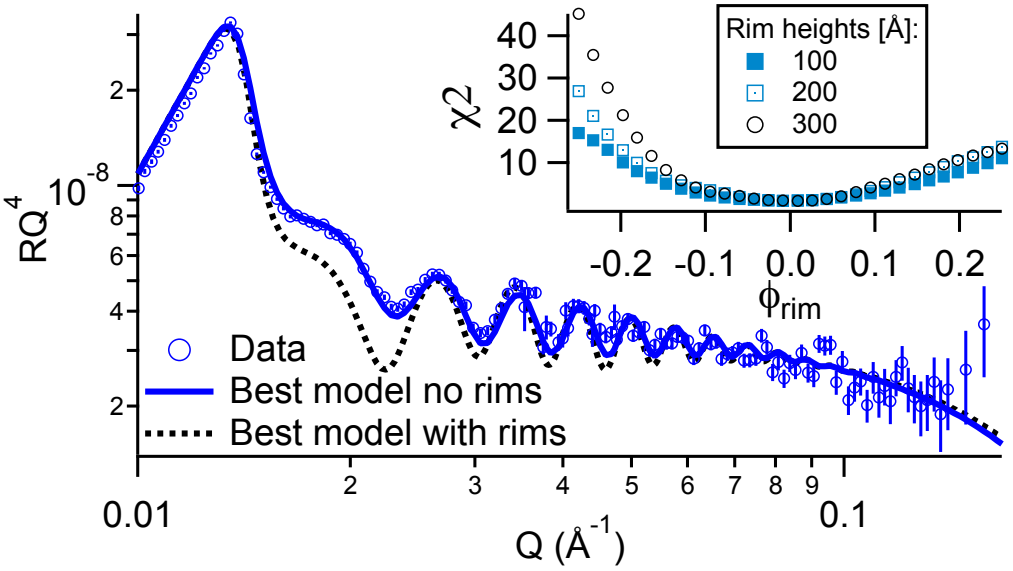

Figure 4: Reflectively curve (multiplied by q_z^4) vs. momentum transfer q_z on a logarithmic scale for an LA film in aqueous solutions of 0.5% BA and 0.1% Pemulen at 27°C (data points). The solid line in the same color code is the best fit to the data assuming no rims. The broken line is the best fit to the data assuming a rim fraction as in Fig. 1 left. Inset: Normalized least square value χ^2 vs. fraction of rims ϕ_{rim} for various heights of rims as indicated in the legend deduced from fitting the specular NR spectra to a model of LA containing a fraction of holes and rims.

Effect of temperature and BA concentration on film swelling in BA/pemulen/D_2O gel

Fig. 5 shows significant swelling of LA films when exposed to BA/Pemulen/D_2O gels for all the cases investigated here. For the case of 0.3%, the swelling ratio (SWR) is calculated as the ratio of the film thickness in the presence of BA/Pemulen/water to that in pure D_2O. This is justified by the fact that LA films do not swell in the presence of pure D_2O even after 24 h at least within the resolution of the NR experiment.[14] At room temperature (21 °C), Fig. 5 shows that the LA film swells by 4.5% at a BA concentration of 0.3% which is the exact same swelling ratio found without the gel.[14] D_2O is unlikely to swell LA films to the extent to be measurable by NR because the Flory-Huggins interaction parameter χ_{LA/D_2O} exceeds 4 at room temperature and therefore can safely be excluded as the swelling molecule.[14] LA

swelling in BA/Pemulen/D_2O is most likely due to BA which has a favorable Flory-Huggins interaction parameter $\chi_{BA/LA}$ between -0.05 and 0.17.[14] Because of its high molecular weight Pemulen can also be excluded as a swelling agent for LA. Even if TEA can swell LA, it is unlikely to account for the measured LA swelling in the present case because it is highly miscible in water. Even in the extreme case of a similar interaction parameter with water ($\chi_{W/TEA}$) and LA ($\chi_{LA/TEA}$), the partitioning of TEA in LA would not exceed the concentration of TEA in water, which is 0.1%, which is within the error bar of the measured SWR. Therefore one can safely attribute the measured SWR to BA uptake by the LA film.

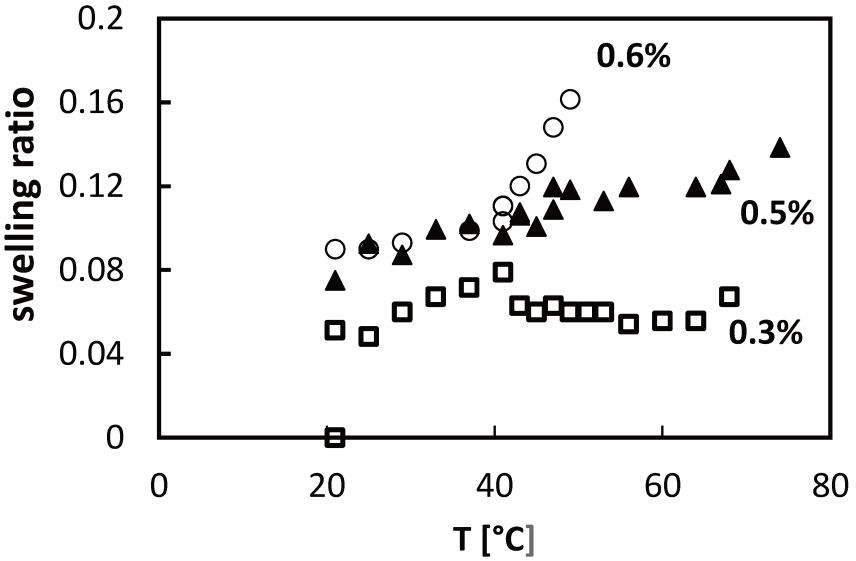

Figure 5: Swelling ratio of a LA film in BA/PTR2/water vs. temperature for BA fractions of 0.3%, 0.5% and 0.6%. The swelling ratio is calculated as the ratio of the film thickness in the presence of BA/PTR2/D_2O at various temperatures to the initial film thickness in pure D_2O. The thickness is extracted from the analysis of NR spectra. For 0.5% and 0.6% the film thickness is extrapolated from dependence of the swelling ratio on $\phi_{Ba/W}$ and film thickness at room temperature.

In order to extract the individual partitions of the involved materials the volume fractions of two constituents can be extracted if the polymer mass conservation is not imposed (eq. 1) or three constituents if the conservation of polymer mass is assumed (eq. 2) from the fitted

NR curves with a two-polymer-layer model as described in the Experimental section. The resulting total volumes of solvent and polymer within the layer without imposing polymer mass conservation are plotted in Fig. 6.

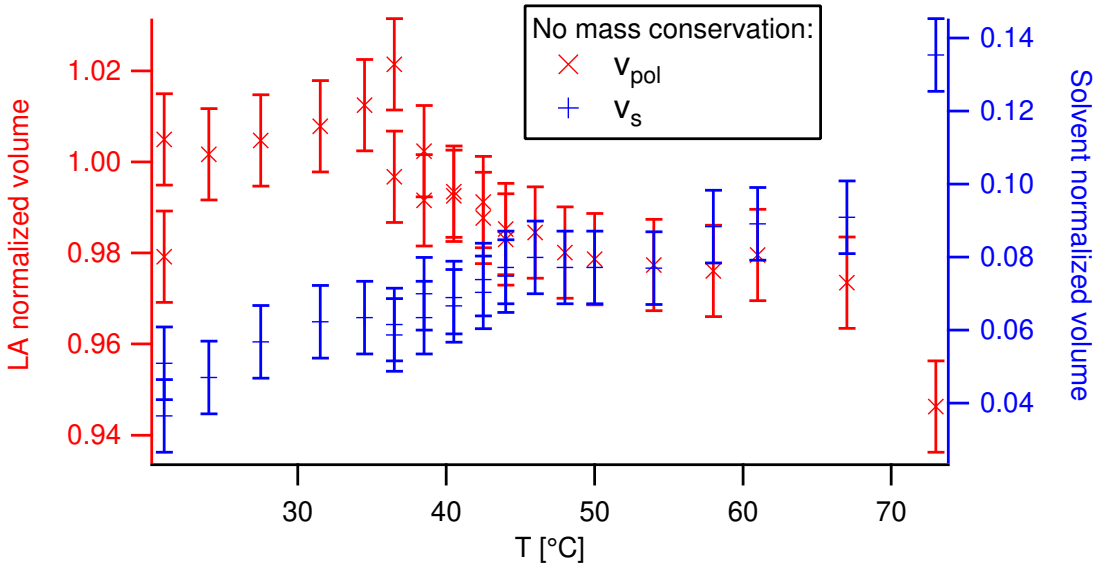

Figure 6: Normalized (excess) volumes of the polymer (red x-crosses, left axis) and liquid (blue crosses, right axis) inside the LA layer from NR of 0.3% BA and 0.1% PTR-2 in D_2O according to the boundary condition eq. 1 as a function of temperature. Note: The two points at R.T. for each fraction were measured at two different times, once at the very beginning and a second time after heating to 40 °C indicating that the polymer loss is irreversible, but the solvent penetration is reversible within error.

As can be seen in the graph the polymer mass seems to be conserved until 38°C with an increasing solvent faction with temperature. Above this temperature there is clearly (irreversible) loss of polymer observed on the expense of more and more solvent penetrating the film. Therefore below this temperature the mass conservation can be assumed and a more detailed partial swelling can be extracted differentiating between water and BA (eq. 2). This result is presented in Fig. 7.

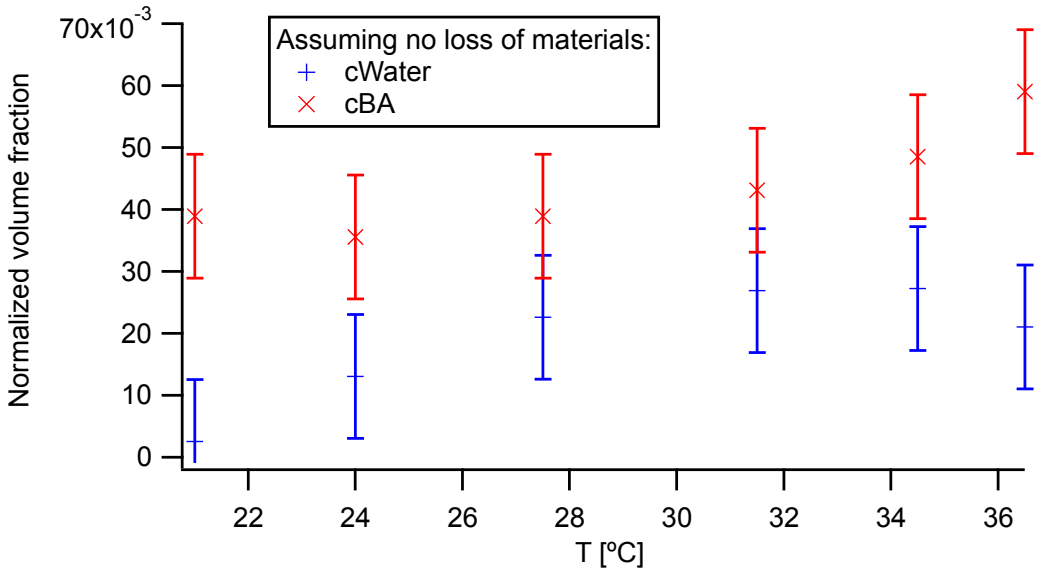

Figure 7: Normalized volume fractions of BA (red x-crosses) and water (blue crosses) from NR of 0.3% BA and 0.1% PTR-2 in D_2O according to the boundary condition eq. 2 as a function of temperature.

As suggested above from the Flory-Huggins interaction parameters indeed the swelling at R.T. is mainly attributed to BA with no significant penetration of water. However, with increased temperature (and time) it seems that the volume fractions of both water and BA are increasing. It has to be noted, however, that the increase in BA fraction with temperature is reversible but the water fraction increase is not. Therefore it seems that there are two parameters influencing the partitions: Increased chemical compatibility of BA and LA with temperature and onset of dewetting by water filled cavities with time.

The fact that the presence of hydrophobic domains from the Pemulen TR2 side group (C10 to C30) does not shift the partitioning balance of BA or water is an important result as Pemulen effectively acts as an emulsifier. This could only infer that the number of hydrophobic moieties at this PTR2 concentration of 0.1% is not enough to perturb the swelling equilibrium. Recovering the same SWR with or without Pemulen at room temperature for 0.3% is a first important result for restoration processes as this means that there is no need to increase the BA concentration when using Pemulen to control solvent transfer to the varnish layer at least when working at room temperature.

Whatever the exact model used for fitting the specular NR of LA in BA/PTR2/D_2O, a SLD growth with temperature (and time) of the LA film is observed, which can only suggest D_2O invasion into the LA film as it is the largest SLD constituent as quantitatively shown above. The film invasion with water can result either from creation of penetrating or non-penetrating holes filled with D_2O or formation of LA/BA/D_2O mixed zones. Assuming holes as the reason for increased water fractions it is possible to calculate SLD density profiles by assuming a Gaussian distribution of cylindrical water filled holes around a mean depth inside a LA film of fitted total thickness. The detailed analysis of the NR spectra with this model assuming LA mass conservation using the least square method yields similar tendencies for the dependence of the surface fraction of holes (ϕ_{hole}) on temperature for fully penetrating holes and for holes with finite depth (see Fig. 8). ϕ_{hole} was found to increase slightly for 0.3% with increasing the temperature up to 70 °C. On the other hand ϕ_{hole} for 0.5% strongly increase up to the breaking temperature and for 0.6% increases rapidly between 37 °C up to the breaking temperature of 49 °C. The absolute values of ϕ_{hole} are higher if the LA mass is allowed to decrease, but the qualitative trend stays the same. We will therefore present the SLD of the fitted LA layer rather than ϕ_{hole} in the following in order to be less model dependent.

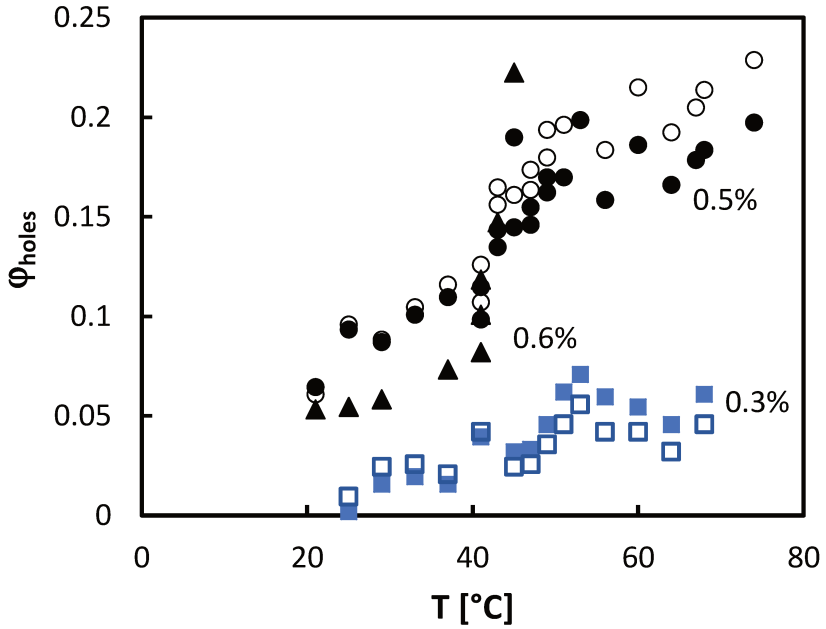

Figure 8: Surface fraction of holes (ϕ_{hole}) containing D_20 vs. temperature for films in contact with BA/PTR2/D_2O for BA fraction of 0.3%, 0.5% and 0.6%. ϕ_{hole} was deduced from fitting the NR spectra to a crossing hole model (full symbols) and non-crossing holes (empty symbols).

Effects of temperature and BA concentration on the film heterogeneities prior to film breaking in the BA/pemulen/D_2O dispersion

Many aspects of the reflectively spectra of Laropal®A81 in BA/pemulen/D_2O point out to the initiation and evolution of significant heterogeneities and defects. This can be seen in the off-specular scattering, film roughness and the process of water invasion. From the first glance, these defects could be analyzed in terms of a simple dewetting process induced by BA as in the case BA/D_2O (without Pemulen). However, significant morphological differences to the case in pure are observed and will be discussed in the following.

Film heterogeneities from OSS

In all NR measurements a clear Yoneda-type scattering was observed around the critical momentum transfers (see Fig. 9). This points towards in-plane SLD correlations present in the system. Quantitative fits of the 2D scattering patterns[54] clearly showed that the origin of this scattering comes from inhomogeneities inside the bulk of the film filled with water. The interface roughness as the only origin of the scattering can be clearly excluded as this would lead to much less scattered intensity. Moreover, it became evident that the SLD contrast contributing to this scattering must come from D2O rich phases inside the polymer, which is the largest SLD contrast when looking at Table S2 in the supporting information. This bares striking similarities to our previous study of LA films in binary water/BA mixtures,[14] where water-filled holes were the origin of the OSS scattering as evidenced by AFM. In the present case AFM measurements were not possible as the gelly solution was sticking to the polymer films and impossible to be removed without detachment of the LA film as well.

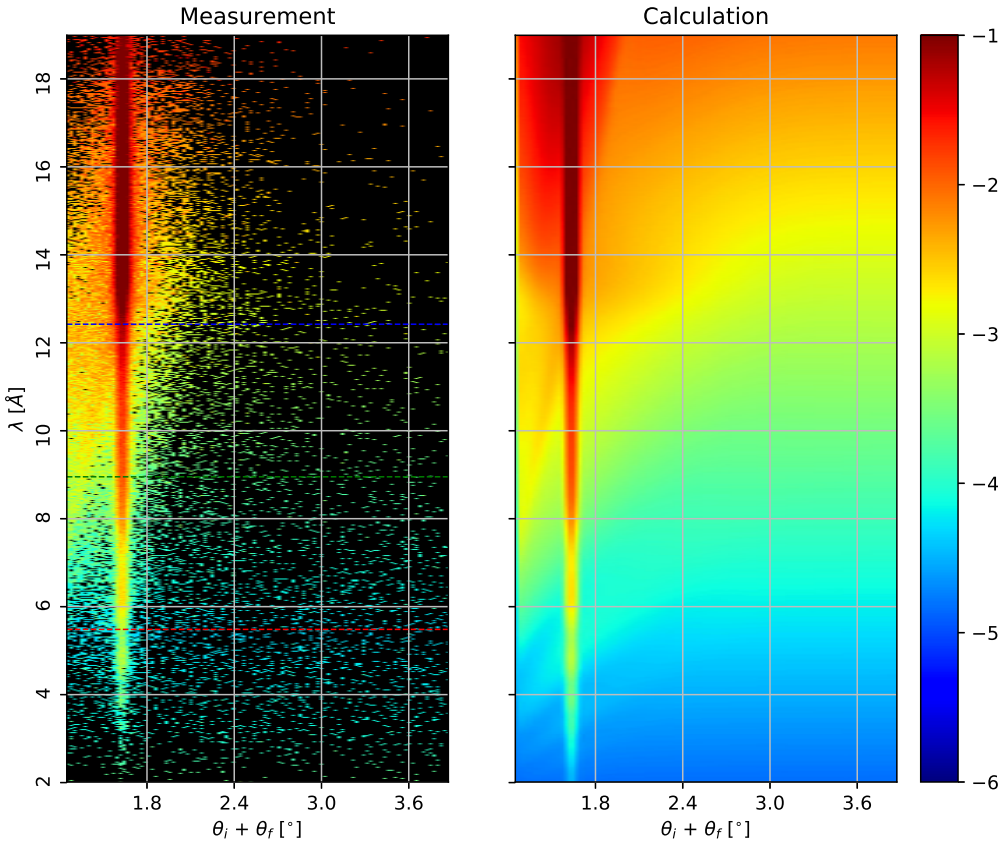

Figure 9: Left: OSS of a LA film in contact with 0.3% BA and 0.1% PTR-2 in D_2O at 72°C. Right: Simulation using the same instrument parameters as in the measurement and using the fitting results from the specular fits and in-plane inhomogeneities filled with water assumed to follow an exponentially decaying SLD on average with a characteristic length of 0.7 μm.

From the quantitative fits of the OSS intensity to an exponentially decaying in-plane SLD inhomogeneity one can extract a characteristic in-plane correlation length, which would correspond to an average hole radius in case of holes. This is plotted in Fig. 10 for a 0.5% BA solution in 0.1% Pemulen as a function of temperature. In addition the SLD from the specular fits is shown on the same graph. In order to put these results into perspective with

the pure water case the results from a similar LA film in contact with a 0.5% BA solution in pure water are added to the graph. These are from the preceding study done at room temperature only.[14] Here another apparent difference between the varnish in contact with a gel and with pure water, both containing BA, can be appreciated: While the SLD is on the same order for both cases at low temperatures it clearly increases significantly for the gelly case at elevated temperatures. The SLD increase is linearly related to the volume fraction of water-filled holes inside the layer, which means that the volume fraction of holes is significantly higher in the Pemulen solution at elevated temperatures compared to the pure water case at R.T. On the other hand the size of the holes is smaller in the case of the polymer dispersion, even at the highest temperature investigated here. This unambiguously testifies a significantly higher hole density in the case of the Pemulen solution. Assuming the hole size extracted from the quantitative OSS fits to be the hole radius, the hole density at R.T for 0.5% BA in pure water is about $0.1\,\mu\mathrm{m}^{-2}$ and for the same BA concentration inside the Pemulen solution at 49 °C is about $3\,\mu\mathrm{m}^{-2}$ if the holes are not overlapping.

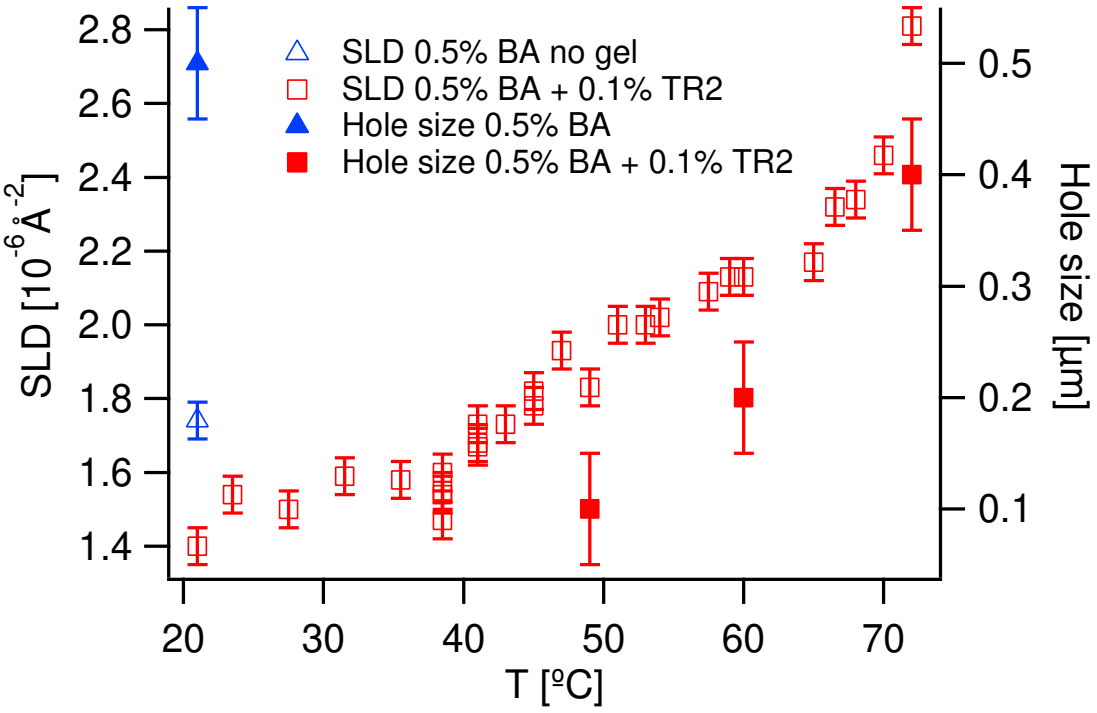

Figure 10: Left axis: SLD as a function of temperature from a LA polymer film in contact with 0.5% BA and 0.1% PTR-2 in D_2O (open squares). Right axis: Extracted hole radius from the OSS simulations of the same sample (filled squares). The triangles correspond to the SLD (open triangle) and the hole radius (filled triangle) of a LA film in contact with a 0.5% BA solution in pure D_2O after 2 h immersion.

Interface between varnish films and PTR2/BA aqueous solutions

The microscopic roughness of the polymer/liquid interface deduced from NR analysis is found to be around 0.6 nm at room temperature and low BA concentrations, while increasing to up to 1.2 nm at higher temperatures or BA concentrations. These values are manifestly higher than the reported one in the case of binary BA/D_2O mixture[14] which never exceeded 0.3 nm. This suggests that adding Pemulen into the aqueous phase favors surface roughness.

An immiscible polymer/polymer interface should develop an interface width σ corresponding to the squared sum of the intrinsic roughness σ_i coming from chemical interactions and scaling with the monomer size a,[55] and the capillary wave roughness σ_{CW} due to interfacial tension

γ if the sample is in equilibrium[56]:

$$\sigma^2 = \frac{k_B T}{2\pi\gamma} \ln(\frac{l_c}{a}) + \sigma_i^2, \tag{3}$$

where the capillary wave spectrum is cut by the neutron coherence length l_c. k_B denotes the Boltzmann constant. The intrinsic width for a high Flory-Huggins interaction parameter χ can be estimated by[55]:

$$\sigma_i = \frac{a\sqrt{N}}{3\sqrt{\chi/2 * N - 1}}, \tag{4}$$

with the polymerization N. The surface energy of Laropal®A81 was determined by measuring the contact angle of different liquids on top of a macroscopic LA film[57] and turned out to be around 30 mN/m.

Using water as the "monomer" with a typical size of a water molecule of 1.8 Å[58] one gets indeed around 3 Å roughness of the interface using the χ values between 2.5 and 4 and $N = 30$ as determined in our previous study[14]. Using around 1 nm as the size of the monomer results in roughness between 4.5 Å and 5.5 Å for the binary mixture. In the case of the lower surface tension of the gelled solvent of around 56 mN/m[32] we get indeed higher values between 3.6 Å and 5.9 Å using 1.8 Å or 1 nm as the monomer size, respectively, assuming the same χ values as for the binary mixtures. This slight roughness increase can explain the interface width of the polymer/D2O/Pemulen system measured at R.T. which is around 6 Å for 0.3% or 0.5% BA, especially taking account that the Pemulen acts as an emulsifier, although its volume fraction is very low (0.1%). The increase of the roughness with temperature up to 70° between 1 Å and 2 Å for the 0.3% or 0.5% BA mixtures, respectively, is, however, more than what would be expected by a mere reduction in interfacial tension with increasing temperature. Moreover, the roughness values above 1 nm in the case of 0.6% BA cannot be explained by a decreased interfacial tension alone, but have to involve a reduction of the Flory-Huggins interaction parameter as a function of temperature. This result is in accord with the increased BA swelling of LA at elevated temperature as observed in Fig. 7.

Interestingly the temperature induced roughness increase of the aqueous/polymer interface seems to plateau at a certain temperature as can be seen in Fig. 11. The origin of this effect remains somewhat unclear. This temperature is close to the glass transition temperature if calculated using the binary mixing model as will be explained later. One could therefore imagine that 'unfreezing' of stresses could be the origin of this stagnation. Note, however, that the change in roughness is reversible as the value at room temperature was measured twice at different moments during the heating protocol (see the two points at R.T. in Fig. 11). Therefore this behaviour is unlikely to be related to non-equilibrium properties. On the other hand, starting from 40 °C a loss of polymer mass is observed (see Fig. 6) by formation of water-filled cavities. It is therefore possible that the roughness contribution due to these cavities is significantly larger than the intrinsic interface roughness and therefore screens the latter as specular NR measures only the sum of the two contributions. Again, the reversibility of the roughness increase even after the appearance of cavities contradicts this hypothesis. Another possibility is that the interaction between BA and LA becomes athermal above 40 °C meaning no further improvement of the polymer/solvent compatibility at higher temperatures. A counter indication to this explanation is that in a test a LA/BA mixture (5% BA) was cooled down to -20° and showed no indication of phase separation, meaning the BA at room temperature is already far away from theta condition, also consistent with the very low Flory-Huggins parameter around zero.

Finally, the roughening of the polymer/liquid interface could also be attributed to the presence of TEA. The presence of weak surface-active molecules might help the formation of interfaces, increasing the actual roughness or lead to a larger SLD gradient upon adsorption, visible as an increased interface roughness (rather than a distinct layer) due to the small size of TEA.

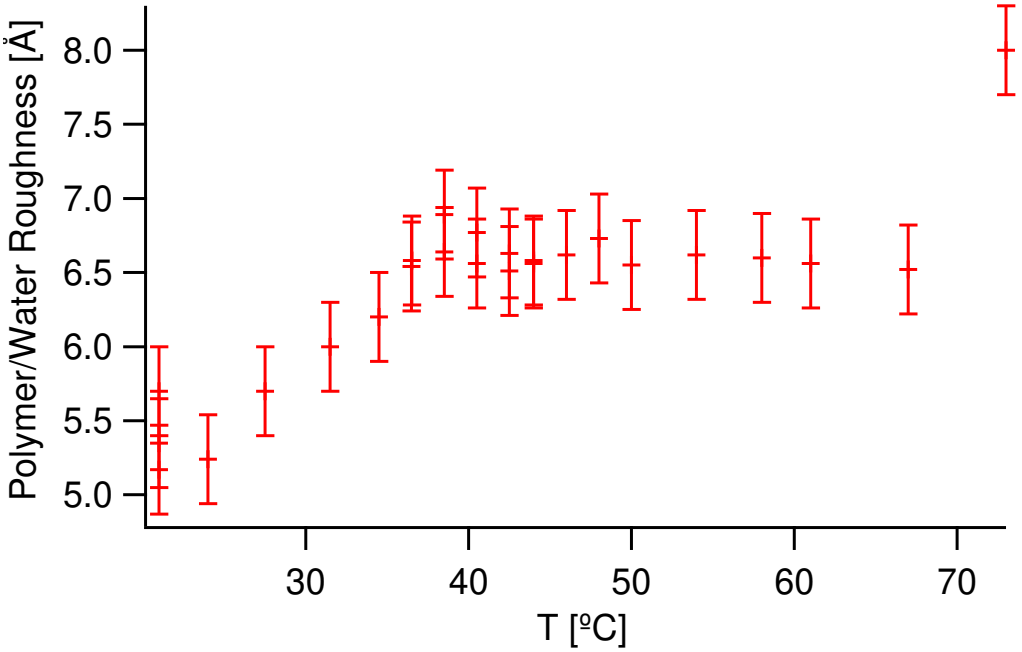

Figure 11: Roughness of the aqueous/polymer interface deduced from NR for a solution of 0.3%BA and 0.1% PTR-2 in D_2O as a function of temperature.

For higher BA concentrations the roughness values are generally higher going up to 1.2 nm but show a similar increasing trend with temperature. Due to the limited temperature ranges available for the other BA concentrations and larger uncertainties their trends are not obvious and therefore they were not analyzed further.

Temperature and solvent influence on the stability of the film

An important outcome of this experiment regarding art restoration field is the onset of film breaking and destruction. Indeed while increasing the temperature most of films investigated here, except for 0.3 %, breaks within the NR experiment yielding a non quantifiable NR spectra. The critical temperature (T_{crit}) for film breaking is found to to be BA fraction dependent and decreases with increasing BA from room temperature to above 72 °C (Fig. 12). At 0.3 %, the film never breaks until the temperature limit of this study (16.5 to 73 °C). At 0.5 %, the temperature of the film breaking was 72 °C, at 0.6 % BA at 44 °C

and at 0.7 % BA only at 21 ° C.

The basic idea behind the strategy of adding moieties of good solvent to a bad solvent gel in art restoration is softening the varnish film to promote its mechanical removal by abrasion. This would lead to reducing its T_g below room temperature via solvent plasticising. The results presented here show that the mechanism is more complex and the chemical interaction plays an important role in this process.

The T_g of the binary LA/BA mixture can be estimated using the partitioning constant of BA between LA and water from NR experiments on thin films[14] and the mixing model:

$$\frac{1}{T_g} = \frac{1-\phi_{BA}}{T_{g(LA)}} + \frac{\phi_{BA}}{T_{g(BA)}}, \tag{5}$$

Using $T_{g(BA)} = -105.15\,°C$[59] for BA and $T_{g(LA)} = 47\,°C$ for LA and the $\phi_{BA/LA}$ concentrations from our previous study.[14] The resulting glass transition temperature as a function of $\Phi_{BA/WA}$ is plotted in Fig. 12 as a black line and decreases from around 35 °C at 0.3% BA to 18 °C at 0.7% BA, the highest solvent concentration examined in this study. The temperature at which a sudden increase in mass loss is observed (film removal) is at 44 ° C for 0.6% BA, 72 °C for 0.5% BA and above 72 °C for 0.3% BA, which is 20-37 °C above the respective glass transition temperature. This suggests that the sudden 'unfreezing' of the film's surface tension stress is not the main motor for film breaking because at 0.3% and 0.5% BA concentrations the film remains largely intact. This does not mean, however, that residual stresses cannot be the origin of hole nucleation as observed for other polymer thin films.[60]

Another important outcome of the fact that the film remains largely intact for extended periods of time more than 20 °C above T_g is that the kinetics driving the film destruction are not controlled by the polymer viscosity. As LA is a low molecular weight polymer its viscosity should decrease by orders of magnitude when crossing T_g. If 'normal' dewetting, which kinetics are governed by viscosity, were to be the origin of film destruction in the here

studied case the kinetics should accelerate by orders of magnitude above T_g as observed with thin polystyrene films dewetting from functionalized silicon substrates: An acceleration of a factor 10 was observed when heating the sample by 10 °C above T_g.[61] In the here studied case the polymer film in contact with a co-polymer solution containing 0.3% BA was withstanding more than 10 h at temperatures significantly above T_g showing a clear layered structure observed by Kiessig fringes in the NR curves despite a high fraction of holes present. If, on the other hand, the BA concentration in the solution is increased to 0.7% the film is almost completely lost within only 3.5 h at 19 °C, which is around T_g. In essence, clearly the BA concentration inside the polymer is driving the kinetics of film destruction and not the polymers' viscosity.

The fact that the polymer softening is not the main driver for film break-up can also be appreciated by the concentration and temperature dependence of the different stages of film destruction. In Fig. 12 the information from T_g estimations, specular and off-specular NR on the state of the varnish film is summarized in a film stability diagram. The boundaries in this diagram are chosen to separate three regimes of film stability depending on $\phi_{BA/W}$ and temperature: a) The area below the black line corresponds to the solid zone below T_g as calculated from eq. 5, b) At higher temperature the polymer is liquid but does not show pronounced hole formation as evidenced by low OSS intensity. It is chosen to separate this phase from the inhomogenous zone at higher temperatures by a threshold of Yoneda peak intensity of 10^4 counts per minute (see Fig. S4 in the supporting information), marked by a blue line. This choice is arbitrary but its exact value will only shift the temperature of the boundary keeping the qualitative behaviour with BA concentration the same. Finally, the red line marks the temperature at which a sudden loss of most of the film's material is observed.

Looking at this film stability diagram it is obvious that the boundaries of film destabilisation are uncorrelated with the T_g evolution: While T_g is decreasing almost linearly with the BA concentration in the investigated range with a rather small slope, the other boundaries

show a much steeper BA dependence and are not necessarily linear.

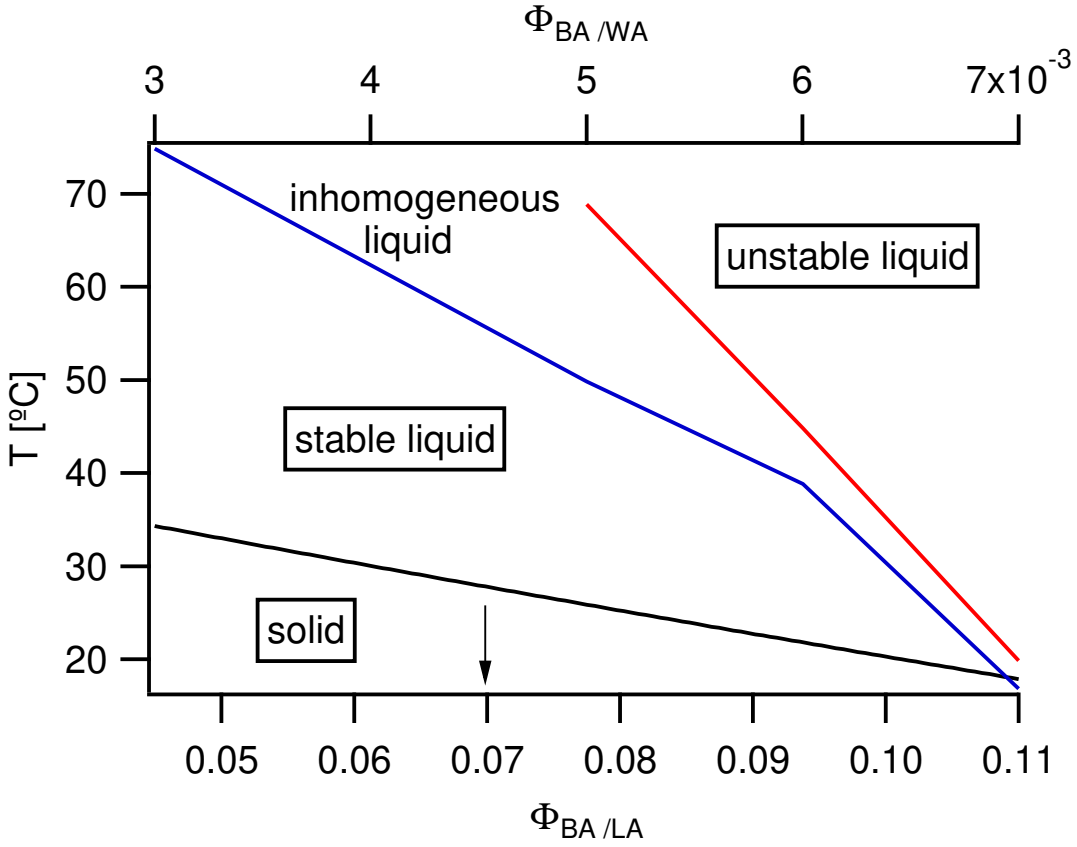

Figure 12: Film stability diagram using the T_g and NR results. The lower black line corresponds to the T_g as calculated from eq. 5 by using the BA in LA volume fractions from the bottom axis. The blue line in the middle corresponds to the threshold temperature where the OSS intensity is 10^4 counts per minute in Fig. S4 from the SI and the red line in the upper right corner marks the temperature at which a sudden loss of most of the film's material is observed. The latter two lines relate to the upper x-axis (BA fraction in water) and are deduced from the experimental data.

Discussion

Given the clear indications that the appearance of water-filled holes growing with time is responsible for the here studied film destruction, dewetting might seem to be the most likely scenario. Moreover, a very similar behaviour of the scattering curves at late stages of film destruction, compared to the case of pure water where dewetting was observed, can be shown as evidenced in the Supporting information. Clearly the driving force is the hydrophilicity

of the used substrate attracting the polar emulsifier and/or water as observed in our previous study.[14] The role of polar forces in dewetting of thin hydrophobic polymer films was also shown for polystyrene supported by silicon wafers immersed in poor solvents[30] or non solvent/poor solvent mixtures.[31]

However, several contradictions to the process of dewetting are observed. The most significant one is probably the fact that the kinetics are not governed by the polymer viscosity, but linked to the amount of solvent swelling. Clearly the retardation of dewetting is gradually switched off by increased solvent concentration inside the polymer. Suppression of dewetting was already observed for thin polystyrene films when their chain ends were functionalized by polar groups, explained by their bonding to the polar substrate and between the chains stabilizing the film.[29] Laropal is known to incorporate a significant amount of polar groups as well[40] and in our previous study of LA films in contact with water/BA mixtures we observed a wetting layer which was not perforated by the dewetting holes testifying the strong bonding of annealed LA to the polar substrate.[14] However, at higher BA concentrations or longer exposure the vast majority of the film vanished, eventually. In the aforementioned study we also observed a retarded swelling of the LA film when exposed to aqueous solutions containing increasing amounts of BA: While for small solvent concentrations almost no swelling was observed, a linear swelling behaviour was recovered as predicted for bulk LA at BA concentrations above 0.2%. We argued that bonding or cross-linking of some sites of the polymer to the substrate were responsible for this swelling retardation, which would be gradually suppressed by the addition of BA.

It is possible that a similar mechanism is at play in the here studied case of the same LA film in contact with a BA containing viscous polymer dispersion. Indeed, for 0.3% BA we again observe a quasi water-free zone close to the substrate (see Fig. 3 Botttom) although this 'wetting layer' is much less pronounced compared to our previously investigated case

without the Pemulen. In addition, contrary to our previous study, at higher BA concentrations this 'dry' layer is not visible anymore. This could be, however, due to the much more polar -OH groups contained in the co-polymer in comparison to water. Therefore the scenario of dewetting retardation due to polar group interactions inside the polymer film and with the polar substrate, which are gradually screened or broken by the polar BA seems to be the most likely scenario. The highly stable film state could be also appreciated by a test where *in situ* shear was applied to the BA swollen film not altering its structure as shown in the supplementary information.

Another contradiction with typical dewetting (and the previous study on binary water/solvent systems) is the here observed absence of rims. However, this could be explained by a) the fact that the polymer/substrate interaction is effectively weaker due to the presence of highly charged groups of the Pemulen, similar to the absence of rims observed for films experiencing plug flow,[62] b) the smaller size of holes, similar to early stages of dewetting of polymer films on non-adsorbing substrates,[28] or most importantly c) the fact that the films are effectively fluid, being above the T_g while the dewetting speed is retarded and thus not limited by viscosity giving the films the time to reach their equilibrium thickness at any stage of dewetting.

Due to the presence of an emulsifier in the system (Pemulen TR-2) we cannot exclude a gradual emulsification of the LA film by its incorporation into the aqueous phase due to the hydrophobic side groups of Pemulen, leaving behind voids leading to holes in the film. Due to the high viscosity of the solution it is technically challenging to establish an equilibrium phase diagram of the here studied system in contrast to the water-based system studied before.[14] However, Pemulen TR-2 is known to form a microgel with typical droplet sizes in the (sub-)micron range when stabilizing an emulsion.[33] Therefore an emulsification process starting from the polymer/gel interface should engender a significant roughening of the poly-

mer surface. As seen in Fig. 11 the measured polymer film roughness for a BA concentration of 0.3% never exceeds 1 nm testifying a molecularly smooth layer just before film rupture. We note that the amount of benzyl alcohol inside the Pemulen solution was up to 0.7% in the current study that is significantly lower than the solubility limit in water (4%). We therefore expect the solvent to be homogeneously distributed as is the case in pure water. Finally, the presence of TEA being a weak surface-active molecule might help the formation of interfaces and intermediate steps in the first stages of dewetting, kinetically favoring the process leading to the observed higher coverage of smaller holes.

On an application level, the results of this paper, such as the presence of holes or the temperature effect, provide new information for painting conservators and restorers. In case the holes pierce the entire varnish layer, the penetration of the solvent contained in the Wolbers gel can reach and get into the paint layer. Thus, inducing an irreversible risk of deformation, swelling and dissolution of this fragile layer. The appearance of (sub-)micron sized holes would also reduce the transparency of the coating. It has to be noted, however, that the here used silicon substrate is slightly hydrophilic and thus not generally representative for the pictorial layer supporting the varnish, being typically hydrophobic. Nonetheless, deeper layers in an easel painting can be hydrophilic as the glue typically used to support the preparation. This could be exposed to the varnish in cases of cracks. Another difference in real paintings is of course the absence of sharp boundaries between the layers. These gradual boundaries have a stabilizing effect on film cohesion.
On the other hand, the results of the combined action of temperature and solvent show that it is possible to remove varnish without mechanical stress, as is currently the case. Now, restorers have a better understanding of the process of removing varnish from paintings using solvent-loaded gels and can re-evaluate this approach in order to guarantee the safety of the paint layer.

Conclusion

The above results on the destruction of Laropal®A81 films in contact with solvent containing viscous polymer dispersions clearly show striking similarities with binary solvent/non-solvent mixtures studied earlier,[14] which points towards a dewetting-type process in the here studied system as well. As in the former case the appearance of water-filled cavities in the film is initiated by the addition of good solvent and significantly accelerated if the amount of solvent is increased. An increase in temperature above T_g, in turn, is not accelerating the dewetting kinetics as much, clearly showing that the dewetting speed is not viscosity limited as it is the case for pure non-polar polymers pointing towards a retardation of film destruction as seen for polymers having polar groups incorporated.[29] It is argued that the addition of polar solvent is screening or breaking the polar interactions inside the film and/or with the polar substrate leading to accelerated film destruction. Another similarity to the pure water case is the loss of polymer mass at late stages of dewetting.

There are, however, significant differences in the here studied case of a gelly matrix in comparison to the dewetting of Laropal®A81 in binary mixtures: No rims are observed, no clear wetting layer is seen and the size of the holes is significantly smaller, although their volume fraction is similar inside the layer. The smaller size of the holes and thus larger hole density can be explained by an increased spreading coefficient of the gel on the Si substrate due to the presence of highly charged -OH groups from the gel. It was shown that the hole density in dewetting polystyrene films on treated Si substrates is larger when in contact with higher energy surfaces.[63] The smaller size of the holes in turn partially explains why no rim is visible as the rim is not present for holes at early stages of visco-elastic film dewetting from non-adsorbing substrates[28,64]. In this case the altered interaction at the polymer/solid interface could be also the reason why no wetting layer is observed. Another explanation for the absence of rims could be the fluid nature of the film as the dewetting speed is obviously not viscosity limited.

In summary, the destruction of LA varnish films as used in art restoration when in contact

with Pemulen TR-2 aqueous solutions containing small amounts of solvent is not principally driven by reduction of the polymer's T_g but clearly governed by the good solvent swelling. The destruction is clearly occurring by the appearance of water-filled holes, similar to the previously reported dewetting-type process of the same films in binary solvent/non-solvent mixtures. Obviously, this behaviour would be catastrophic for art-restoration, it has to be noted, though, that the here used support (silicon) is hydrophilic, while the surfaces supporting the protective varnish layers in easel paintings are typically hydrophobic. However, the presence of polar groups inside Laropal®A81 seems to play a determining role for film stability, which is gradually screened by addition of polar solvent. This brings to evidence the importance of polar interactions in LA film removal, which should be taken into account in restoration recipes.

The presence of the gellifying polymer, however, apparently changes the interface width between the varnish and the polymer solution without shifting the solvent partition in the bulk of the materials. This opens a way for art restoration to tune the chemical and surface interactions, not only by varying the concentrations of the involved materials but notably by changing temperature. This is potentially a way to make varnish removal safe for art restoration by the use of gels in a temperature-controlled way. The smaller size of the holes can be also less evident concerning optical distortions.

Acknowledgement

We thank the ILL for neutron beam time on FIGARO (doi.ill.fr/10.5291/ILL-DATA.1-03-36). We thank the Partnership for Soft Condensed Matter at ILL for the use of complimentary techniques. The Laboratoire de Rhéologie et Procédés is part of the LabEx Tec 21 (Investissements d'Avenir - grant agreement n° ANR-11-LABX-0030) and of the PolyNat Carnot Institut (Investissements d'Avenir - grant agreement n° ANR-11-CARN-030-01).

Supporting Information Available

Additional NR fitting results, pre-characterization of LA layers, comparison of NR and OSS between LA films in contact with gel and pure water containing high BA concentrations and additional optical micrographs of LA films after long exposure to pure water and BA. *In situ* Rheo-NR of BA swollen LA films in contact with gel+BA.

References

(1) Debnath, K.; Bucio, T. D.; Al-Attili, A.; Khokhar, A. Z.; Saito, S.; Gardes, F. Y. Photonic crystal waveguides on silicon rich nitride platform. *Optics express* **2017**, *25*, 3214–3221.

(2) Crudden, C. M.; Horton, J. H.; Narouz, M. R.; Li, Z.; Smith, C. A.; Munro, K.; Baddeley, C. J.; Larrea, C. R.; Drevniok, B.; Thanabalasingam, B., et al. Simple direct formation of self-assembled N-heterocyclic carbene monolayers on gold and their application in biosensing. *Nature communications* **2016**, *7*, 1–7.

(3) Teh, L.; Tan, N.; Wong, C.; Li, S. Growth imperfections in three-dimensional colloidal self-assembly. *Applied Physics A* **2005**, *81*, 1399–1404.

(4) Boissière, C.; Grosso, D.; Prouzet, E. Inorganic Nanomaterials Synthesis Using Liquid Crystals. *Encyclopedia of Inorganic Chemistry* **2006**,

(5) Stolow, N. Action of solvents on dried linseed oil films. *Nature* **1957**, *179*, 579.

(6) Stolow, N. The measurement of film thickness and of solvent action on supported films. *Studies in Conservation* **1957**, *3*, 40–44.

(7) Michalski, S. A physical model of the cleaning of oil paint. *Studies in Conservation* **1990**, *35*, 85–92.

(8) Phenix, A.; Sutherland, K. The cleaning of paintings: effects of organic solvents on oil paint films. *Studies in Conservation* **2001**, *46*, 47–60.

(9) Fife, G. R.; Stabik, B.; Kelley, A. E.; King, J. N.; Blümich, B.; Hoppenbrouwers, R.; Meldrum, T. Characterization of aging and solvent treatments of painted surfaces using single-sided NMR. *Magnetic Resonance in Chemistry* **2015**, *53*, 58–63.

(10) Brandi, C.; Déroche, C. *Théorie de la restauration*; École nationale du patrimoine, 2001.

(11) Stolow, N. Application of science to cleaning methods: Solvent action studies on pigmented and unpigmented linseed oil films. *Studies in Conservation* **1961**, *6*, 84–88.

(12) Graham, I. The effect of solvents on linoxyn films. *F. Oil Col* **1953**, *36*, 500–500.

(13) Carretti, E.; Bonini, M.; Berrie, L. D. B.-H.; Angelova, L.-V.; Baglioni, P.; Weiss, R.-G. New frontiers in Materials Science for Art Conservation: Responsive Gels and Beyond. *Accounts of Chemical Research* **2010**, *43*, 751–760.

(14) Castel, A.; Gutfreund, P.; Cabane, B.; Rharbi, Y. Swelling, dewetting and breakup in thin polymer films for cultural heritage. *Soft Matter* **2020**,

(15) Wolbers, R. *Cleaning painted surfaces: aqueous methods*; 2000.

(16) Bertolucci, S.; Bianchini, E.; Biave, C.; Caliari, F.; Cremonesi, P.; Gravina, S.; Zammataro, M.; Zangani, B. Preparazione e utilizzo di soluzioni acquose addensate, reagenti per la pulitura di opere policrome. *Progetto restauro* **2001**, *7*, 28–33.

(17) Sun, M.; Zou, J.; Zhang, H.; Zhang, B. Measurement of reversible rate of conservation materials based on gel cleaning approach. *Journal of Cultural Heritage* **2015**, *16*, 719–727.

(18) Guizzo, S.; Tortolini, C.; Pepi, F.; Leonelli, F.; Mazzei, F.; Di Turo, F.; Favero, G. Application of microemulsions for the removal of synthetic resins from paintings on canvas. *Natural product research* **2016**, 1–11.

(19) Rodriguez, S. H. Les propriétés, actions et principales problématiques des gels de Pemulen® TR-2. Le choix de la base dans la formulation des gels. CeROArt. Conservation, exposition, Restauration d'Objets d'Art. 2017.

(20) Salama, K. K.; Ali, M. F.; El-Sheikh, M. S. The Conservation of an Egyptian Coptic Fresco Painting from Saint Jeremiah Monastery: The Use of Nano-Materials in Cleaning and Consolidation. Journal of Nano Research. 2017; pp 148–153.

(21) Baglioni, P.; Berti, D.; Bonini, M.; Carretti, E.; Dei, L.; Fratini, E.; Giorgi, R. Micelle, microemulsions, and gels for the conservation of cultural heritage. *Advances in Colloid and Interface Science* **2014**, *205*, 361–371.

(22) Chelazzi, D.; Giorgi, R.; Baglioni, P. Microemulsions, micelles, and functional gels: how colloids and soft matter preserve works of art. *Angewandte Chemie International Edition* **2018**, *57*, 7296–7303.

(23) Singh, A.; Mukherjee, R. Swelling Dynamics of Ultrathin Polymer Films. *Marcomolecules* **2003**, *36 (23)*, 8728–8731.

(24) Miller-chou, B.-A.; Koenig, J.-L. A review of polymer dissolution. *Progress in Polymer science* **2003**, *28 (8)*, 1223–1270.

(25) Ellison, C.-J.; Torkelson, J.-M. The distribution of glass-transition temperatures in nanoscopically confined glass formers. *Nature Materials* **2003**, *2(10)*, 695–701.

(26) Nieto Simavilla, D.; Huang, W.; Housmans, C.; Sferrazza, M.; Napolitano, S. Taming the Strength of Interfacial Interactions via Nanoconfinement. *ACS Central Science* **2018**, *4*, 755–759.

(27) Seemann, R.; Herminghaus, S.; Neto, C.; Schlagowski, S.; Podzimek, D.; Konrad, R.; Mantz, H.; Jacobs, K. Dynamics and structure formation in thin polymer melt films. *Journal of Physics: Condensed Matter* **2005**, *17*, S267–S290.

(28) Reiter, G. Dewetting of highly elastic thin polymer films. *Physical Review Letters* **2001**, *87*, 186101.

(29) Henn, G.; Bucknall, D. G.; Stamm, M.; Vanhoorne, P.; Jérôme, R. Chain End Effects and Dewetting in Thin Polymer Films. *Macromolecules* **1996**, *29*, 4305–4313.

(30) Xu, L.; Sharma, A.; Joo, S. W. Dewetting of Stable Thin Polymer Films Induced by a Poor Solvent: Role of Polar Interactions. *Macromolecules* **2012**, *45*, 6628–6633.

(31) Xu, L.; Sharma, A.; Joo, S. W.; Liu, H.; Shi, T. Unusual Dewetting of Thin Polymer Films in Liquid Media Containing a Poor Solvent and a Nonsolvent. *Langmuir* **2014**, *30*, 14808–14816, PMID: 25402851.

(32) Simovic, S.; Tamburic, S.; Milic-Askrabic, J.; Rajic, D. An investigation into interactions between polyacrylic polymers and a non-ionic surfactant: an emulsion preformulation study. *International Journal of Pharmaceutics* **1999**, *184*, 207 – 217.

(33) Szűcs, M.; Sandri, G.; Bonferoni, M. C.; Caramella, C. M.; Vaghi, P.; Szabó-Révész, P.; Erős, I. Mucoadhesive behaviour of emulsions containing polymeric emulsifier. *European journal of pharmaceutical sciences* **2008**, *34*, 226–235.

(34) Feller, R.-L.; Stolow, N.; Jones, E.-H. In *On picture varnishes and their solvents. Revised and enlarged edition*; National Gallery of Art distributed by The Foundation of the American Institute for Conservation of Historic,, Works, A., Eds.; 1971.

(35) Diethert, A.; Metwalli, E.; Meier, R.; Zhong, Q.; Campbell, R.-A.; Cubitt, R.; Müller-Buschbaum, P. In situ neutron reflectometry study of the near-surface solvent concentration profile during solution casting. *Soft Matter* **2011**, *7 (2-3)*, 6648–6659.

(36) Michalski, S. A physical model of the cleaning of oil paint. *Studies in Conservation* **1990**, *35:sup1*, 85–92.

(37) Wolff, M.; Kuhns, P.; Liesche, G.; Ankner, J. F.; Browning, J. F.; Gutfreund, P. Combined neutron reflectometry and rheology. *Journal of Applied Crystallography* **2013**, *46*, 1729–1733.

(38) https://www.basf.com.

(39) la Rie, E. D.; Lomax, S.; Palmer, M.; Glinsman, L.; Christopher, A. An investigation of the photochemical stability of urea-aldehyde resin retouching paints. *Studies in Conservation* **2000**, *45:sup1*, 51–59.

(40) Bonaduce, I.; Colombini, M.; I.Degano,; Girolamo, F. D.; Nasa, J. L.; Modugno, F.; Orsini, S. Mass spectrometric techniques for characterizing low-molecular-weight resins used as paint varnishes. *Analytical and Bioanalytical Chemistry* **2012**, *405 (2-3)*, 1047–1065.

(41) Maines, C. A.; la Rie, E. D. Size-exclusion chromatography and differential scanning calorimetry of low molecular weight resins used as varnishes for paintings. **2004**, *52*, 39–45.

(42) http://www.ctseurope.com.

(43) Madsen, F.; Eberth, K.; Smart, J. D. A rheological assessment of the nature of interactions between mucoadhesive polymers and a homogenised mucus gel. *Biomaterials* **1998**, *19*, 1083–1092.

(44) Ravenel, N. Pemulen® TR-2: An Emulsifying Agent with Promise. *WAAC Newsletter Volume* **2010**, *32*, 10–12.

(45) Shahin, M.; Hady, S. A.; Hammad, M.; Mortada, N. Optimized formulation for topical

administration of clotrimazole using Pemulen polymeric emulsifier. *Drug development and industrial pharmacy* **2011**, *37*, 559–568.

(46) Hall, D. B.; Underhill, P.; Torkelson, J. M. Spin coating of thin and ultrathin polymer films. *Polymer Engineering & Science* **1998**, *38*, 2039–2045.

(47) Campbell, R. A.; Wacklin, H. P.; Sutton, I.; Cubitt, R.; Fragneto, G. FIGARO: The new horizontal neutron reflectometer at the ILL. *Eur. Phys. J. Plus* **2011**, *126*.

(48) Gutfreund, P.; Saerbeck, T.; Gonzalez, M. A.; Pellegrini, E.; Laver, M.; Dewhurst, C.; Cubitt, R. Towards generalized data reduction on a chopper-based time-of-flight neutron reflectometer. *Journal of Applied Crystallography* **2018**, *51*, 606–615.

(49) Abelès, F. Recherches sur la propagation des ondes électromagnétiques sinusoïdales dans les milieux stratifiés-Application aux couches minces. Annales de physique. 1950; pp 596–640.

(50) Nelson, A. Co-refinement of multiple-contrast neutron/X-ray reflectivity data using MOTOFIT. *Journal of Applied Crystallography* **2006**, *39*, 273–276.

(51) https://refl1d.readthedocs.io/en/latest/.

(52) https://www.ncnr.nist.gov/resources/activation/.

(53) Lauter, V.; Lauter, H.; Glavic, A.; Toperverg, B. Reference module in materials science and materials engineering. 2016.

(54) Hafner, A. Full Off-Specular and Specular Reflectometry for Soft Thin Film Analysis. Ph.D. thesis, Université libre de Bruxelles, Faculté des Sciences – Physique, Bruxelles, 2019.

(55) de Gennes, P. G. Dynamics of fluctuations and spinodal decomposition in polymer blends. *The Journal of Chemical Physics* **1980**, *72*, 4756–4763.

(56) Sferrazza, M.; Heppenstall-Butler, M.; Cubitt, R.; Bucknall, D.; Webster, J.; Jones, R. A. L. Interfacial Instability Driven by Dispersive Forces: The Early Stages of Spinodal Dewetting of a Thin Polymer Film on a Polymer Substrate. *Physical Review Letters* **1998**, *81*, 5173–5176.

(57) Good, R. J.; Girifalco, L. A. A THEORY FOR ESTIMATION OF SURFACE AND INTERFACIAL ENERGIES. III. ESTIMATION OF SURFACE ENERGIES OF SOLIDS FROM CONTACT ANGLE DATA. *The Journal of Physical Chemistry* **1960**, *64*, 561–565.

(58) Braslau, A.; Deutsch, M.; Pershan, P. S.; Weiss, A. H.; Als-Nielsen, J.; Bohr, J. Surface Roughness of Water Measured by X-Ray Reflectivity. *Phys. Rev. Lett.* **1985**, *54*, 114–117.

(59) Tylinski, M.; Chua, Y.; Beasley, M.; Schick, C.; Ediger, M. Vapor-deposited alcohol glasses reveal a wide range of kinetic stability. *The Journal of chemical physics* **2016**, *145*, 174506.

(60) Reiter, G.; Hamieh, M.; Damman, P.; Sclavons, S.; Gabriele, S.; Vilmin, T.; Raphaël, E. Residual stresses in thin polymer films cause rupture and dominate early stages of dewetting. *Nature materials* **2005**, *4*, 754–758.

(61) Bäumchen, O.; Fetzer, R.; Jacobs, K. Reduced Interfacial Entanglement Density Affects the Boundary Conditions of Polymer Flow. *Physical Review Letters* **2009**, *103*, 247801.

(62) Debrégeas, G.; Martin, P.; Brochard-Wyart, F. Viscous bursting of suspended films. *Physical review letters* **1995**, *75*, 3886.

(63) Ashley, K. M.; Meredith, J. C.; Amis, E.; Raghavan, D.; Karim, A. Combinatorial investigation of dewetting: polystyrene thin films on gradient hydrophilic surfaces. *Polymer* **2003**, *44*, 769 – 772.

(64) Brochard-Wyart, F.; Debregeas, G.; Fondecave, R.; Martin, P. Dewetting of Supported Viscoelastic Polymer Films: Birth of Rims. *Macromolecules* **1997**, *30*, 1211–1213.

CHAPTER 6
TEMPORAL EVOLUTION OF VARNISH FILMS IN THE PRESENCE OF SOLVENT/NONSOLVENT MIXTURES FOR CULTURAL HERITAGE

This chapter is presented in the form of a paper for an upcoming publication. It is a continuation of the article "Swelling, Dewetting and Breakup in thin polymer films for cultural heritage" [13] which focuses this time on a thick film and shows whether the thickness of the film has an influence on the behaviour of Laropal®A81 Film in contact with a small amount of benzyl alcohol in water or whether the results are similar to thin films. It brings together the data obtained by the QCM-D and SANS experiments for thick Laropal®A81 films immersed or not in a benzyl alcohol/water mixture. The analysis of these data mainly gives information about the kinetics of benzyl alcohol and water invasion during the swelling of Laropal®A81 thick films. The data reveal that the behaviour of these films immersed for a few hours in a benzyl alcohol/water mixture is similar to that of thin films. Indeed, like thin films, the swelling of thick films is accompanied by instability. These instabilities take the form of holes, characteristic of the dewetting phenomenon. The growth of the holes depends on the increasing concentrations of BA in contact with the film. When the amount of BA is sufficient, the holes can pass through the entire polymer film and come into contact with the substrate. Above a critical concentration (0.6 % BA), the films break irreversibly. This rupture is accompanied by water penetration and departure of Laropal®A81.

Temporal evolution of varnish films in the presence of solvent/nonsolvent mixtures for cultural heritage[†]

Amélie Castel[*a], Philipp Gutfreund[b‡], Bernard Cabane[*c] and Yahya Rharbi[*d]

Abstract: The removal of thick amorphous polymer films in contact with nonsolvent/solvent binary mixtures is investigated by means of small-angle neutron scattering. A distribution profiles of benzyl alcohol and heavy water in Laropal®A81 (LA) was given in order to address the scientific aspect of one of the most destructive treatments in art restoration, the removal of varnish from easel paintings. During immersion, the structural change of thick films was observed. The film swells followed by instabilities. Then, structural defects until the polymer is completely dissolved. The purpose of this article is to understand whether the origin of these instabilities is intrinsically due to this swelling. The behaviour of thick polymer films in contact with solvent/nonsolvent mixtures is compared to the behaviour of thin polymer film under the same conditions. A similar behaviour was determined by comparing the predictive swelling and distribution of solvents in the thin (Amélie Castel et al. [13]) and thick films. For this, the structure of thick polymer films prepared by dipping was observed during kinetic penetration of the solvent by small angle scattering (SANS).

Keywords: Diffusion; Dissolution; Laropal®A81; Neutron; Neutron reflectively; Polymer; Solubility; Solvents; Varnish

6.1 Introduction

Remove a polymer film on a surface by the action of a solvent is a challenging task which impacts many industrial applications such as microlithography, membrane science, recycling

plastics, drug delivery, tissue regeneration [91] and art restoration. In the field of Cultural Heritage, polymers films are present on painting to protect the paint layer from external abrasive agents and most of paintings have a varnish film. The film is usually deposited during restoration campaigns on the paint layer. For this operation, the restorers remove the old vanish and apply a fresh one. In function of the surface state and the desired film thickness, restorers choose to depose the polymer by brush or spray techniques directly on the paint surface thus forming the protective polymeric film. The techniques used and the number of the layers deposited, define the thickness of the final varnish film: thin [13] (<100 nm) or thick (>100 nm).

The physics of swelling and dissolution of glassy polymer films is essential in Cultural Heritage in order to remove altered varnish films on paintings by the use of solvents. The most difficult part is never reach, swell and dissolve the colored layer located just below. The risk is that solvents penetrate into the deeper layers, weaken the structure of the paint layer (cracks, loss of materials, etc.) and change irreversible the physico-composition of the painting. To avoid the destruction of the original material of the painting, it is essential to understand each physical mechanisms governing the swelling and instabilities formation, the dissolution [98] and the rupture of the polymer [91] film regardless its thickness and the concentration of solvent in contact with it.

The kinetic of the swelling and the dissolution of ultrathin polymer (Laropal®A81) films ($\sim$ 100 nm) by a solvent/nonsolvent binary mixtures was well studied by neutron reflectometry (mainly FIGARO, ILL, Grenoble) and atomic force microscopic (ESRF, Grenoble) in 2020 in a previous paper "Swelling, Dewetting and Breakup in thin polymer films for cultural heritage" by Amélie Castel et al. published in Soft Matter [13]. The aim was to investigate if the swelling of the Laropal®A81 polymer by a solvent (benzyl alcohol) or a solvent/nonsolvent mixture is done by a homogeneous or a heterogeneous process. It was shown that the swelling of the polymer or the surface state is most probably heterogeneous. Indeed, the presence of heterogeneities (holes) of large sizes was confirmed in addition to the neutron reflectivity by images with an atomic force microscopic. The presence of these instabilities inside the film are characteristic of dewetting and film rupture. The spatial scale and the volume fraction of these heterogeneities was determined. Finally, the role of the bad solvent in the apparition of the dewetting was poured.

The behaviour of ultrathin polymer films which includes swelling with instabilities, holes coalescence and film dissolution, until film breakage has been accurately investigated and understood. Now the question is whether changing the film thickness to a thicker film will give the same or different results. The capillary pressure of a thicker polymer film is lower, but the Van Der Waals forces are lower than for thinner films. It can be expected that the physics of swelling and dissolution of thick polymer films is different (fast and without dewetting process) compared to thin films. The physics of swelling and dissolution of thick polymer films can be expected to be different (fast and without dewetting process) compared to thin films. Thicker films should dissolve faster than thinner films due to imperfections (pores and cracks) created during the manufacturing and annealing time of the film. These imperfections increase the free volume and surface area [147]. Molecules preferentially lodge in these free volumes and promote rapid dissolution of the thick film.

In this paper, a quantitative view of the swelling and dissolution of thick amorphous glassy polymer films with a small amount of solvent in a non-solvent by SANS was presented. Given the initial motivation to remove the varnish layer from easel paintings without altering the paint layer below, Laropal®A81 (LA), a polymer resin currently used as a varnish by art restorers,

was chosen for this study. Small angle neutron scattering is a very powerful technique for studying polymer materials. It allows to establish the critical concentrations at the off set of the film dissolution and to perform experiments to understand the effect of benzyl alcohol and D_2O penetration on LA films. The solvent/non-solvent on thick Laropal®A81 films will be compared to the previous paper on thin polymer films [13].

6.2 Experimental

6.2.1 Materials

Laropal®A81 is a condensation product of urea and aliphatic aldehydes. This low molecular weight resin is in the form of small semi-transparent pellets. Its glass transition temperature (T_g) is 48 °C. It is soluble in alcohols, esters, ketones and aromatic hydrocarbons and is very heat stable. Size-exclusion chromatography (SEC) estimated its weight-average molecular weight (Mw) to be 3640 Da and its number-average molecular weight (Mn) to be 1266 Da [28]. Its molecular structure was characterize by Bonaduce *et al.* using flow injection analysis coupled to electrospray ionisation and quadrupole time-of-flight mass spectrometry (FIA-ESI-Q-ToF) and gel chromatography (GC). They concluded that Laropal®A81 is a product of the reactions between 4-hydroxy-6-isopropyl-5,5-dimethyl-tetrahydropyrimidin-2(1*H*)-one and aldehydic compounds. In addition, they have shown that that hydroxyl groups have a strong effect on the physical properties of the polymer[95]. This resin is often used by art restorers to make the varnish layers and as a correction material for paint retouching [32]. The Laropal®A81 used in this study was produced by BASF [121]. The softening point indicated by the manufacturer is 80-95 ˚C. Its density is 1,1 g/cm^3 at 20 ˚C. It can be dissolved in aprotic and dipolar solvents and is insoluble in water.

6.2.2 Thick film preparation and characterization

For QCM-D experiment, LA films were deposited on the quartz sensor by spin-coating and annealed for 30 min at 114 ˚C taking care not to make a thermal shock on the fragile sensor. The quartz sensor was rigorously cleaned before spin-coating. The LA/toluene solutions at 170 g/L were spin-coated at 2250 rpm for 44 seconds at room temperature (21°C). Film thicknesses were measured using the mass measured as function of the coated surface. The film thickness was $\sim$ 500 nm.

For SANS experiment, LA films were produced by dip-coating on single quartz cells. Substrates was immersed in a solution of 400 g/L Laropal®A81 in toluene at a constant and controlled speed. The single quartz cells was rigorously cleaned before dip-coating subsequently sonicate in water plus one drop on Decon 90 mixture, clean water, ethanol, acetone, chloroform and ending with clean water during 15 min for each products and dried at room temperature. All samples were annealed at 114 ˚C during 30 min in an oven vacuum. Film thicknesses were measured using a contact profilometer across a scratch. The thickness measured was approximately 1.2 µm.

6.2.3 QCM-D

Quartz Crystal Microbalance with Dissipation Monitoring (QCM-D) is a nanogram sensitive technique which allows to measure in real-time the mass of the polymer films on the quartz sensor by measuring the resonance frequencies of a vibrating piezoelectric quartz crystal [148].

Three LA films of 500 nm on quartz sensor were measured in solutions of D_20 containing an increasing BA concentration $\phi BA/W$ (pure D_2O, 0.2 % BA until 0.7 %). Frequency changes were monitored during few hours on the QCM-D. It has been verified that each film gave the same results for the repeatability of the experiment, but only the results of one sample are presented afterwards.

6.2.4 SANS

SANS experiments were performed on D11 [149] at the Institut Laue-Langevin (ILL), Grenoble, France. Three sample-to-detector distances were used to cover the full q-range, namely 1.4 m, 8 m and 39 m at a constant neutron wavelength of 0.55 nm. In front of the sample a 14 mm circular diaphragm was placed. Measurement times were set to 10 min for the short detector distance, 30 min for the intermediate one and between 30 min and 4 h for the longest sample-to-detector distance.

LA films of approximately 1.2 µm on single quartz cells were put in vats of 4.6 x 2.5 x 0.5 cm^3 containing the solutions of different concentrations of benzyl alcohol in D_2O (0 %; 0.2 %; 0.4 %; 0.6 % and 0.7 %) or D_2O+H_2O (0.6 %) at the beginning of the experiment and the temporal evolution of the SANS spectra was recorded. The background emerging from a cell filled with the same solution, but without a polymer film, was subtracted from the spectra.

SANS measures the scattering of neutrons at small angles arising from variations of the neutron scattering length density (SLD) of the bulk material. The SLDs involved in this experiment are depicted in Table 6.1.

Table 6.1 – Scattering length densities of the materials used in this study. For LA the range of measured values during different experiments is given [13]. In case of the other materials literature values are given assuming the chemical composition of BA to be C_7H_8O at 1.02 g/cm^3 density.

Material	bulk SLD [10^{-6}Å^{-2}]
D_2O	6.36 (literature value)
H_2O	-0.57 (literature value)
BA	1.298 (literature value)
Laropal®A81	0.9±0.1

6.2.5 Analysis of SANS data

The measured SANS data is analyse using Igor Pro software. Data are reduced and plotted by a model of Porod. The Igor's Power Law fit function is:

$$f(x) = A * x^{pow} + y_0 \tag{6.1}$$

with Y_0 is held at zero as it is common to use the law of power. This equation following the correlation length model:

$$I(q) = \frac{1}{q^s} * \frac{C}{1 + (q\chi)^m} + B, \tag{6.2}$$

where, χ is the characteristic length. m is the *high-q* Porod exponent. And, S is a "stretching" factor in the *low-q* mass fractal structure.

Basically, from equation 6.1, the A represents the signal intensity and x^{pow} is the scattering invariant q.

6.3 Results and Discussion

The figure 6.1 shows typical SANS spectra for a 1.2 µm LA polymer film immersed in D_2O containing 0.7 % of BA as a function of time. For completeness, the SANS curve of the dry film is also shown as well (red crosses) although the SANS signal for this sample is close to the background, making it difficult to extract the actual foreground. A similar curve was obtained for a LA film immersed in pure D_2O (not shown). Although the error bars largely include zero diffusion cross section for these curves (error bars omitted for clarity in this figure), it appears that the diffusion cross section is not zero at small q-values but of the order of 1000 cm^{-1}, which is clearly not compatible with a homogeneous homo-polymer melt. This result is consistent with SAXS measurements performed on 1 mm self-supporting films of the same polymer. It is clear that some inhomogeneities are present even in dry films. As soon as the film is placed into contact with a solution containing BA, the SANS signal increases significantly, showing clear Porod diffusion. And, the q-dependence is given by $\frac{d\sigma}{d\Omega} \sim q^{-4}$ typical for surface appearance. The large scattering cross section of $10^5\,cm^{-1}$ to $10^6\,cm^{-1}$ at low q values shows that a strong SLD contrast has to exist across the interface. Looking on table 6.1 the contrast has to come from D_2O. Indeed a control experiment where the water was contrast matched to LA by dilution with H_2O showed zero scattering corroborating the D_2O/BA interface to be the origin of the observed SANS signal.
In order to extract quantitative information the SANS curves were fitted with the Porod law for low q-values where background did not affect the curve:

$$\frac{d\sigma}{d\Omega}(q) = 2\pi S(\Delta SLD)^2 q^{-4}, \tag{6.3}$$

where S represents the total area and ΔSLD the difference in SLD between the two phases across the interface. The resultant plot of the pre-factor A = $2\pi S(\Delta SLD)^2$ is plotted in Fig. 6.2 as a function of time for two BA concentrations.

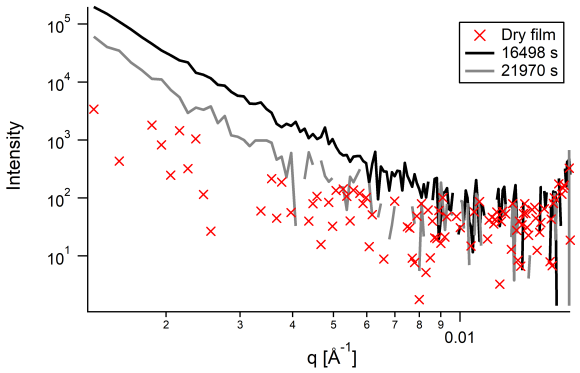

Figure 6.1 – SANS spectra, scattering cross-section of 1.2 µm LA films in contact with 0.7 % BA in D_2O as function of time.

It can be seen that in contact with the 0.6 % BA solution the signal increases rapidly as compared to the dry film and reaches a maximum after about 3 h. Afterwards a decrease is observed although still significantly above the level of the dry film followed again by a slight increase after about 10 h of immersion. Similar, but apparently accelerated behaviour is observed for the highr BA concentration. In the latter case the initial increase in intensity happens faster than the observed time window and also the minimum is reached already after 7 h to be followed by an increase again.
In order to understand this cyclic behaviour of the scattered intensity we refer to our previous

work on the same system, but using about ten times thinner films [13]. In this work we highlighted the presence of dewetting type holes for 100 nm thin films immersed in BA/W mixtures beyond 0.3 % BA by using neutron reflectometry (NR) and atomic force microscopy (AFM). A visual inspection of the 1.2 µm thick films used in this study showed clearly an opaque appearance after contact with the BA/W mixture, very similar to the films in our previous work. This corroborates the assumption that also in this case a de-wetting type phenomenon takes place. In this case the initial rapid increase in surface area could be the appearance and growth of holes filled with D_2O. Indeed for 100 nm thick films this process was leveling off after about 1 h at 0.5 % BA [13]. The same timescale is observed for ten times thicker films at 0.6 % (2-3 h). At 0.7 % BA the 100 nm films were already in a too advanced strage of de-wetting to be analyzed by NR after 20 min. For the micron thick films the initial maximum is also reached before the first SANS spectrum was recorded at 5 h immersion time.
For the following decrease in SANS intensity two possible explanations are discussed. 1) Part of the film could disappear into the bulk due to dissolution or an emulsification process as discussed in our previous work. 2) An alternative explanation would be the coalescence of holes leading to fewer holes and thus smaller surface area.

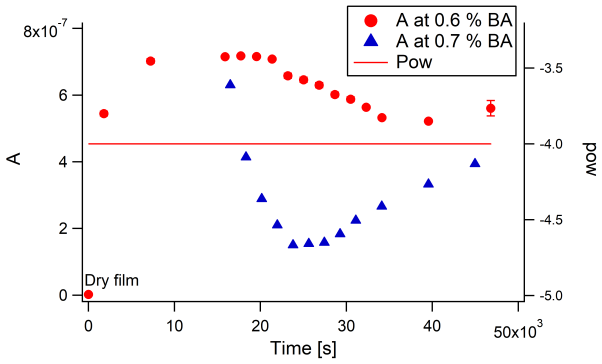

Figure 6.2 – A (intensity) obtained from fitted SANS data by Porod's law of 1.2 µm LA films in contact with 0.6 % BA and 0.7 % BA in D_2O.

In order to shed further light onto the dissolution process QCM-D measurements were performed on 500 nm thick films. In case of no change of viscoelastic properties of the film fequency change in QCM-D is directly proportional to the bound mass to the quartz crystal. Fig. 6.3 shows the frequency change as a function of time of the film immersed in D_20 and at increasing concentrations of BA as indicated in the graph (0 %, 0.2 %, 0.3 %, 0.4 %, 0.5 %, 0.6 % and 0.7 % BA). After a short equilibration in pure D_2O the frequency slightly lowers for BA concentrations below 0.3 % probably mainly due to BA swelling as also observed in our NR study [13]. Starting from 0.3 % a significant mass uptake is seen in accordance with the appearance of water filled holes. At 0.7 % BA the same cyclic behaviour of mass uptake and loss is observed on similar time scales as for the SANS experiment.

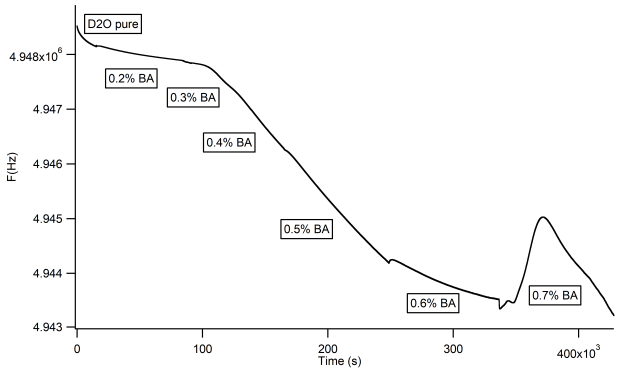

Figure 6.3 – Frequency change of a 500 nm Laropal®A81 film prepared by spin coating and immersed in an increasing concentration of BA in D_2O as a function of time as reveled by QCM-D.

6.4 Conclusions

In this work the late stages of Laropal®A81 film destruction were investigated by means of SANS and QCM-D. BA in water concentrations of 0.6 and 0.7 % were used which were found to be critical concentrations of immediate film rupture in the case of ultra-thin films investigated previously [13]. Similar to our previous work the process of film destruction is an intrinsically heterogeneous dewetting type process by hole formation. The micrometer thick films, which are closer to real applications in art restoration, behave similar to thin films, so this seems to be an intrinsic feature of Laropal®A81. This is not trivial as van der Waals forces are much weaker on a micron length scale. On the other hand the Laplace pressure of a film droplet with a radius equal to the film thickness is much weaker for a thicker film. The thickness of the polymer film and the concentration of solvent have an influence on the kinetics of swelling, dissolution and the rupture of the polymer film. It was observed cyclic changes of bound mass and SANS scattering signal, which could be explained by two opposing effects, on the one hand dewetting of the film leading to incorporation of water and on the other hand the (emulsified or patchy) dissolution of the polymer. An alternative explanation for this cyclic behaviour could be the growth and coalescence of holes.

Acknowledgements

We thank the ILL for neutron beam time on D11 (doi:10.5291/ILL-DATA.1-03-36). We thank the Partnership for Soft Condensed Matter at ILL for the use of complimentary techniques. We thank Yuri Gerelli for the help during the QCM-D measurements.

GENERAL CONCLUSION

Varnish inevitably changes over time. This change, a normal degradation of the material, can lead to alteration of the paint layer or impeding the appreciation of the painting. Its removal is a difficult treatment involving the deposition of solvent conducing to its swelling and eventually to its breaking. During this process, restorers must be able to guarantee the safe removal of the varnish. With current knowledge, it is no longer necessary to prove that using pure solvents and solvent mixtures is a risky treatment for the painted layer because of the difficulty of controlling the process. Soft materials have an important wide range of applications. In the case of moisturizer in cosmetics, the aim is to penetrate the skin barrier by water molecules in a gel mixture. If one compares the skin barrier to the polymer film barrier and the water to the solvent, gels can also be applied to the proceed of the removal of varnish treatment. In this case, gels are composed mainly by water ($\sim$ 90% or more) and a little amount of solvent in the water/gel mixture. With the use of this solvent/gel system, theoretically it seems possible to have a better control of the action of the solvent, to predict the kinetics of the solvent molecules into the varnish film, to reduce the amount of solvent transferred, to facilitate the application and to allow a short or long action time. The visual macroscopic results of using these kinds of materials of high molecular weight shown by scientists or restorers prove the effectiveness of the action of these solvent/gel systems on the polymer film. But there is a lack of knowledge in the understanding of the physics of the interactions between the polymer/solvent, polymer/water, polymer/solvent/gel and polymer/gel. And that was exactly the purpose of this study.

In summary, the microscopic and nanoscopic behavior of thin and ultrathin synthetic, hydrophobic polymer film of Laropal®A81 in contact with two systems was investigated: water/solvent solutions and gel/solvent mixture. The impact of shear and temperature was also explored. This work has been possible by the use of many instruments (AFM, Optical Miscroscopy, DSC, QCM, ellispometry, X-rays and rheology) and more particularly by the use of neutrons (NR and SANS) mainly at ILL in Grenoble.

First of all it was necessary to fix the materials of the study. It was chosen to use a resin of Laropal®A81 (LA), a synthetic resin commonly used for Cultural Heritage composed from urea, isobutyraldehyde, and formaldehyde, as a model varnish polymer film of this study. The solvent was benzyl alcohol (BA), a solvent also used by restorers to remove the varnish from the paint layer. For water (W), D_20 at 99,9% D for neutron scattering experiments, AFM and SAXS was chosen ; and MilliQ water with a resistance superior to 18MΩcm for others experiments. The Pemulen TR-2 in form of powder was the gel of this study. Pemulen TR-2 makes it possible to associate a hydrophobic solvent with water thanks to its ability to form a stable emulsion at low or high concentrations of the oil phase and also at very low viscosity. The approach of this study was to cover all the fields which allow the global comprehension of each element which composes the project according to 6 axes: I. Historical and material context of the varnish as well as the initial motivations of this project from Cultural Heritage, II. Scientific knowledge of Neutron scattering and polymers, III. Description of the materials chosen, Experimental protocol and Instrumentations, IV. The first paper submitted entitled "Swelling, Dewetting and Breakup in Thin Polymer Films for Cultural Heritage" [13] on the behavior of ultrathin film in contact with a solvent/nonsolvent mixture mainly by NR and AFM, V. The second paper submitted soon entitled "Stability of fluid Ultrathin Polymer Films in contact with solvent-loaded Gels for Cultural Heritage". on the behavior of ultrathin film in contact with a solvent/gel mixture by NR, and finally, VI. the results of the behavior of thick film immersed in a solvent/water mixture by SANS and QCM-D presented also in the form of a short publication.

I. The motivation was exposed by guiding the reader in the global understanding of what restoration, varnishes are used and how restorers use them. Then describing the problem encountered and the state of the art about the problem. This allows us to have a good overview of the subject and adjust to the best target the difficulties of the removal of the varnish layer, this risky treatment for the painted layer.

II. Then, the basic physics of polymers and of neutron scattering, which are the main parts of this project, give the essential scientific aspects to understand the key points of this subject.

III. A specific protocol was established in order to produce identical samples, reproducible and adapted to the constraints of each instrument. Thick films more than 1 µm were produced by dip coating and casting process for SANS and SAXS experiments, thin films of 500 nm were made by spin coating process for QCM-D and NR and ultrathin films were made by spin coating for NR, SANS, AFM, and Optical Microscopy. And that accompanied by several mixtures of water/BA, water/gel, water/gel/solvent were prepared.

Materials of LA, BA and Pemulen TR 2 gel were characterized by an extensive literature review and the state of art and some complementary experiments. The LA was characterized by DSC measurement. The DSC allows us to measure the glassy transition (T_g) of LA immersed or not in BA/W. The T_g decreases when BA is transferred into the polymer film. This allowed highlighting the role of the T_g in the process of destruction of the varnish film. The swelling and dissolution process was first studied by measuring of the change of mass per unit area of LA thanks to oscillation frequency measurement with a QCM-D. The Pemulen TR-2 gel was characterized by rotary rheology experiments with a cone-plate geometry. The influence of the quantity of Pemulen TR-2 and solvent on the viscosity change of the gel at fixed pH were observed. The viscosity increased with increasing amount of Pemulen TR-2 and decreased with solvent addition. The Pemulen TR-2 gel behaves as a non-Newtonian shear thinning with a slight thixotropy. And it has a good adhesion when it is in contact with a rough or flat surface. These observations corroborate well the known elements of the literature on this gel.

IV. Neutrons scattering is a fantastic tool to explore thin polymer films during the process and to obtain various information such as the thickness, the roughness and the SLD of the polymer films. Thanks to these neutron data, the partial volume fractions of $\phi_{BA/LA}$ and $\phi_{W/LA}$ or $\phi_{PTR2gel/LA}$ in LA films were calculated. In parallel, the study of the Yoneda peak, the OSS scattering intensity close to the total reflection, allowed us to follow the kinetics of the swelling in situ. In contact with a solvent/nonsolvent mixture, ultrathin film followed a dewetting process inducing holes and rims. The size of holes depends of the amount of solvent. Beyond a critical concentration, films breaks.

V. Thanks to neutron scattering, significant results were obtained in the comprehension of the swelling, dewetting and breakup of thin polymer films in contact with solvent-loaded gels for Cultural Heritage. Pemulen TR-2 gel matrix plays a role during the swelling and dissolution processes. As well as the solvent/nonsolvent case, the swelling of ultrathin film in contact with a solvent-loaded gel is accompanied by a dewetting process. It appears in the form of holes. However, there are some differences compared to the typical dewetting, in particular the absence of rims. The combination of temperature with solvent also has a high impact on the stability of the film. Beyond a critical temperature which depends on the solvent fraction, the film breaks.

VI. Small angle neutron scattering (SANS) allows the investigation of thick polymer films dry or immersed in a solution mixture. Experiments carried out with SANS and QCM-D have shown that the behaviour of thick films in contact with a solvent/non-solvent mixture is the same as for thin films. The destruction of film is accompanied by a heterogeneous dewetting process observable in the form of holes on all the film surface.

Appendices

APPENDIX A
PUBLICATIONS

A. Castel, Y. Rharbi, P. Gutfreund, B. Cabane "Swelling, Dewetting and Breakup in thin polymer films for cultural heritage", SoftMatter,2020,16,1485 (Accepted 25th November 2019 and published on 13th January 2020) DOI: 10.1039/c9sm01976f

APPENDIX B
CONFERENCE PRESENTATIONS

B.1 PRESENTATIONS

- **ILL Clip session** A. Castel, Y. Rharbi, P. Gutfreund, B. Cabane 'Using neutron to protect our works of art' (Grenoble, France. 2019)
- **MLZ Conference : Neutron for Culture and Art** A. Castel, Y. Rharbi, P. Gutfreund, B. Cabane 'Coupled Neutron reflectivity/rheology for safe removal of synthetic varnish layer on easel paintings' (Munich, Allemagne. 2018)
- **ILL Clip session** A. Castel, Y. Rharbi, P. Gutfreund, B. Cabane 'Using neutron to protect our works of art' (Grenoble, France. 2018)
- **ILL Ph.D seminar** A. Castel 'The moderations of neutrons' (Grenoble, France. 2017)
- **ILL Ph.D seminar** A. Castel, Y. Rharbi, P. Gutfreund, B. Cabane 'Using neutron to protect our works of art' (Grenoble, France. 2017)
- **LRP Séminaire des doctorants** A. Castel, Y. Rharbi, P. Gutfreund, B. Cabane 'La science au service de l'Art' (Grenoble, France. 2017)
- **ILL Clip session** A. Castel, Y. Rharbi, P. Gutfreund, B. Cabane 'Using neutron to protect our works of art' (Grenoble, France. 2017)

B.2 POSTERS

- **HERCULES SCHOOL** Amélie Castel, Philipp Gutfreund, Yahya Rharbi and Bernard Cabane 'Using neutrons to protect our works of art'(Grenoble, France. 2018)
- **MLZ Conference : Neutron for Culture and Art** Amélie Castel, Philipp Gutfreund, Yahya Rharbi and Bernard Cabane 'Using neutron reflectivity to understand the nanoscopic behavior of a synthetic varnish layer during the swelling process by a solvent in an aqueous gel' (Munich, Germany. 2018)
- **European User meeting** Amélie Castel, Philipp Gutfreund, Yahya Rharbi and Bernard Cabane 'Using neutron reflectivity to understand the nanoscopic behavior of a synthetic varnish layer during the swelling process by a solvent in an aqueous gel" (Grenoble, France. 2018)

BIBLIOGRAPHY

[1] C. Brandi, *Teoria del restauro*. Ed. di storia e letteratura, 1963.

[2] S. Walden, *Outrage à la peinture*, E. Ivrea, Ed. Paris, 2003, p. 134.

[3] S. Bergeon and P. Curie, *Peinture & dessin: vocabulaire typologique et technique*. Éditions du patrimoine, Centre des monuments nationaux, 2009.

[4] K. Nicolaus, *Manuel de restauration des tableaux*. 1999.

[5] C. Bételu, "Est-il utile ou nuisible de restaurer ? réflexion sur l'acte de restauration et ses acteurs en 1796", 2 avril 2016. [Online]. Available: https://grham.hypotheses.org.

[6] E. Delacroix and R. Piot, *Journal de Eugène Delacroix*. Plon, 1895, vol. 1.

[7] E. D. la Rie and C. McGlinchey, "New synthetic resins for picture varnishes", *International Institute for Conservation of Historic and Artistic Works*, pp. 168–173, 1990.

[8] S. Langle and P. Curie, *Peinture et dessin*, E. du Patrimoine, Ed. Paris, 2009.

[9] trad. Déroche of C. Brandi, *Theorie de la restauration*, E. N. du Patrimoine, Ed. Paris, 2001.

[10] R.-L. Feller, N. Stolow, and E.-H. Jones, "On picture varnishes and their solvents. revised and enlarged edition", *National Gallery of Art distributed by The Foundation of the American Institute for Conservation of Historic and Artistic Works*, 1971.

[11] S. Michalski, "A physical model of the cleaning of oil paint", *Studies in Conservation*, vol. 35:sup1, pp. 85–92, 1990.

[12] D. Bucknall, "Influence of interfaces on thin polymer film behaviour", *Progress in Materials Science*, vol. 49, U. of Oxford, Ed., pp. 713–786, 2004.

[13] A. Castel, P. Gutfreund, B. Cabane, and Y. Rharbi, "Swelling, dewetting and breakup in thin polymer films for cultural heritage", *Soft Matter*, vol. 16, pp. 1485–1497, 6 2020. [Online]. Available: http://dx.doi.org/10.1039/C9SM01976F.

[14] M. Thoury, "Identification non-destructive des vernis des oeuvres d'art par fluorescence uv", PhD thesis, Université Pierre et Marie Curie, 2006.

[15] F. Perego, *Dictionnaire des matériaux du peintre*, Belin, Ed. Paris, 2005.

[16] Vitruve, *De l'architecture*, E. B. lettres, Ed. 1673, vol. Vol.7, C.9.

[17] P. l'Ancien traduction by Stéphane Schmitt, *Histoire naturelle*. Bibliothèque de la Pléiade, 2013, vol. Vol. 37.

[18] R. Feller, N Stolow, E. Jones, and O. P. Varnishes, "Their solvents", *National Gallery of Art, Washington, DC*, 1985.

[19] C. Cennini, C. D. Cennini, and G. De Beer, *The craftsman's handbook*. Courier Corporation, 1954, vol. 2.

[20] D. V. Thompson, *The materials and techniques of medieval painting*. Courier Corporation, 1956, vol. 327.

[21] S. G. Stadtbibliothek, *The Strasburg Manuscript: A Medieval Painters' Handbook*. Transatlantic Arts, 1966.

[22] J. Watin, *L'Art du peintre, doreur, vernisseur*, 2e edi. Grangé et Durand neveu, Ed. Paris, 1773.

[23] A. Genty, "Les chancis des vernis et des couches picturales des peintures de chevalet à l'huile: contribution à la caractérisation physico-chimique, à la connaissance des mécanismes de formation et aux traitements de restauration.", PhD thesis, Cergy-Pontoise, 2017.

[24] E. D. la Rie, "Old master paintings : a study of the varnish problem", *Analitical chemistry*, 1228A–1240A, 1989.

[25] O. Chiantore and M. Lazzari, "Photo-oxidative stability of paraloid acrylic protective polymers", *Polymer*, vol. 42, issue 1, elsevier, Ed., pp. 17–27, 2001.

[26] S. Koob, "The use of paraloid b-72 as an adhesive: its application for archaeological ceramics and other materials", *Studies in Conservation*, vol. 31, issue 1, T. Francis, Ed., pp. 7–14, 2001.

[27] E. D. la Rie, "The influence of varnishes on the appareance of paintings", *Studies in Conservation*, vol. 32, pp. 1–13, 1987.

[28] C. A. Maines and E. D. la Rie, "Size-exclusion chromatography and differential scanning calorimetry of low molecular weight resins used as varnishes for paintings", *Progress in Organic Coatings*, vol. 52, pp. 39–45, 2004.

[29] H. Piena, "Regalrez in furniture conservation", *Journal of the American Institute for Conservation*, vol. 40, issue 1, pp. 59–68, 2001.

[30] G. Vasari, *Vies des peintres, sculpteurs et architectes*. Tessier, 1839, vol. 1.

[31] R. S. Berns and E. R. De la Rie, "The effect of the refractive index of a varnish on the appearance of oil paintings", *Studies in conservation*, vol. 48, no. 4, pp. 251–262, 2003.

[32] E. D. la Rie, S. Lomax, M. Palmer, L. Glinsman, and A. Christopher, "An investigation of the photochemical stability of urea-aldehyde resin retouching paints", *Studies in Conservation*, vol. 45:sup1, pp. 51–59, 2000.

[33] G. Hedley, "Solubility parameters and varnish removal: a survey", *The conservator*, vol. 4, no. 1, pp. 12–18, 1980.

[34] C. Stavroudis and S. Blank, "Solvents & sensibility", 1989.

[35] C. McGlinchey, "Boundaries of the teas solubility concept", 2002.

[36] T. Fardi, E. Stefanis, C. Panayiotou, S. Abbott, and S. van Loon, "Artwork conservation materials and hansen solubility parameters: a novel methodology towards critical solvent selection", *Journal of cultural heritage*, vol. 15, no. 6, pp. 583–594, 2014.

[37] G. D. Smith and R. Johnson, "Strip teas: solubility data for the removal (and application) of low molecular weight synthetic resins used as inpainting media and picture varnishes", *WAAC newsletter*, vol. 30, no. 1, pp. 11–19, 2008.

[38] P. Cremonesi, *L'usi dei solventi organici nella pulitura di opere policrome*, I. Prati, Ed. 2004, pp. 87–115.

[39] L. Masschelein-Kleiner, *Les solvants*, I. R. du Patrimoine Artistique, Ed. 1994, vol. 2.

[40] D. Horsin, *De la Conservation et de la Restauration des tableaux, chap I and III*, H. Bossange, Ed. Paris: Oxford University Press, 1851.

[41] F. Graham, "The effect of solvents on linoxyn films", *F. Oil Col*, vol. 36, U. of Oxford, Ed., 1953.

[42] N. Stolow, *Some investigations of the action of solvents on drying oil films*. University of London: PhD Thesis, 1956.

[43] ——, "The action of solvents on drying-oil films: part ii", *Journal of the Oil and Colour Chemists' Association*, vol. 40, no. 5-6, pp. 488–499, 1957.

[44] N Stolow, *Solvent action: some fundamental researches into the picture-cleaning problem*, 1959.

[45] K. Sutherland, "The extraction of soluble components from an oil paint film by a varnish solution", *Studies in conservation*, vol. 45, no. 1, pp. 54–62, 2000.

[46] A. Phenix and K. Sutherland, "The cleaning of paintings : effects of organic solvents on oil paint films", *Studies in Conservation*, vol. 46, pp. 47–60, 2001.

[47] R. Wolbers, *Cleaning painted surfaces: aqueous methods*. 2000.

[48] T. Graham, "Xxxv.—on the properties of silicic acid and other analogous colloidal substances", *Journal of the Chemical Society*, vol. 17, pp. 318–327, 1864.

[49] E. Carretti, L. Dei, and R. G. Weiss, "Soft matter and art conservation. rheoreversible gels and beyond", *Soft Matter*, vol. 1, no. 1, pp. 17–22, 2005.

[50] E. Carretti, L. Dei, and P. Baglioni, "Aqueous polyacrylic acid based gels: physico-chemical properties and applications in cultural heritage conservation", pp. 280–283, 2004.

[51] E. Carretti and L. Dei, "Gels as cleaning agents in cultural heritage conservation", pp. 929–938, 2006.

[52] R. Giorgi, M. Baglioni, D. Berti, and P. Baglioni, "New methodologies for the conservation of cultural heritage: micellar solutions, microemulsions, and hydroxide nanoparticles", *Accounts of Chemical Research*, vol. 43, no. 6, pp. 695–704, 2010.

[53] P. Baglioni, D. Berti, M. Bonini, E. Carretti, M. D. C. C. Perez, D. Chelazzi, L. Dei, E. Fratini, R. Giorgi, I. Natali, *et al.*, "Gels for the conservation of cultural heritage", *MRS Online Proceedings Library Archive*, vol. 1418, 2012.

[54] P. Baglioni, D. Berti, M. Bonini, E. Carretti, L. Dei, E. Fratini, and R. Giorgi, "Micelle, microemulsions, and gels for the conservation of cultural heritage", *Advances in Colloid and Interface Science*, vol. 205, pp. 361–371, 2014.

[55] P. Baglioni, E. Carretti, and D. Chelazzi, "Nanomaterials in art conservation", *Nature Nanotechnology*, vol. 10, no. 4, p. 287, 2015.

[56] M. Baglioni, Y. J. Benavides, D. Berti, R. Giorgi, U. Keiderling, and P. Baglioni, "An amine-oxide surfactant-based microemulsion for the cleaning of works of art", *Journal of colloid and interface science*, vol. 440, pp. 204–210, 2015.

[57] M. Baglioni, J. A. Domingues, E. Carretti, E. Fratini, D. Chelazzi, R. Giorgi, and P. Baglioni, "Complex fluids confined into semi-interpenetrated chemical hydrogels for the cleaning of classic art: a rheological and saxs study", *ACS applied materials & interfaces*, vol. 10, no. 22, pp. 19 162–19 172, 2018.

[58] D Chelazzi, E Fratini, R Giorgi, R Mastrangelo, M Rossi, and P Baglioni, *Gels for the cleaning of works of art*, 2018.

[59] N. Bonelli, G. Poggi, D. Chelazzi, R. Giorgi, and P. Baglioni, "Poly (vinyl alcohol)/poly (vinyl pyrrolidone) hydrogels for the cleaning of art", *Journal of colloid and interface science*, vol. 536, pp. 339–348, 2019.

[60] E. Carretti, M. Bonini, L. D. B.-H. Berrie, L.-V. Angelova, P. Baglioni, and R.-G. Weiss, "New frontiers in materials science for art conservation: responsive gels and beyond", *Accounts of Chemical Research*, vol. 43, pp. 751–760, 2010.

[61] P. Baglioni and R. Giorgi, "Soft and hard nanomaterials for restoration and conservation of cultural heritage", *Soft Matter*, vol. 2, no. 4, pp. 293–303, 2006.

[62] D. Chelazzi, R. Giorgi, and P. Baglioni, "Microemulsions, micelles, and functional gels: how colloids and soft matter preserve works of art", *Angewandte Chemie International Edition*, vol. 57, no. 25, pp. 7296–7303, 2018.

[63] B. Hammouda, "Probing nanoscale structures-the sans toolbox", *National Institute of Standards and Technology*, pp. 1–717, 2008.

[64] F. Hippert, E. Geissler, J. L. Hodeau, E. Lelièvre-Berna, and J.-R. Regnard, *Neutron and X-ray Spectroscopy*. Springer Science & Business Media, 2006.

[65] J. Baruchel, J.-L. Hodeau, M. S. Lehmann, J.-R. Regnard, and C. Schlenker, *Neutron and synchrotron radiation for condensed matter studies*. Springer, 1993.

[66] M. Angst, T. Brückel, D. Richter, and R. Zorn, *Scattering methods for condensed matter research*, PreJuSER-136382. Streumethoden, 2012.

[67] K. Lefmann, "Neutron scattering: theory, instrumentation, and simulation", *Niels Bohr Institute, University of Copenhagen*, 2017.

[68] G. L. Squires, *Introduction to the theory of thermal neutron scattering*. Cambridge university press, 2012.

[69] R. Pynn, "Neutron scattering: a primer", *Los Alamos Science*, vol. 19, pp. 1–31, 1990.

[70] P. Gutfreund, "The microscopic origin of surface slip: a neutron and x-ray scattering study on the near surface structure of flowing liquids", PhD thesis, Physik und Astronomie der Ruhr-Universitat Bochum, 2011.

[71] A. Hafner, "Full off-specular and specular reflectometry for soft thin film analysis", PhD thesis, Université Libre de Bruxelles, 2019.

[72] [Online]. Available: http://www.ill.eu.

[73] [Online]. Available: www.nuclear-power.net.

[74] V. F. Sears, "Neutron scattering lengths and cross sections", *Neutron news*, vol. 3, no. 3, pp. 26–37, 1992.

[75] N. Zettili, *Quantum mechanics: concepts and applications*, 2003.

[76] [Online]. Available: https://www.ncnr.nist.gov/resources/sldcalc.html.

[77] E. Fermi, *Reflection of neutrons on mirrors*. Manhattan District, 1946, vol. 56.

[78] L. G. Parratt, "Surface studies of solids by total reflection of x-rays", *Physical review*, vol. 95, no. 2, p. 359, 1954.

[79] I. Hamley and J. S. Pedersen, "Analysis of neutron and x-ray reflectivity data. i. theory", *Journal of applied crystallography*, vol. 27, no. 1, pp. 29–35, 1994.

[80] L Nevot and P Croce, "Caractérisation des surfaces par réflexion rasante de rayons x. application à l'étude du polissage de quelques verres silicates", *Revue de Physique appliquée*, vol. 15, no. 3, pp. 761–779, 1980.

[81] C. Strazielle and H. Benoit, "Some thermodynamic properties of polymer-solvent systems. comparison between deuterated and undeuterated systems", *Macromolecules*, vol. 8, no. 2, pp. 203–205, 1975.

[82] J. Daillant and A. Gibaud, *X-ray and neutron reflectivity principles and applications*, ser. Lecture notes in physics m58. Berlin New York: Springer, 1999, 1 vol. (XXIII, 331 p.) ISBN: 3-540-66195-6. [Online]. Available: http://www.sudoc.fr/046622063.

[83] P. Gutfreund, T. Saerbeck, M. A. Gonzalez, E. Pellegrini, M. Laver, C. Dewhurst, and R. Cubitt, "Towards generalized data reduction on a chopper-based time-of-flight neutron reflectometer", *Journal of Applied Crystallography*, vol. 51, no. 3, pp. 606–615, 2018. [Online]. Available: https://doi.org/10.1107/S160057671800448X.

[84] T. Saerbeck, R. Cubitt, A. Wildes, G. Manzin, K. H. Andersen, and P. Gutfreund, "Recent upgrades of the neutron reflectometer d17 at ill", *Journal of Applied Crystallography*, vol. 51, no. 2, pp. 249–256, 2018.

[85] F. Abelès, "Recherches sur la propagation des ondes électromagnétiques sinusoïdales dans les milieux stratifiés-application aux couches minces", in *Annales de physique*, EDP Sciences, vol. 12, 1950, pp. 596–640.

[86] A. Nelson, "Co-refinement of multiple-contrast neutron/x-ray reflectivity data using motofit", *Journal of Applied Crystallography*, vol. 39, pp. 273–276, 2006.

[87] S. Sinha, E. Sirota, Garoff, S, and H. Stanley, "X-ray and neutron scattering from rough surfaces", *Physical Review B*, vol. 38, no. 4, p. 2297, 1988.

[88] Y Yoneda, "Anomalous surface reflection of x rays", *Physical review*, vol. 131, no. 5, p. 2010, 1963.

[89] V Lauter, H. Lauter, A Glavic, and B. Toperverg, *Reference module in materials science and materials engineering*, 2016.

[90] J Teixeira, "Small-angle scattering by fractal systems", *Journal of Applied Crystallography*, vol. 21, no. 6, pp. 781–785, 1988.

[91] B.-A. Miller-chou and J.-L. Koenig, "A review of polymer dissolution", *Progress in Polymer science*, vol. 28 (8), elsevier, Ed., pp. 1223–1270, 2003.

[92] P.-G. De Gennes and P.-G. Gennes, *Scaling concepts in polymer physics*. Cornell university press, 1979.

[93] P. J. Flory, *Principles of polymer chemistry*. Cornell University Press, 1953.

[94] R. L. Scott, "The thermodynamics of high polymer solutions. v. phase equilibria in the ternary system: polymer 1—polymer 2—solvent", *The Journal of chemical physics*, vol. 17, no. 3, pp. 279–284, 1949.

[95] I. Bonaduce, M. Colombini, I.Degano, F. D. Girolamo, J. L. Nasa, F. Modugno, and S. Orsini, "Mass spectrometric techniques for characterizing low-molecular-weight resins used as paint varnishes", *Analytical and Bioanalytical Chemistry*, vol. 405 (2-3), pp. 1047–1065, 2012.

[96] G. Wypych, *Handbook of plasticizers*. ChemTec Publishing, 2004.

[97] D. Baughman and Y. Liu, *Neural networks in bioprocessing and chemical engineering*. Academic Press, 2014.

[98] K Ueberreiter, *The solution process*, 1968.

[99] A. Ouano and J. Carothers, "Dissolution dynamics of some polymers: solvent-polymer boundaries", *Polymer Engineering & Science*, vol. 20, no. 2, pp. 160–166, 1980.

[100] W. J. Cooper, P. D. Krasicky, and F. Rodriguez, "Dissolution rates of poly (methyl methacrylate) films in mixed solvents", *Journal of applied polymer science*, vol. 31, no. 1, pp. 65–73, 1986.

[101] M. Fixman, "Radius of gyration of polymer chains. ii. segment density and excluded volume effects", *The Journal of Chemical Physics*, vol. 36, no. 12, pp. 3123–3129, 1962.

[102] A. Sharma and G. Reiter, "Instability of thin polymer films on coated substrates: rupture, dewetting, and drop formation", *Journal of Colloid and Interface Science*, vol. 178, pp. 383–399, 1996.

[103] R. Konnur, K. Kargupta, and A. Sharma, "Instability and morphology of thin liquid films on chemically heterogeneous substrates", *Physical Review Letters*, vol. 84, no. 5, p. 931, 2000.

[104] C. Neto and K. Jacobs, "Dynamics of hole growth in dewetting polystyrene films", *Physica A: Statistical Mechanics and its Applications*, vol. 339, no. 1-2, pp. 66–71, 2004.

[105] A. Sharma and R. Khanna, "Pattern formation in unstable thin liquid films", *Physical Review Letters*, vol. 81, no. 16, p. 3463, 1998.

[106] R Xie, A. Karim, J. F. Douglas, C. C. Han, and R. A. Weiss, "Spinodal dewetting of thin polymer films", *Physical Review Letters*, vol. 81, no. 6, p. 1251, 1998.

[107] G. Reiter, "Unstable thin polymer-films-rupture and dewetting processes", *Langmuir*, vol. 9, pp. 1344–1351, 1993.

[108] G. Reiter and P.-G. de Gennes, "Spin-cast, thin, glassy polymer films: highly metastable forms of matter", *The European Physical Journal*, vol. 6 (1), pp. 25–28, 2001.

[109] F Saulnier, E Raphaël, and P.-G. De Gennes, "Dewetting of thin polymer films near the glass transition", *Physical review letters*, vol. 88, no. 19, p. 196 101, 2002.

[110] R. Seemann, S. Herminghaus, C. Neto, S. Schlagowski, D. Podzimek, R. Konrad, H. Mantz, and K. Jacobs, "Dynamics and structure formation in thin polymer melt films", *Journal of Physics: Condensed Matter*, vol. 17, no. 9, S267–S290, 2005. [Online]. Available: https://doi.org/10.1088%2F0953-8984%2F17%2F9%2F001.

[111] A. A. Pahlavan, L Cueto-Felgueroso, A. E. Hosoi, G. H. McKinley, and R. Juanes, "Thin films in partial wetting: stability, dewetting and coarsening", *Journal of Fluid Mechanics*, vol. 845, pp. 642–681, 2018.

[112] G. Schramm, *A practical approach to rheology and rheometry*. Haake Karlsruhe, 1994.

[113] P. Oswald, M. Saint-Jean, and M. Saint-Jean, *Rhéophysique: Ou comment coule la matière*. Belin, 2005.

[114] C. W. Macosko and I. M. Krieger, "Rheology: principles, measurements, and applications", *Journal of Colloid and Interface Science*, vol. 178, no. 1, p. 382, 1996.

[115] M. Renaud, M. N. Belgacem, and M. Rinaudo, "Rheological behaviour of polysaccharide aqueous solutions", *Polymer*, vol. 46, no. 26, pp. 12 348–12 358, 2005.

[116] Y. S. Lee, E. D. Wetzel, and N. J. Wagner, "The ballistic impact characteristics of kevlar® woven fabrics impregnated with a colloidal shear thickening fluid", *Journal of materials science*, vol. 38, no. 13, pp. 2825–2833, 2003.

[117] N. J. Wagner and J. F. Brady, "Shear thickening in colloidal dispersions", *Physics Today*, vol. 62, no. 10, pp. 27–32, 2009.

[118] [Online]. Available: https://www-liphy.ujf-grenoble.fr/pagesperso/verdier/Cours.pdf.

[119] I. Bonaduce, M. P. Colombini, I. Degano, F Di Girolamo, J. La Nasa, F. Modugno, and S. Orsini, "Mass spectrometric techniques for characterizing low-molecular-weight resins used as paint varnishes", *Analytical and bioanalytical chemistry*, vol. 405, no. 2-3, pp. 1047–1065, 2013.

[120] Y.-f. Zhang, X.-r. Zeng, and B.-y. Ren, "Synthesis and structural characterization of urea–isobutyraldehyde–formaldehyde resins", *Journal of Coatings Technology and Research*, vol. 6, no. 3, pp. 337–344, 2009.

[121] [Online]. Available: https://www.basf.com.

[122] [Online]. Available: http://www.ctseurope.com.

[123] M. Shahin, S. A. Hady, M. Hammad, and N. Mortada, "Optimized formulation for topical administration of clotrimazole using pemulen polymeric emulsifier", *Drug development and industrial pharmacy*, vol. 37, no. 5, pp. 559–568, 2011.

[124] C. Dupuy, "Les solvants organiques neutres épaissis pour le nettoyage d'une couche picturale. comparaison des acides polyacryliques et des éthers de cellulose comme épais-

sissant des solvants organiques", in *CeROArt. Conservation, exposition, Restauration d'Objets d'Art*, Association CeROArt asbl, 2012.

[125] D. Stulik, D. Miller, H. Khanjian, J. Carlson, N. Khandekar, and R. Wolbers, *Solvent gels for the cleaning of works of art: the residue question*. Getty Publications, 2004.

[126] N. Ravenel, "Pemulen® tr-2: an emulsifying agent with promise", *WAAC Newsletter Volume*, vol. 32, pp. 10–12, 2010.

[127] E. D. Goddard and J. V. Gruber, *Principles of polymer science and technology in cosmetics and personal care*. CRC Press, 1999.

[128] N. Sahu, B Parija, and S Panigrahi, "Fundamental understanding and modeling of spin coating process: a review", *Indian Journal of Physics*, vol. 83, no. 4, pp. 493–502, 2009.

[129] P. U. D.B. Hall and J. Torkelson, "Spin coating of thin and ultrathin polymer films", *Polymer engineering and science*, vol. 38, pp. 2039–2045, 1998.

[130] [Online]. Available: https://louisville.edu/micronano/files/documents/standard-operating-procedures/SpinCoatingInfo.pdf.

[131] C. M. D.E. Bornside and L. Scriven, "Spin coating: one-dimensional model", *Journal of Applied Physics*, vol. 66 (11), pp. 5185–5193, 1989.

[132] E. Rio and F. Boulogne, "Withdrawing a solid from a bath: how much liquid is coated?", *Advances in Colloid and Interface science*, vol. 247, pp. 100–114, 2017.

[133] M. Faustini, B. Louis, P. A. Albouy, M. Kuemmel, and D. Grosso, "Preparation of sol-gel films by dip-coating in extreme conditions", *The Journal of Physical Chemistry C*, vol. 114, no. 17, pp. 7637–7645, 2010.

[134] G. Jellison Jr, "Data analysis for spectroscopic ellipsometry", *Thin Solid Films*, vol. 234, no. 1-2, pp. 416–422, 1993.

[135] H. Fujiwara, *Spectroscopic ellipsometry: principles and applications*. John Wiley & Sons, 2007.

[136] [Online]. Available: https://www.mlz-garching.de/.

[137] R. A. Campbell, H. P. Wacklin, I. Sutton, R. Cubitt, and G. Fragneto, "Figaro: the new horizontal neutron reflectometer at the ill", *Eur. Phys. J. Plus*, vol. 126, no. 107, 2011.

[138] M. Wolff, P. Kuhns, G. Liesche, J. F. Ankner, J. F. Browning, and P. Gutfreund, "Combined neutron reflectometry and rheology", *Journal of Applied Crystallography*, vol. 46, no. 6, pp. 1729–1733, 2013.

[139] http://www.mlz-garching.de/nrex.

[140] C. M. Stafford, C. Harrison, K. L. Beers, A. Karim, E. J. Amis, M. R. VanLandingham, H.-C. Kim, W. Volksen, R. D. Miller, and E. E. Simonyi, "A buckling-based metrology

for measuring the elastic moduli of polymeric thin films", *Nature materials*, vol. 3, no. 8, p. 545, 2004.

[141] G. Binnig, C. F. Quate, and C. Gerber, "Atomic force microscope", *Physical review letters*, vol. 56, no. 9, p. 930, 1986.

[142] Y Yan, "Tribology and tribo-corrosion testing and analysis of metallic biomaterials", in *Metals for Biomedical Devices*, Elsevier, 2010, pp. 178–201.

[143] G. Sauerbrey, "The use of quarts oscillators for weighing thin layers and for microweighing", *Z. Phys.*, vol. 155, pp. 206–222, 1959.

[144] X. Qiao, X. Zhang, Y. Tian, and Y. Meng, "Progresses on the theory and application of quartz crystal microbalance", *Applied Physics Reviews*, vol. 3, no. 3, p. 031 106, 2016.

[145] M. D. Ward and D. A. Buttry, "In situ interfacial mass detection with piezoelectric transducers", *Science*, vol. 249, no. 4972, pp. 1000–1007, 1990.

[146] K. M. Ok, E. O. Chi, and P. S. Halasyamani, "Bulk characterization methods for noncentrosymmetric materials: second-harmonic generation, piezoelectricity, pyroelectricity, and ferroelectricity", *Chemical Society Reviews*, vol. 35, no. 8, pp. 710–717, 2006.

[147] Ö Pekcan, Ş Uĝur, and Y Yılmaz, "Real-time monitoring of swelling and dissolution of poly (methyl methacrylate) discs using fluorescence probes", *Polymer*, vol. 38, no. 9, pp. 2183–2189, 1997.

[148] M. C. Dixon, "Quartz crystal microbalance with dissipation monitoring: enabling real-time characterization of biological materials and their interactions", *Journal of biomolecular techniques: JBT*, vol. 19, no. 3, p. 151, 2008.

[149] P. Lindner and R. Schweins, "The d11 small-angle scattering instrument: a new benchmark for sans", *Neutron News*, vol. 21, no. 2, pp. 15–18, 2010.